



Hochschule für Angewandte Wissenschaften Hamburg  
*Hamburg University of Applied Sciences*

## **Bachelor's Thesis**

David Joaquin Garcia Merida

# **Theoretical and experimental determination of balsa wood elastic properties to supplement the stiffness prediction of a physically based FRP Sandwich Model**

*Fakultät Technik und Informatik  
Department Fahrzeugtechnik und Flugzeugbau*

*Faculty of Engineering and Computer Science  
Department of Automotive and  
Aeronautical Engineering*

**David Joaquin Garcia Merida**

**Theoretical and experimental  
determination of balsa wood elastic  
properties to supplement the stiffness  
prediction of a physically based FRP  
Sandwich Model**

Bachelor's thesis submitted within the Bachelor's examination

in the degree program Aeronautical Engineering  
at the Department of Automotive and Aeronautical Engineering  
of the Faculty of Engineering and Computer Science  
of the University of Applied Sciences Hamburg

in cooperation with:  
Fraunhofer Institut for Wind Energy Systems IWES  
Modeling of Polymers and Composites  
Am Seedeich 45  
27572 Bremerhaven

First examiner: Prof. Dr.-Ing. Dipl.-Kfm. Markus Linke  
Second examiner: Dr.-Ing. Alexandros Antoniou

Date of submission: 30.04.2021

## **Abstract**

**David Joaquin Garcia Merida**

### **Thema der schriftlichen Ausarbeitung**

Theoretische und experimentelle Bestimmung der elastischen Eigenschaften von Balsaholz zur Unterstützung der Steifigkeitsvorhersage eines physikalisch-basierten FVK Sandwich Modells

### **Stichworte**

Balsaholz, Sandwich, faserverstärkter Kunststoff, Vier-Punkt Biegung, Biegesteifigkeit, Schubmodul, Feuchtegehalt, Rotorblatt, Windkraftanlage

### **Kurzreferat**

Um die Steifigkeitsvorhersage eines physikalisch-basierten Faserverbundkunststoff Sandwich Modells zu unterstützen, wird eine Übersicht der internationalen Literatur zu den Eigenschaften von Balsaholz gegeben. Daraus wird eine generische Datenbasis der elastischen Eigenschaften gewonnen. Die veröffentlichten Daten werden mit Bezug auf die Holzdichte aufbereitet und dargestellt. Der am besten beschreibende Korrelationsgrad wird ermittelt und die natürliche Streuung der Daten, sowie der Einfluss der Holzdichte werden diskutiert. Die Modelvorhersage wird anhand quasi-statischer Vierpunktbiegeversuche an Sandwichproben verschiedener Kerndicken überprüft. Die der Auswertung zugrunde liegende Analytik beschreibt die Biegelinie der neutralen Achse des Sandwichs. Die Genauigkeit der Steifigkeitsvorhersagen wird durch die Implementierung der generischen Datenbasis maßgeblich gesteigert und durch die experimentellen Ergebnisse bestätigt.

**David Joaquin Garcia Merida**

### **Title of the paper**

Theoretical and experimental determination of balsa wood elastic properties to supplement the stiffness prediction of a physically based FRP Sandwich Model

### **Keywords**

balsa wood, sandwich, fiber reinforced plastic, four-point bending, bending stiffness, shear modulus, moisture content, rotor blade, wind turbine

### **Abstract**

To supplement the stiffness prediction of a physically based fiber reinforced plastic sandwich model the international literature on balsa wood material properties is reviewed. Therefrom a generic database for the elastic properties is derived. The available published data are collected, evaluated and presented in dependence of the balsa wood density. To characterize the type of dependence on the density the best correlating fitting approach is implemented. Furthermore, the natural scatter of the data and the relative moisture content are discussed. The model's stiffness prediction is compared to quasi-static four-point bending tests on sandwich specimens with different core thicknesses. The analytical expressions used for the evaluation model the deformation of the sandwich neutral axis. The accuracy of the model's stiffness prediction is significantly improved by the implemented database and found to be in good agreement with the experimental results.

# Contents

<b>1</b>	<b>Introduction.....</b>	<b>1</b>
1.1	Motivation .....	1
1.2	Description of the existing physically based model.....	2
1.3	Scope and Goals .....	3
<b>2</b>	<b>Theory.....</b>	<b>5</b>
2.1	Pure Balsa .....	5
2.1.1	Literature review for mechanical properties of pure balsa .....	7
2.1.2	Discussion of literature values, methods and influences .....	14
2.1.2.1	Methodology and plausibility of literature sources .....	14
2.1.2.2	Influence of moisture content.....	25
2.1.2.3	Applicable fitting method.....	28
2.1.3	Determination of universal literature values.....	31
2.2	Theoretical background of experiments.....	34
2.2.1	Differential equation of the bending line .....	35
2.2.2	Four-point bending evaluation approaches.....	38
2.2.3	Correlation between strain and bending moment in a beam.....	39
2.3	Simplified rule of mixture approach by Thomsen and Larsen .....	39
<b>3</b>	<b>Experimental methods and procedures of four-point bending test .....</b>	<b>46</b>
3.1	Test Setup according to ASTM C393 .....	46
3.2	Testing machine and tools.....	46
3.3	Preparation of specimens .....	47
3.3.1	Infusion and manufacturing process of balsa core sandwich specimens .....	47
3.3.2	Measuring Systems .....	50
3.4	Test procedure .....	51
3.5	Determination of bending stiffness and shear modulus .....	52
3.6	Modified tests and other test configurations .....	53
<b>4</b>	<b>Experimental results .....</b>	<b>55</b>
4.1	Specimen geometry.....	55
4.2	Bending stiffness and shear modulus .....	55
<b>5</b>	<b>Model validation .....</b>	<b>59</b>
5.1	Implementation of literature database and resulting predictions.....	59
5.2	Discussion of experimental results and validation of model predictions .....	61
5.3	Discussion of the simplified rule of mixture approach by Thomsen and Larsen.....	64
<b>6</b>	<b>Conclusions and future research.....</b>	<b>66</b>
<b>7</b>	<b>References .....</b>	<b>68</b>
	<b>Appendix A: Tables literature data .....</b>	<b>74</b>
	<b>Appendix B: Baltek SB technical data sheet.....</b>	<b>83</b>
	<b>Appendix C: Saertex X-E-812g/m<sup>2</sup>-1270mm technical data sheet .....</b>	<b>86</b>

---

**Appendix D: EPIKOTE Resin MGS RIMR 035c, EPIKURE Curing Agent  
MGS RIMH 037 technical data sheet .....87**

## List of Figures

Figure 1: development renewable energies in Germany for the last decade [1, p. 9].....	1
Figure 2: development of height, rotor diameter and power generation since 1998 [4, p. 40].....	2
Figure 3: cross section wind turbine rotor blade [3, p. 313] .....	2
Figure 4: schematic of a tree trunk cross section showing growth rings and anisotropy directions [8, p. 8690].....	5
Figure 5: balsa end grain panel with marked radial directions of single blocks.....	6
Figure 6: axial compression test setup Doyle et al. [10, p. 26].....	8
Figure 7: plate shear test setup Doyle et al. [10, p. 29].....	8
Figure 8: shear test setup Da Silva and Kyriakides [8, p. 8709] .....	9
Figure 9: shear test setup Osei-Antwi et al. incl. Iosipescu specimen with tracking dots [11, p. 234] .....	10
Figure 10: lap shear test setup Newaz et al. [23, p. 212].....	11
Figure 11: literature values Young's modulus axial compression .....	15
Figure 12: comparison axial Young's moduli from Baltek TDS .....	16
Figure 13: literature values radial Young's modulus from compression.....	17
Figure 14: literature values tangential Young's modulus from compression .....	17
Figure 15: literature values shear modulus in axial-radial plane .....	19
Figure 16: literature values shear modulus in axial-tangential plane .....	19
Figure 17: data sets Osei-Antwi et al. for shear moduli in axial-radial/axial-tangential plane.....	20
Figure 18: shear load in Iosipescu specimen with different grain orientation.....	20
Figure 19: shear distribution in the notch of an Iosipescu specimen.....	20
Figure 20: literature values shear modulus in radial-tangential plane.....	21
Figure 21: literature values axial-radial Poisson's ratio.....	21
Figure 22: literature values axial-tangential Poisson's ratio .....	22

Figure 23: literature values tangential-radial Poisson's ratio.....	23
Figure 24: literature values tangential-axial Poisson's ratio .....	24
Figure 25: literature values radial-axial Poisson's ratio.....	24
Figure 26: literature values radial-tangential Poisson's ratio.....	25
Figure 27: axial Young's modulus over moisture content for a specific density including moisture range.....	26
Figure 28: moisture diagram Báder et al. [47, p. 1016].....	27
Figure 29: moisture diagram Neroth [18, p. 840] .....	27
Figure 30: axial-tangential shear modulus from Doyle et al. with linear and polynomial fitting .....	30
Figure 31: Young's modulus axial direction, linear regression.....	31
Figure 32: four-point bending test setup ASTM C393 incl. load distribution [5, p. 53].....	34
Figure 33: bending stiffness measurement with dial gauge by Zenkert [53, p. 340].....	38
Figure 34: representative volume element described by combination of springs [58, p. 263].....	40
Figure 35: RVE Otten [5, p. 33].....	43
Figure 36: spring system RVE Otten .....	43
Figure 37: four-point bending test rig according to ASTM C393 .....	47
Figure 38: schematic vacuum assisted resin transfer moulding [53, p. 423].....	48
Figure 39: principle layup of sandwich manufacturing with VARTM [59, slide 57] .....	48
Figure 40: VARTM panel manufacturing with two vacuum bags .....	49
Figure 41: four-point bending test setup with installed DIC system .....	51
Figure 42: strain over force four-point bending, specimen 9.....	56
Figure 43: resulting bending stiffness ASTM D7250.....	58
Figure 44: resulting shear modulus ASTM D7250 .....	58
Figure 45: detailed view of gap between specimen and rubber pads occurring irregularly during testing (photos taken during two different tests).....	62

## List of Tables

Table 1:	mean moisture contents of balsa wood specimens of selected sources .....	25
Table 2:	coefficients of determination for fittings of literature mechanical properties.....	29
Table 3:	Poisson's ratios resulting from literature review.....	33
Table 4:	specimen geometries.....	55
Table 5:	four-point bending results, based on strain and on DIC data.....	57
Table 6:	mean values and standard deviations of four-point bending test results .....	58
Table 7:	balsa-resin core properties; model 1 including mixture approach of Thomsen and Larsen and literature data base; model 2 including literature data base; model 3 without supplements (old model) .....	60
Table 8:	model predictions for bending stiffness and shear modulus; model 1 including mixture approach of Thomsen and Larsen and literature data base; model 2 including literature data base; model 3 without supplements (old model) .....	60
Table 9:	overview experimental results and model predictions.....	63
Table A-1:	literature data Doyle et al. ....	77
Table A-2:	literature data Da Silva, Kyriakides .....	78
Table A-3:	literature data Easterling et al. ....	78
Table A-4:	literature data Osei-Antwi et al. ....	79
Table A-5:	literature data Newaz et al. ....	79
Table A-6:	specimens' dimensions Newaz et al. ....	79
Table A-7:	literature data Kotlarewski et al. ....	79
Table A-8:	literature data Feichtinger .....	81
Table A-9:	literature data Soden et al.....	82
Table A-10:	literature data Wood Handbook .....	82
Table A-11:	literature data Baltek TDS.....	82



## List of Abbreviations

CCD	charge-coupled device
CLT	classical laminate theory
DIC	digital image correlation
FE	finite elements
FRP	fiber reinforced plastic
FVC	fiber volume content
IWES	Fraunhofer Institute for Wind Energy Systems
LVDT	linear variable differential transformer
PU	polyurethane
PVC	polyvinyl chloride
RVE	representative volume element
TDS	technical data sheet
VARTM	vacuum assisted resin transfer molding

## List of Symbols

Symbol	Meaning	Unit
$A$	area	$mm^2$
$A_g$	cross section area grid RVE Thomsen and Larsen	$mm^2$
$a$	width of vessel cells RVE Otten	$mm$
$a_{TL}$	length RVE Thomsen and Larsen	$mm$
$B$	coefficient of determination	-
$b$	specimen/beam width	$mm$
$b_{TL}$	width RVE Thomsen and Larsen	$mm$
$b_x, b_y$	distance between vessel cells RVE Otten	$mm$
$C_{1-6}$	integration constants	-
$c$	core thickness	$mm$
$c_z$	measuring distance Zenkert	$mm$
$D$	bending stiffness Zenkert	$Nmm^2$
$D_x$	bending stiffness	$Nmm^2$
$D_{Qx}$	shear stiffness normalized over core thickness	$\frac{N}{mm}$
$D_{SL}$	distance between supporting and next loading bar	$mm$
$d$	distance between the center lines of the faces	$mm$
$E_A$	axial Young's modulus	$MPa$
$E_{A,ten}$	axial Young's modulus derived from tension	$MPa$
$E_{A,com}$	axial Young's modulus derived from compression	$MPa$
$E_{B,x}$	balsa wood Young's modulus x-direction	$MPa$
$E_{B,y}$	balsa wood Young's modulus y-direction	$MPa$
$E_{B,z}$	balsa wood Young's modulus z-direction	$MPa$
$E_f$	Young's modulus foam RVE Thomsen and Larsen	$MPa$
$E_g$	Young's modulus resin grid RVE Thomsen and Larsen	$MPa$
$E_R$	radial Young's modulus	$MPa$
$E_r$	resin Young's modulus RVE Otten	$MPa$

$E_T$	tangential Young's modulus	$MPa$
$E_x$	specimen/beam Young's modulus x-direction	$MPa$
$E_{x,RVE}$	Young's modulus x-direction RVE Otten	$MPa$
$E_y$	specimen/beam Young's modulus y-direction	$MPa$
$E_{y,RVE}$	Young's modulus y-direction RVE Otten	$MPa$
$E_{y,TL}$	Young's modulus y-direction RVE Thomsen and Larsen	$MPa$
$E_z$	specimen/beam Young's modulus z-direction	$MPa$
$E_{z,RVE}$	Young's modulus z-direction RVE Otten	$MPa$
$F$	bending force	$N$
$G_A$	axial shear modulus Feichtinger	$MPa$
$G_{AR}$	axial-radial shear modulus	$MPa$
$G_{AT}$	axial-tangential shear modulus	$MPa$
$G_{AR/AT}$	axial-radial axial-tangential mixed shear modulus (out-of-plane)	$MPa$
$G_{B,xy}$	balsa wood shear modulus x-y-plane	$MPa$
$G_{B,xz}$	balsa wood shear modulus x-z-plane	$MPa$
$G_{B,yx}$	balsa wood shear modulus y-x-plane	$MPa$
$G_{B,yz}$	balsa wood shear modulus y-z-plane	$MPa$
$G_{RT}$	radial-tangential shear modulus	$MPa$
$G_{xy}$	specimen/beam shear modulus x-y-plane (in-plane)	$MPa$
$G_{xy,RVE}$	shear modulus x-y-plane RVE Otten	$MPa$
$G_{xz}$	specimen/beam shear modulus x-z-plane (out-of-plane)	$MPa$
$G_{xz,RVE}$	shear modulus x-z-plane RVE Otten	$MPa$
$G_{yz}$	specimen/beam shear modulus y-z-plane (out-of-plane)	$MPa$
$G_{yz,RVE}$	shear modulus y-z-plane RVE Otten	$MPa$
$h$	thickness RVE Thomsen and Larsen	$mm$
$I_y$	axial moment of inertia	$mm^4$

$k_{[...]}$	spring constant (various)	$\frac{N}{mm}$
$L$	distance between loading bars	$mm$
$l$	specimen length	$mm$
$L_1$	distance between loading bars Zenkert	$mm$
$L_2$	distance between supporting bars Zenkert	$mm$
$L_{RVE}$	length RVE Otten	$mm$
$M_I$	bending moment section I	$Nmm$
$M_{II}$	bending moment section II	$Nmm$
$M_x, M_y$	bending moment	$Nmm$
$m$	number of vessel cells in y-direction RVE Otten	-
$n$	number of vessel cells in x-direction RVE Otten	-
$P$	bending force Zenkert	$N$
$Q_x$	transverse shear force normalized over beam width	$\frac{N}{mm}$
$Q_I$	normalized transverse shear force section I	$\frac{N}{mm}$
$Q_{II}$	normalized transverse shear force section II	$\frac{N}{mm}$
$r$	correlation coefficient	-
$S$	sum of divagation squares	-
$S$	distance between supporting bars	$mm$
$s_x, s_y$	width resin filled slits RVE Otten	$mm$
$t$	specimen/beam thickness	$mm$
$t_1, t_2$	face thickness	$mm$
$t_a$	width resin bar width-direction RVE Thomsen and Larsen	$mm$
$t_b$	width resin bar length-direction RVE Thomsen and Larsen	$mm$
$t_c$	specimen core thickness	$mm$
$t_{RVE}$	thickness RVE Otten	$mm$
$W_{RVE}$	width RVE Otten	$mm$
$w_I$	deflection section I	$mm$
$w_{II}$	deflection section II	$mm$
$w_{b,I}$	bending deflection section I	$mm$
$w_{b,II}$	bending deflection section II	$mm$
$w_{s,I}$	shear deflection section I	$mm$

$w_{s,II}$	shear deflection section II	mm
$w_Z$	deflection Zenkert	mm

<b>Greek Symbols</b>		
<b>Symbol</b>	<b>Meaning</b>	<b>Unit</b>
$\varepsilon$	strain	-
$\varepsilon_l$	strain lower strain gauge	-
$\varepsilon_u$	strain upper strain gauge	-
$\nu_{AR}$	axial-radial Poisson's ratio	-
$\nu_{AT}$	axial-tangential Poisson's ratio	-
$\nu_{B,xy}$	balsa wood Poisson's ratio x-y-orientation	-
$\nu_{B,yx}$	balsa wood Poisson's ratio y-x-orientation	-
$\nu_{RA}$	radial-axial Poisson's ratio	-
$\nu_{RT}$	radial-tangential Poisson's ratio	-
$\nu_{TA}$	tangential-axial Poisson's ratio	-
$\nu_{TR}$	tangential-radial Poisson's ratio	-
$\rho$	density	$\frac{kg}{m^3}$
$\varphi$	fiber volume content	-
$\psi$	twist of beam cross section	-

# 1 Introduction

## 1.1 Motivation

In the year 2020 the electrical energy produced by wind turbines in Germany was 131 TWh and thus 4% higher than in the year 2019 [1, p. 8]. The annually growth of the produced wind energy is an ongoing trend looking at the data for the last decade displayed in Figure 1. The current wind energy production equals 24% of the German gross energy consumption [1, p. 9] and is the most important renewable energy source in the overall energy mix.

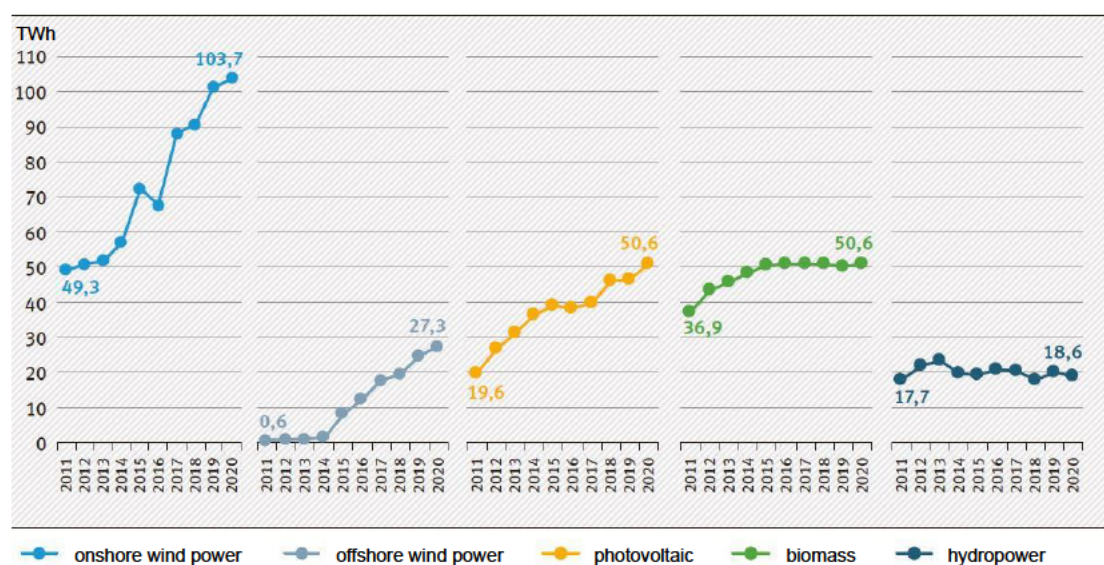


Figure 1: development renewable energies in Germany for the last decade [1, p. 9]

This trend of growing installation of wind power capacities can be observed globally and especially the Asian-Pacific region has a high energy demand in general and for wind energy in particular [2]. Overall, the wind energy is an important pillar of the measures against the human-caused global warming. To fulfill the need for wind energy on the one hand it is necessary to build more wind turbines. On the other hand, the capacity and efficiency of the single wind turbine needs to be improved. This leads to the development of larger wind turbines with higher towers and larger rotor diameters as it can be seen in Figure 2, because the power production basically increases proportional to the square of the diameter [3, p. 652]. Following the square-cube law the mass increases theoretically cubic-proportional. However, due to design process advances the exponent is practically between 2.4 - 2.8 [3, p. 324]. This leads to the necessity to construct the rotor blades as light as possible. Furthermore, the loads caused by the mass of the rotor blades also have an impact on many other parts of the wind turbine. Thus, weight optimized rotor blades are also important for the economic efficiency of wind turbines [3, pp. 875 ff.].

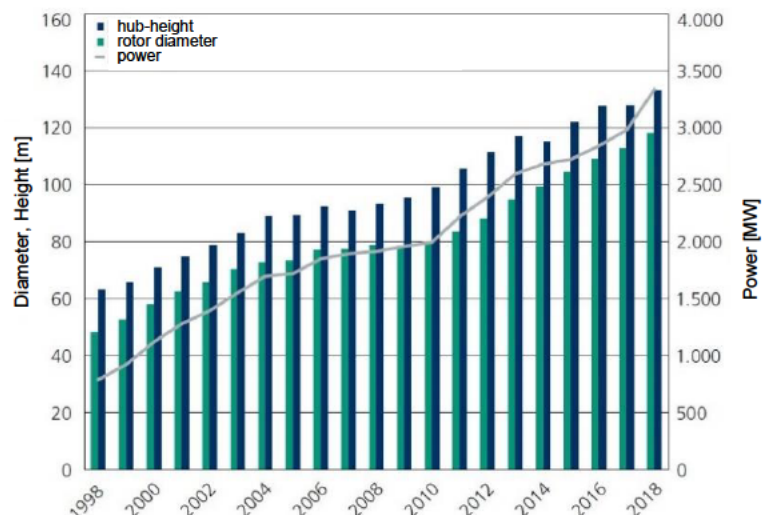


Figure 2: development of height, rotor diameter and power generation since 1998 [4, p. 40]

The need for weight optimized rotor blades leads to the utilization of high-performance, lightweight materials. Therefore, fiber reinforced plastic (FRP) sandwiches are commonly used for large parts of the aerodynamic surface of the rotor blade. This can be seen highlighted in red on the rotor blade cross section in Figure 3. One variant for these sandwiches is a combination of glass fiber-epoxy face sheets with a balsa wood core. The optimal utilization of the sandwich structure with regards to the named demands, requires an accurate prediction of its masses and mechanical properties.

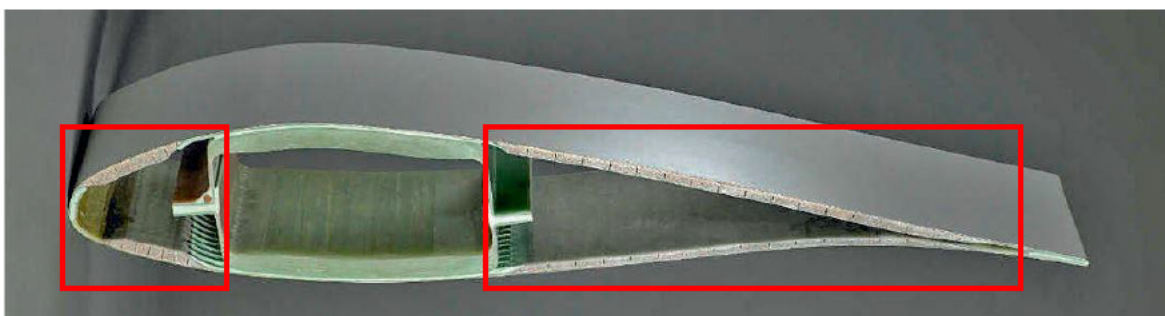


Figure 3: cross section wind turbine rotor blade [3, p. 313]

## 1.2 Description of the existing physically based model

One step towards the necessary prediction of rotor blade masses and their elastic properties respectively, is the modeling of flat sandwich panels. Therefore, Otten [5] developed a physically based FRP sandwich model with special focus on the balsa core resin uptake in his Master's thesis. A brief introduction of the model is described in the following paragraphs.

The model is written in Microsoft Excel (Microsoft Corporation, Redmond, Washington, USA). It consists of two major parts, the mass calculation and the stiffness calculation. Both calculations are performed with special attendance to the resin uptake of the balsa panel during the manufacturing process. It is influenced by the widening of the slits of the balsa panels and the porous structure of the balsa wood. The user can define the sandwich layout individually. The stiffness calculation

includes the bending stiffness, the in-plane and the transverse shear moduli of the whole sandwich. It is based on the classical laminate theory (CLT). The balsa wood properties necessary for the calculation, are based on the data of a single literature source.

The model predictions are intended to be verified by experimental results. They are found to be sufficiently accurate for the mass prediction, with a relative error of less than 10% [5, p. 85]. For the verification of the bending stiffness and shear moduli, four-point bending tests according to ASTM C393 [6] are performed. The bending stiffness is calculated by applying the bending line theory for beams. One evaluation approach is based on strains measured with strain gauges on the upper and lower surface of the specimen. Another approach is to measure the deflection via the path of the machine cross head. For both cases, the experimental results show large differences to the model predictions and thus do not verify them. One reason is found to be the compliance of the machine cross head, leading to mismeasurements of the deflection. The used bending line equations are sensitive to minimal changes of deflection and thus the results become inaccurate. Another factor stated is, that the sandwich shear modulus strongly depends on the balsa core shear modulus. This is derived from a single literature source, "based on a semi-empirical equation for wood in general" [5, p. 86] and thus not reliable.

### 1.3 Scope and Goals

The described uncertainties in the existing physically based model and the inaccuracies of the model predictions lead to the scope and goals of this Bachelor's thesis.

In order to improve the reliability of the balsa wood elastic properties, which the model calculations and predictions are based on, a literature review is performed. The respective, current properties derived from single literature sources shall be replaced by a generic database. Therefore, an overview of the relevant literature dealing with the elastic characterization of balsa wood is given in chapter 2.1.1, including detailed information on the used testing methods and specimens' configurations. The data is processed, compared and analyzed, while deviations and potential improper testing methods are discussed. On this basis the data is filtered to exclude misleading test results from further processing. Additionally, the influence of the wood moisture on the properties is discussed in chapter 2.1.2.2. Finally, in chapter 2.1.3, one universal value for each elastic property of the balsa wood is derived as a function of the density of the balsa wood. This dependence is already available in all sources. In chapter 2.3 an alternative approach for the modeling of the balsa-resin mixture in the core is described, which occurred during the research.

To verify the predictions of the supplemented model, four-point bending tests according to ASTM C393 [6] are performed again. The theory used for the evaluation of the tests is explained in chapter 2.2. To prevent potential problems in the deflection measurement via the machine path, two different measurement methods are applied and described in chapter 3.3.2. The specimens are manufactured with the vacuum assisted resin transfer molding (VARTM) technique, described in chapter 3.3.1. To differentiate the database the tests are performed on



sandwich specimens with two different core thicknesses. Furthermore, another face sheet layout compared to Otten's tests is used. The test procedure and evaluation are described in chapters 3.4 and 3.5. Chapter 3.6 contains the description of modified test configurations, developed during the initial testing. The experimental results of the four-point bending tests are then displayed in chapter 4. The derived, generic literature database is implemented in the existing model in chapter 5.1. Also, the alternative balsa-resin mixture approach is implemented. The resulting, new model predictions are displayed and compared with the old predictions. In chapter 5.2 the four-point bending tests and their results are discussed with special attendance to the improvement of measurement systems. Finally, they shall verify the model predictions. The alternative mixture approached is discussed separately in chapter 5.3. In the last chapter, 6, the results of this thesis are summarized and an outlook on future research is given.

The goal is to receive sufficiently accurate model predictions for the bending stiffness and shear modulus of an FRP sandwich verified by experimental results to enable the characterization and modelling of lightweight optimized wind turbine rotor blades sandwich components.

## 2 Theory

### 2.1 Pure Balsa

As outlined before, balsa wood is the most common core material in sandwich constructions used in wind turbine blades, besides polyvinyl chloride (PVC) and polyurethane (PU) foams [7, p. 1]. In contrast to the foams, balsa wood is described as an anisotropic material in the literature, with its mechanical properties depending on the anisotropy direction [8, p. 8689]. Other sources describe it as an orthotropic material, again with its mechanical properties depending on the “three mutually perpendicular axes” [9, pp. 5-1 f.]. In some sources, orthotropy is also referred to as rhombic anisotropy. Three principal directions, axial, radial and tangential are to be found in the international literature. These are defined respectively as a. parallel to the grain [9, p. 3-13], b. perpendicular to the grain and radial to the growth rings and c. perpendicular to the grain and tangential to the growth rings. Some authors refer to the axial direction as longitudinal [9, pp. 5-1 f., 10, pp. 2 f.] but within this work the indication “axial” will be used. The directions are oriented on the tree trunk as displayed in Figure 4. To describe an orthotropic material properly, twelve constants are required. Thus the Young’s moduli  $E_A$ ,  $E_R$ ,  $E_T$ , the shear moduli  $G_{AR}$ ,  $G_{AT}$ ,  $G_{RT}$  and the Poisson’s ratios for all direction combinations  $\nu_{AR}$ ,  $\nu_{AT}$ ,  $\nu_{TR}$ ,  $\nu_{TA}$ ,  $\nu_{RA}$ ,  $\nu_{RT}$  need to be determined, with nine of them independent from each other [9, p. 5-2].

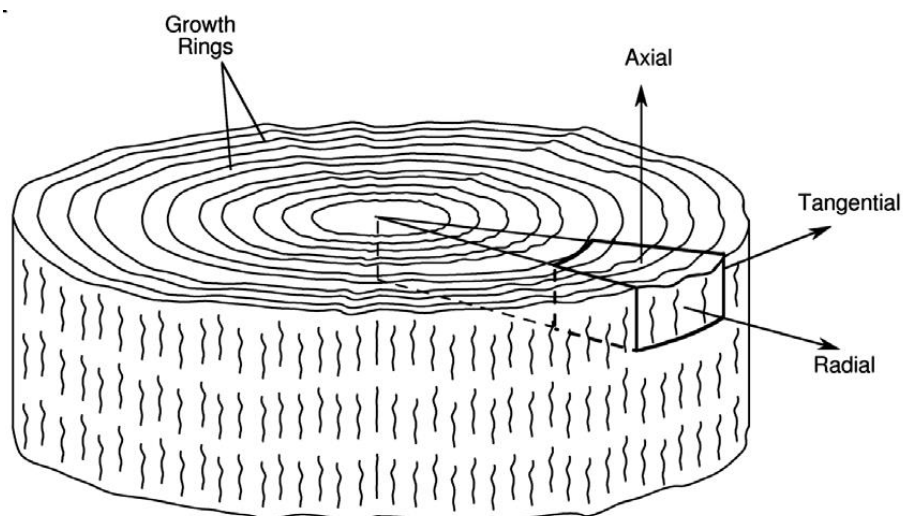


Figure 4: schematic of a tree trunk cross section showing growth rings and anisotropy directions [8, p. 8690]

Balsa wood as a naturally grown material strongly varies in its density “with age and habitat of the tree. It covers densities from about [...] 40 – 380 kg/m<sup>3</sup>” [8, p. 8686]. The balsa plates from different manufacturers, such as Baltek (3A Composites Core Materials - Airex AG, Sins, Switzerland) or Gurit (Gurit Holding AG, Wattwil, Switzerland), used in wind turbine blades usually consist of selected “cubic blocks of balsa with the fiber direction perpendicular to the panel plane [...]. In this way, end grain balsa panels of relatively uniform density can be produced” [11, p. 231]. These panels are cut as slices from larger blocks of joint rods of end grain balsa from different trees [5, p. 10, 12, p. 336]. The uniform density is important for the industrial use, as the mechanical properties of balsa strongly depend on the density

[13, pp. 37 ff.]. Within the panels the orientation of the single blocks varies regarding the radial and tangential orientation as it is displayed in Figure 5.

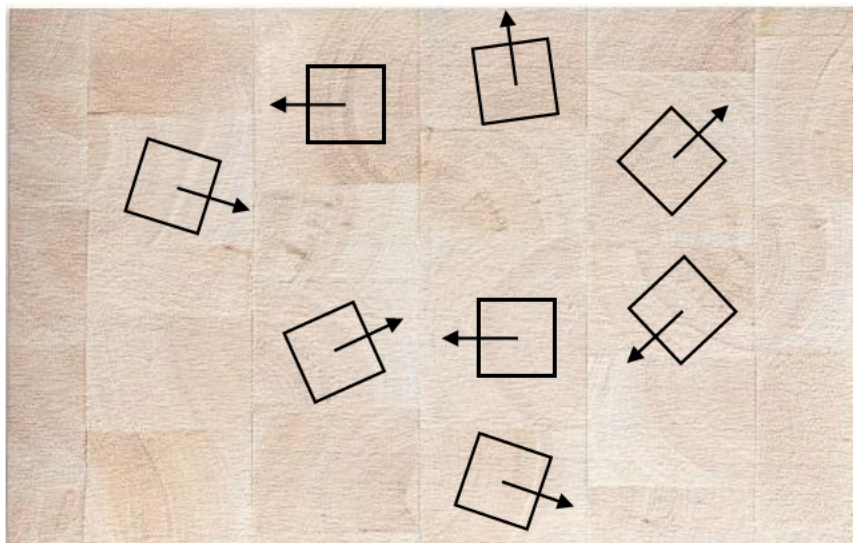


Figure 5: balsa end grain panel with marked radial directions of single blocks

This leads to the conclusion, that the radial and tangential direction and so their different mechanical properties cannot be distinguished in the balsa plates anymore. To approximate values for the in-plane properties the radial and tangential values must be combined.

In the following, an overview of the international literature values for the different mechanical properties is given. It includes a short explanation of the respective testing methods, with which the values were determined. Some sources display their results as mechanical property over density and others over specific gravity. These two terms can be directly converted into each other, as the specific gravity could also be called specific density and is “the ratio of the density of a material to the density of pure water” at 4°C [14, pp. 4 f.], which is 997 kg/m<sup>3</sup>. In this thesis the property values will be displayed as a function of the density.

The moisture content of the used balsa specimens is documented since it shows a large impact on the properties of the chemical components of the cell wall material and thus on the wood mechanical performance [15,16, p. 127]. The effect is negative. With increasing moisture content the mechanical properties deteriorate [17, p. 230] until a threshold level of about 30% [18, p. 840]. Some sources suggest “up to 6 per cent change in mechanical properties” [17, p. 230] per 1% moisture change at a nominal density. Furthermore, the moisture content has an impact on the actual density as it increases the mass and also the volume of the wood. This effect is called swelling [18, p. 834]. Often carried out experiments to investigate the influence of moisture content on balsa specimens volumes [5, pp. 57–59]. Yet it is stated that “the equilibrium moisture content [...] at a given temperature and relative humidity is nearly the same regardless of [...] density” [14, p. 2]. This makes specimens comparable, if they are conditioned in the same way until saturation.

Furthermore, the methods and values are discussed to sort out potentially improper test results. Average mechanical properties for the balsa wood are then derived.

## 2.1.1 Literature review for mechanical properties of pure balsa

### Elastic Properties of Wood – Doyle, Drow, McBurney – 1962

A standard reference regarding the mechanical properties of balsa wood is the work of Doyle, Drow and McBurney from 1962 [10]. The authors carry out tests to determine the Young's moduli, Poisson's ratios and shear moduli without a particular standard being applied. To obtain the Young's moduli and Poisson's ratios, the specimens are compressed in the direction of their length while axial compression and lateral expansion are measured. The tests are performed on 27 specimens with axial and between 13 to 20 each with radial and tangential orientation in the direction of their length. All specimens are cut directly out of pure balsa and conditioned in a humidity room at 70 °F and 64% relative humidity until they reach a constant weight, i.e. under standard climate conditions [18, p. 834]. This leads to a moisture content of averaged 8.97 - 9.44% in the specimens. The compression specimens are prisms with the size of 2 by 2 by 8 inches and the shear specimens are 8 by 8 by 0.25 inches. The authors present their data in tables and diagrams. Although the database is the same, the tables contain already sorted, summarized and averaged data. To get a larger and more original data pool, the data points of the diagrams [10, pp. 30–41] are used for this thesis. Therefore, all diagrams are digitalized using the Engauge Digitizer Version 12.1 (Freeware, © Mark Mitchell) and the data points are read out. Afterwards the data is converted into metric units if necessary. This procedure is performed for all sources with data points in diagrams, which are not simply listed in tables but already processed.

The axial compression is measured with a Lamb's roller extensometer over a central 6-inch gage length. The lateral expansion is measured with a Lamb's roller lateral extensometer that is partly self-build and modified to eliminate inaccuracies. It should be mentioned that the measuring mechanisms are very sensitive to manufacturing inaccuracies and that all measuring is done analogue by hand. Figure 6 shows the axial compression test setup. The extensometers applied horizontally and vertically to the specimen can be seen. The exact operating principle of the utilized mirror system can be found on pages 7 to 10 of the paper [10, pp. 7–10]. The moduli of rigidity are obtained by a test in a "plate shear" apparatus, constructed by the forest laboratory. In it the four corners of the flat specimen are loaded equally. The force on two opposing corners is acting upwards and on the other opposing corners downwards. The modulus of rigidity can then be calculated from the load and measured deflections on the diagonals of the specimen. A detailed description of the test can be found in Forest Products Laboratory Report No. 1301 [19]. The setup is displayed in Figure 7. The test results are listed in appendix A Table A-1.

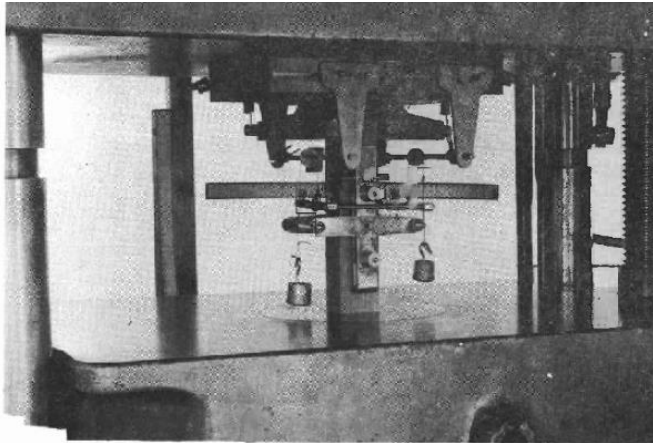


Figure 6: axial compression test setup Doyle et al. [10, p. 26]

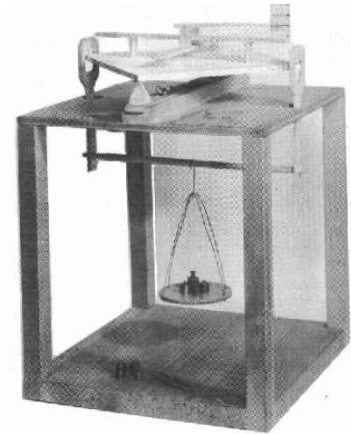


Figure 7: plate shear test setup Doyle et al. [10, p. 29]

### Compressive response and failure of balsa wood – Da Silva, Kyriakides – 2007

In their paper from 2007, Da Silva and Kyriakides deal with the microstructure and mechanical properties of balsa wood. They carry out extensive compression until failure tests as well as shear tests without a particular standard being applied [8]. They hereby determine the Young's moduli of balsa for all three directions and the shear moduli in the axial-radial and the axial-tangential plane. The compression tests are performed on 61 specimens in axial direction and on an unknown number in radial and tangential direction. The axial specimens are 1 by 1 by 3 inches, except for the lowest densities where a square cross section with 1.5 inches is chosen. The radial and tangential specimens are 2 inches tall with a square cross section of 1 inch. All compression specimens are cut-out of Baltek balsa plates with different densities (SL45, SL1112, SL1415). More precisely they were cut-out of single blocks within the plates, to avoid block interfaces within the specimen. Furthermore, 29 shear tests are performed in the axial-tangential plane and 19 in the axial-radial plane on specimens that are glued directly to custom mounting plates. They are 3 by 1 by 1 inches, with their ends radiused to a test section of 0.75 by 0.625 inch, for reducing stress concentrations. All specimens are conditioned between 9 - 12% relative moisture content and weighed before the testing.

In the displacement-controlled compression tests an extensometer is used to record the strain within a computer operated data acquisition system. The shear test setup is displayed in Figure 8. Shear is applied by applying "a horizontal displacement to the lower part of the fixture" [8, p. 8709] under displacement control. To measure the relative displacement a miniature linear variable differential transformer (LVDT) is used. The test results selected and published by the authors are listed in appendix A Table A-2.

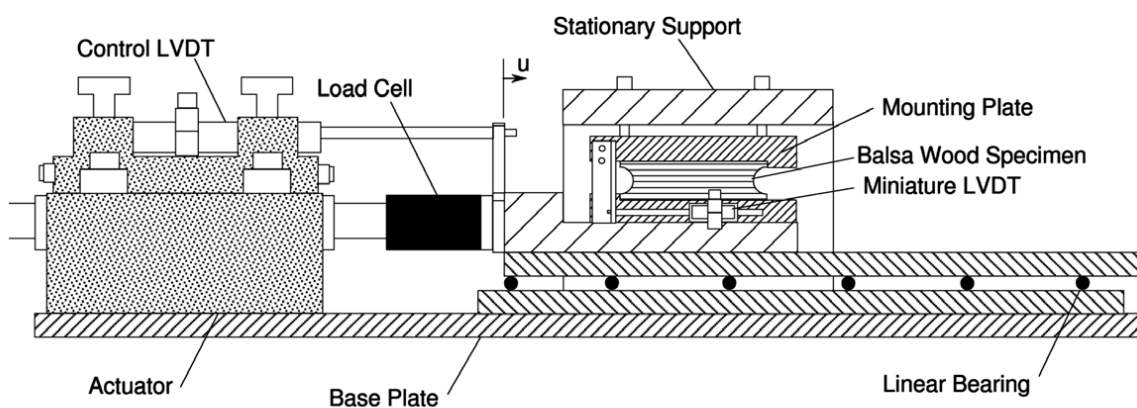


Figure 8: shear test setup Da Silva and Kyriakides [8, p. 8709]

### On the mechanics of balsa and other woods – Easterling, Harrysson, Gibson, Ashby – 1982

In their 1982 published paper, the authors carry out compression test on balsa specimens until failure. They examine the correlation between the microscopic structure of balsa, including the properties of the cell wall material and its mechanical properties [13]. The Young's moduli for the three principal directions are measured on specimens categorized in four density classes. The Poisson's ratios are measured for one density class under radial and tangential compression. They are derived from the table [13, p. 34], whereas the Young's moduli data is extracted from the diagram [13, p. 38]. The specimens are cut from "well seasoned dry balsawood" [13, p. 32], without the moisture content being measured exactly.

The compression tests are recorded with an Instron. It is not mentioned what is used to measure the perpendicular strain for the calculation of the Poisson's ratios. Furthermore, the authors claim to measure the bending stiffness of long beams for each density class, with a test setup, which is explained. Also, no results can be found in the paper. The determined Young's moduli and Poisson's ratios are listed in appendix A Table A-3.

### Shear mechanical characterization of balsa wood as core material of composite sandwich panels – Osei-Antwi, de Castro, Vassilopoulos, Keller – 2013

In this paper the authors perform shear tests on Iosipescu specimens according to ASTM D5379 [20] to examine the shear moduli and strength of balsa [11]. They explicitly deal with balsa as a core material in sandwich panels and therefore with balsa panels made from joint blocks. Tests are performed on specimens in three different planes related to the grain. One of directions aligns with the radial-tangential plane. The other ones align with axial-radial or axial-tangential or a mix of them, which is not specified in the paper. In one type, the shear plane is parallel to end and in the other to flat grain. To reflect the adhesive joints in the balsa panel, the specimens contain these joints as well. To keep the results comparable with other sources, only the results for specimens of pure balsa, without joints, are taken into further consideration. The specimens are made of Baltek SB150 panels with a

moisture content of approximately 12%, measured according to ASTM 4442-07 A [21].

The shear tests are performed according to standard ASTM D5379 [20] to avoid high stress concentrations, which occurred in previous tests according to ASTM C273-94 [22]. For measuring the shear deformations, a video extensometer is used. With it four black dots on the specimen are tracked. The test setup with visible tracking dots is displayed in Figure 9. The determined shear moduli are listed in appendix A Table A-4.

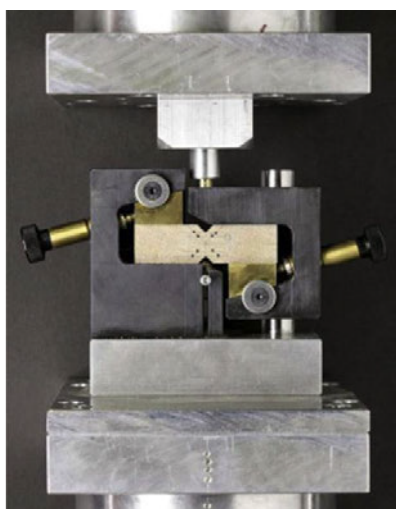


Figure 9: shear test setup Osei-Antwi et al. incl. Iosipescu specimen with tracking dots [11, p. 234]

Characterization of balsa wood mechanical properties required for continuum damage mechanics analysis – Newaz, Mayeed, Rasul – 2016

The authors carry out several tests to evaluate the mechanical properties of balsa wood for the use in continuum damage mechanics analysis [23]. They compare their results with literature results and with results obtained from numerical solutions using LS-DYNA. For the given scope in this Bachelor's thesis, only the experimental results are used. The specimens' orientation in the test is distinguished in along and across the grain. The orientation along the grain aligns with the axial orientation. The orientation across the grain is the radial or tangential orientation or a mix of both. The authors derive the Young's moduli from compression and tension tests by calculating an equivalent modulus, introduced by Yao and Ye [24]. Furthermore, they derive the given Poisson's ratios from calculations using the measured strain and stress from compression and tension tests. The longitudinal and lateral deformation are not directly measured. Shear moduli are derived from a lap shear test. None of the tests follows a particular standard. Specimens for all tests are made of pure balsa. They are cut-out of a sheet from Balsa Wood Inc. with a uniform density, which shows a deviation of  $\pm 1.5\%$ . The moisture content is considered to be 12%, but not specifically measured. All specimens have a plate like shape of different size for the different tests. The number of specimens per test remains unknown.

All tests are performed displacement controlled on an MTS testing machine. No additional measuring system is mentioned. For the shear tests, a custom-made fixture is used with the specimens glued to it. It is displayed in Figure 10. All results

are listed in appendix A Table A-5 and the dimensions of the specimens for each test can be found in appendix A Table A-6.



Figure 10: lap shear test setup Newaz et al. [23, p. 212]

Mechanical properties of Papua New Guinea balsa wood – Kotlarewski, Belleville, Gusamo, Ozarska – 2015

The authors perform various tests according to ASTM D143-09 [25] on balsa wood from Papua New Guinea [26]. They determine Young's modulus, modulus of rupture, hardness, compression strengths and shear strengths. The results are compared with results from South American balsa wood e.g. Baltek uses for its panels. The specimens are cut directly from the trunk. They are in general seasoned to 12% moisture content before testing. Individual moisture content measurements on each specimen, reveal deviations from that value. Moisture content and density are measured according to AS/NZS 1080.1:2012 [27] and AS/NZS 1080.3:2000 [28].

The elastic modulus is determined by conducting a three-point static bending test until failure. It is performed on 26 specimens with 25 by 25 mm cross section by 410 mm length using an Instron Model 5569 universal testing machine. The results are listed in appendix A Table A-7. The specimens are categorized in three density classes. To enable the presentation in a common diagram, the middle value of each density class is considered to be the value for the whole range. This is done for all sources where it is applicable.

Test Methods and Performance of Structural Core Materials-1. Static Properties – Feichtinger – 1989

In his paper, the author describes mechanical characterization methods for several structural core materials in sandwich constructions [12]. He performs corresponding tests on end grain balsa specimens. The characterization includes the Young's modulus in axial direction, derived from compression tests according to ASTM C365-57 [29]. The specimen dimensions are 3 by 3 by 3 inches. The shear



modulus for a combination of axial-radial and axial-tangential planes is derived from lap shear test according to ASTM C273-61 [30]. The specimen dimensions are 6 by 2.5 by 0.5 inches. The specimens are cut-out of balsa panels of own production. They are conditioned at  $50\pm 4\%$  relative humidity and  $73\pm 2^\circ\text{F}$  according to MIL-STD-401B [31]. Compression and shear tests in radial and tangential orientation are performed on 48 specimens each.

All tests are performed on an Instron Model 4206 universal testing machine under displacement control. The strain in the compression tests is measured using a gauge. It is fixed on the side of the specimen by two steel drill blanks inserted into the core. The decrease in gauge length is measured with an extensometer. The load is taken directly from the load cell of the machine. For the shear tests, the specimens are directly bonded to the steel plates. The displacement between the plates is measured with a modified extensometer. The author displays the shear results for axial-radial and axial-tangential plane individually in a diagram [12, p. 349]. There is no table with the data listed. In the diagram, the data point symbols cannot be distinguished from each other, due to the low resolution of the source and missing colors. As described before, the orientation of the single blocks in balsa panels is mixed anyway. With this argument, the author proceeds to derive a single analytical model for the mixed orientations by regression through all data points. In contrast to most of the other sources, no linear correlation between the properties and the density is stated. The Young's modulus is determined as [12, p. 342]

$$E_A = 2.839 * \rho^{1.442} \quad (1)$$

and the shear modulus as [12, p. 348]

$$G_A = 54.68 * e^{7.023*10^{-3}*\rho} \quad (2)$$

with  $[E_A]=\text{MPa}$ ,  $[G_A]=\text{MPa}$  and  $[\rho]=\text{kg/m}^3$ . The data points are still extracted from the diagrams [12, pp. 341, 349] and can be found in appendix A Table A-8.

#### Variables affecting the strength of balsa wood – Soden, McLeish – 1976

The authors examine the strength of pure balsa wood specimens dependent on the density and different angles of the grain, as it is used as modelling material in design competitions [17]. Beside the strengths, they also derive the Young's moduli from their tests. Tension and compression tests are performed. The tension tests are performed according to standards B.S. 373 1958 and ASTM 143-52 1972 [32], with some modifications regarding the dimensions of the specimens. However, the standard B.S. 373 1958 does not exist. It is assumed that the referenced standard instead must be BS 373:1957 [33]. It contains corresponding content. The compression tests are performed without any referenced standard. For the tension tests, 105 specimens with a test cross section of 1.5 by 5 mm are cut from four sheets of wood under different grain angles. 43 specimens for the compression tests are cut from five sheets. They have a nominal cross section of 6 by 5 up to 19 by 19 mm. The Young's modulus is determined separately for tension and compression. It is determined only from the samples with an angle of  $0^\circ$ , so axial orientation. All

samples are conditioned at  $103\pm 2^\circ\text{C}$  until constant weight. The relative moisture constant is not measured.

All tests are performed on an Instron TT-C testing machine with strain-gauged load cells under displacement control. For the determination of Young's moduli an Instron G/51-11 extensometer is used. The authors state that "mechanical properties of wood can usually be related to [their] density by equations of the form" [17, p. 228]

$$P_\rho = K * \rho^n \quad (3)$$

Using the method of least squares for the curve fitting, the resulting correlations for Young's moduli for tension and compression are [17, p. 229]

$$E_{A,ten} = 1000 * 5.17 * \left(\frac{\rho}{170}\right)^{1.5} \quad (4.1)$$

$$E_{A,com} = 1000 * 3.77 * \left(\frac{\rho}{170}\right)^{1.5} \quad (4.2)$$

with  $[E_A]=\text{MPa}$  and  $[\rho]=\text{kg/m}^3$ . The data points are still extracted from the diagrams [17, p. 229] and can be found in appendix A Table A-9.

#### Wood Handbook – Forest Products Laboratory – 2010

The Wood Handbook is one of the reference sources when it comes to the use of wood as an engineering or building material [9]. It deals with all usual commercially used types of wood. The Young's moduli in chapter five are derived from static bending tests. They include a 10% value correction concerning an effect of shear deflection [9, pp. 5-1 ff.]. Young's moduli for the radial and tangential directions and shear moduli are then calculated with the use of elastic ratios. For none of the tests any standard is referenced. Furthermore, the Poisson's ratios are experimentally determined. All the tests are performed on pure, straight grained balsa wood. The number of specimens, the tests are performed on, is not exactly mentioned. All properties are averaged ones. The given values refer to specimens with a moisture content of 12%. They are given for only one density. They are listed in appendix A Table A-10.

#### Baltek Technical Data Sheet

The balsa panels used for the tests in this thesis are of the product series Baltek SB. Baltek delivers a technical data sheet (TDS) with several mechanical properties listed for each panel type, which are distinguished depending on their density. The TDS can be found in appendix B. The listed compressive Young's modulus in axial direction is determined according to ISO 844 [34], which applies to the determination of compression properties of rigid cellular plastics. The tensile Young's modulus in axial direction is determined according to ASTM C297 [35]. The shear modulus is

determined according to ASTM C273 [36]. No further information about the testing is given. The data can be found in appendix A Table A-11.

Furthermore the works of Borrega et al. [37], Malek and Gibson [16], Brøndsted and Toftegaard [38], Monti et al. [39], Branner and Berring [40], Widagdo et al. [41], Caprino and Langella [42], Grenestedt and Bekisli [43] and Shishkina et al. [44] are reviewed, but found to be not relevant for the determination of balsa mechanical properties. This is due to the use of other core materials, no performance of own experiments or other significant reasons.

## **2.1.2 Discussion of literature values, methods and influences**

In this chapter, the discussion of the literature results displayed in the previous chapter is performed in two steps. The first step is to review the general plausibility of the single sources. The choice of testing methods, test performance, calculations and assumptions in the preparation and evaluation of the tests are assessed. It should be mentioned again that balsa wood is a naturally grown material. This leads to strong scattering of its mechanical properties. The second step is the discussion of the most accurate fitting method to describe the dependence of the respective mechanical property on the density with a mathematical function. In the literature there are different approaches for the most accurate description. The fitting is only performed for sources with data for more than one density. The other single data points potentially support the assumptions of the other sources. Therefore, they are also further displayed and discussed.

### **2.1.2.1 Methodology and plausibility of literature sources**

Before presenting all results for Young's and shear moduli in the Figures 11, 13 to 16 and 20, it is necessary to sort the results of some sources. This makes them presentable in a uniform way and enables the further work with them. The sources that only deliver a function are represented by this function. All other sources are represented by the derived data points from the diagrams.

In most of the sources, the Young's moduli are derived from compression tests. In some cases, they are referred to a standard. In other cases, they are individually planned. As outlined before, Newaz et al. describe in their paper that they perform compression and tension tests for all principal directions of the balsa. They derive deviating Young's moduli dependent on the load direction [23, pp. 208 ff.]. They conclude that balsa has bi-modulus behavior. Therefore, they state, that the Young's moduli for each principal direction can be calculated with the results for compression and tension. To do so, they use the equation of equivalent modulus, introduced by Yao and Ye [23, p. 211]. Looking up the pursuant paper [24], it must be noticed that the referenced equation cannot be found and nothing similar is mentioned in it. As the in Newaz et al. used, equivalent modulus is not transparent, only their results from compression tests are taken into consideration. This keeps all sources comparable to each other.

The same divergence between Young's moduli, derived from compression and from tension tests, can be found in the results of Soden and McLeish and on the Baltek TDS. This supports the correctness of the assumption that balsa has bi-modulus behavior, even though Soden and McLeish do not investigate this deviation. Furthermore, this assumption is not opposed by the other sources, as they do not perform tension tests at all. Nonetheless, for Soden and McLeish's paper and the Baltek TDS only the resulting values from the compression tests are considered, too.

The most literature data can be found for the Young's modulus in axial direction, displayed in Figure 11. Here it becomes obvious, that the data delivered by Kotlarewski et al. does not fit in with the rest of the data. As already explained, they perform their tests explicitly on Papua New Guinean balsa wood to compare it with South American balsa wood. This is suspected to be the main reason for the obvious deviation. Furthermore, they derive the Young's modulus from static bending tests, whereas all other sources use compression test. In general, static bending tests are qualified to determine the Young's modulus. But in this case the different test method could be another reason for the deviation. The authors themselves note that the literature data "cannot be directly compared with the results of [their] study because different standards [...] were used" [26, p. 86]. Last, they categorize the density classes of the balsa wood in wide ranges of 40 kg/m<sup>3</sup> which leads to less exact results. With these arguments the source is not considered for the further proceeding of the values.

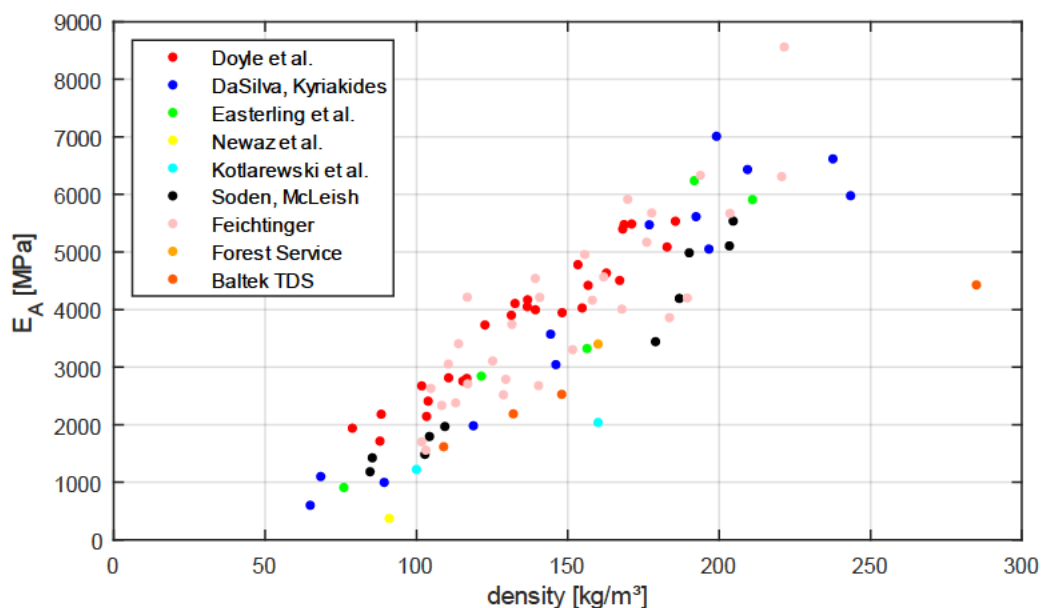


Figure 11: literature values Young's modulus axial compression

The given Young's modulus for Baltek SB150, with a density of 285 kg/m<sup>3</sup>, is much lower as it can be expected by the other literature values. Comparing the TDS' compression with the tension data confirms that the modulus is excessively low. The deviation between the compression and tension data for the lower densities is much lower than for the high density. This is also displayed in Figure 12, where linear regressions for the tension and compression data with and without the data point for Baltek SB150 are performed. That the linear regression is applicable, is

discussed at the end of this chapter. As there is no further information about testing and with these comparisons, the given data point is found to be probably erroneous. It is excluded from further consideration. The Baltek data set is reduced to three data points.

Also, the value from Newaz et al. is low and not within the expected range. There are no hints on an improper test setup or performance nor on evaluation. Thus, the data is further considered.

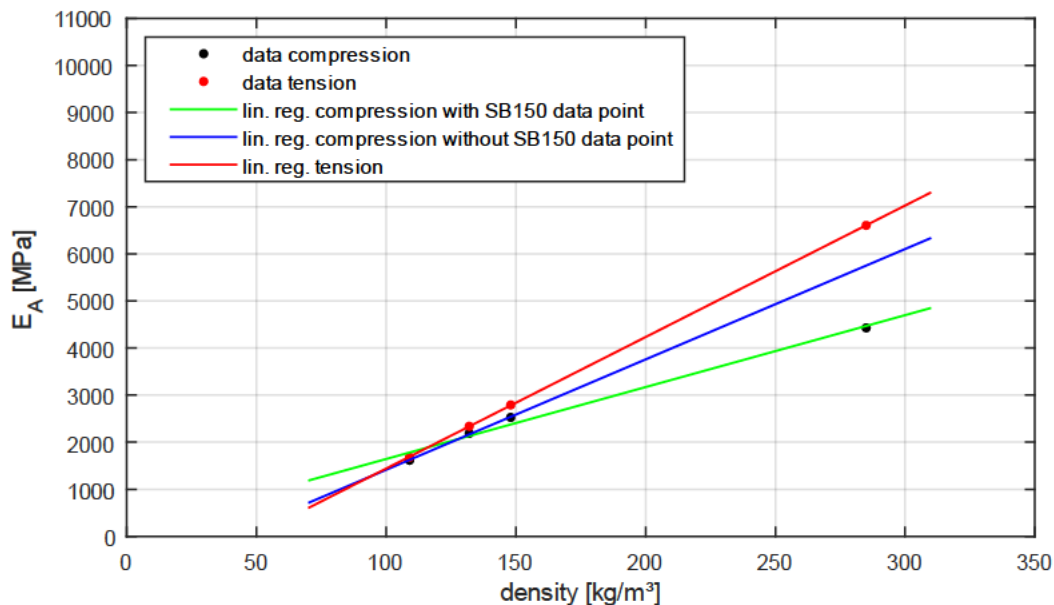


Figure 12: comparison axial Young's moduli from Baltek TDS

First thing to be noticed, when looking at the data for Young's moduli in radial and tangential direction is, that there are less sources and accordingly less data for these properties. The data is displayed in Figures 13 and 14. All in all, the data appears coherent. But again, the data of Newaz et al. needs to be discussed. It cannot be derived from their paper, if the given data applies to radial or tangential direction. Comparing it with the other data, it seems like theirs is the tangential Young's modulus. But as shown before, they derive significantly lower results from the compression tests. Thus, this criterion is not sufficient for the allocation of the results. A clear allocation of the data is not possible at this point. The data could also be a mixture of radial and tangential tests. Furthermore, only a single data point is present. Therefore, the data will be first considered when it comes to the combination of radial and tangential values for the calculation of balsa panel properties.

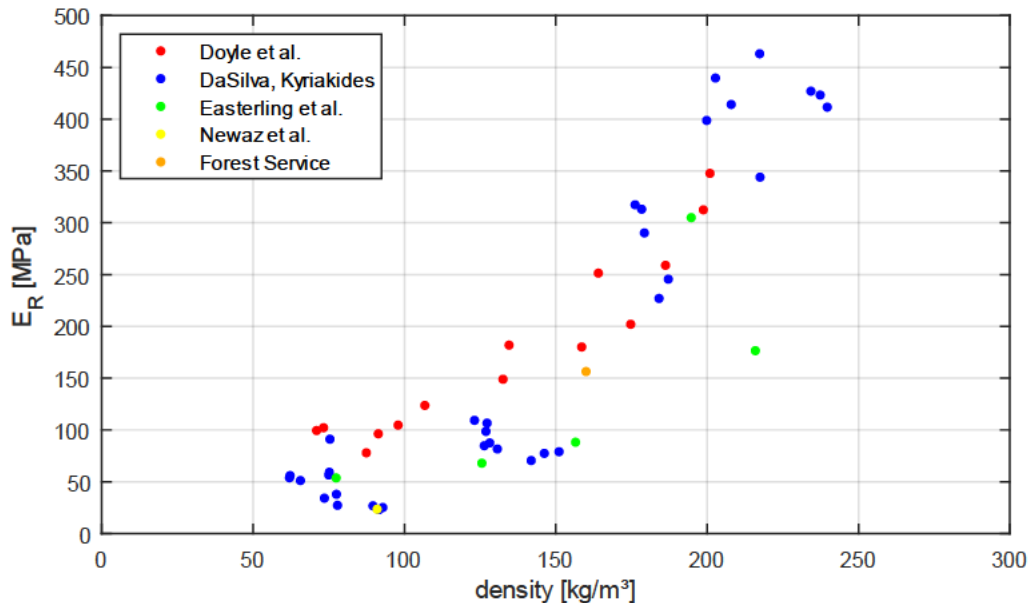


Figure 13: literature values radial Young's modulus from compression

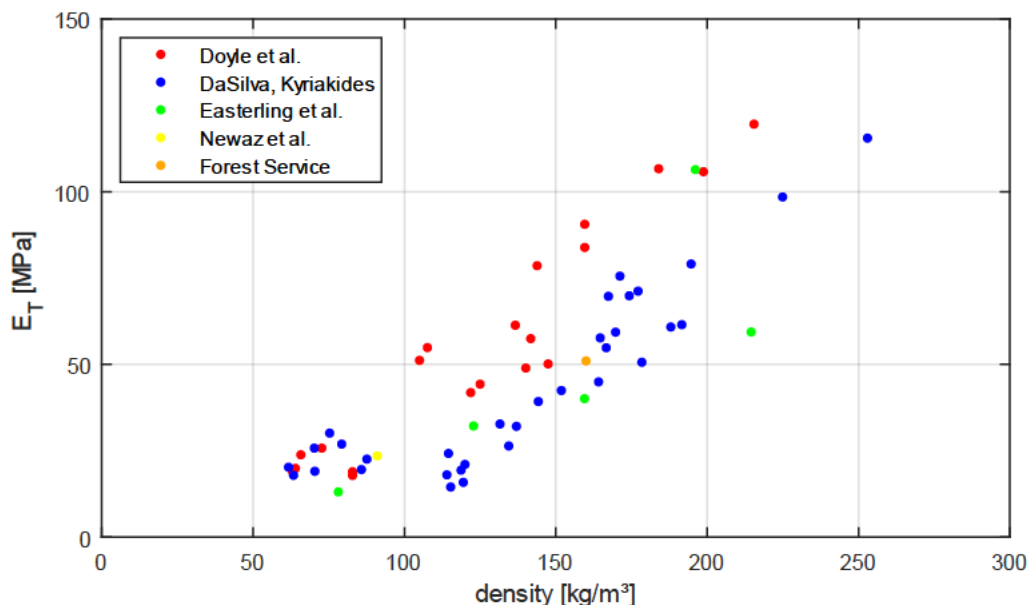


Figure 14: literature values tangential Young's modulus from compression

Looking at the shear modulus for the axial-radial and axial-tangential plane in Figures 15 and 16, the data of Osei-Antwi et al. stands out. First difference to the other sources is that they tested denser specimens of balsa wood. The authors cut their specimens from balsa panels of a high density class (Baltek SB150). In all other sources the specimens are cut from balsa directly from the trunk or from less dense balsa panels. The allocation of Osei-Antwi's et al. data to the shear modulus of the axial-radial or the axial-tangential plane is problematic because the tests are performed on specimens defined by their orientations to the grain. Their orientation is not associated with the principal directions. The test specimens are cut from balsa panels consisting of blocks of random orientation. This leads to the assumption, that the results come from a mixture of axial-radial and axial-tangential orientation. Furthermore, the data consists of two sets. One results from tests with the shear

plane parallel to end grain, which complies with axial-radial/tangential direction. The other one from tests with the shear plane parallel to flat grain, which complies with radial/tangential-axial orientation. As it can be seen in Figure 17, the results of the end grain test suggest a higher Young's modulus than the results of the tests parallel to flat grain. That is, what the authors state as well.

In theory, a shear load can be displayed as a combination of tension and compression forces acting under  $45^\circ$  as displayed in Figure 18. Compared with the sketched grain orientation of the specimens in Figure 18, it should not matter whether axial-radial/tangential or radial/tangential-axial orientation is tested. In both cases the grain is under the same load. This is also inherent in the determination that wood is an orthotropic material. In favor of this argument, it can be noticed that no other source differentiates between these orientations. This leads to the most important difference between Osei-Antwi et al. paper and the other sources. The authors derive the shear moduli from tests according to ASTM D5379 (Iosipescu) [20], whereas other authors rely on variations of lap shear tests. The general applicability of the Iosipescu shear test for the determination of the shear modulus of wood, is discussed in a paper of Yoshihara, Ohsaki, Kubojima and Ohta from 1999 [45]. To investigate the applicability of Iosipescu shear tests according to ASTM D5379 but with proportionally larger specimens, the authors compare the results with results obtained from a torsion test. The strains are measured with bonded triaxial strain gauges on each side in the middle of the specimen. It is shown that the results from axial-radial and radial-axial oriented specimens are similar and coincide with the torsion test results. They conclude that the Iosipescu method effectively measures the shear modulus. What is not discussed in the paper, is the problem of the uneven load distribution in the middle of the specimen as displayed in Figure 19. It could lead to different strain results depending on the placement of the strain gauges, as the shear in the middle is higher than the nominal shear and tends towards zero on the edges. Besides, there are several differences to the tests of Osei-Antwi et al. First, the mounting for the specimens and the measuring method are different. The used optical measurement of Osei-Antwi et al. inflicts measurement errors. There is an additional interaction with bending effects, because the tracked points cannot be located exactly in the middle axis [11, p. 233]. The most important difference can be found in the results. They are significantly different for axial-radial and radial-axial orientation, even though the results for the axial-radial orientation are strongly scattered. Because of these reasons and the associated uncertainties in the applicability of Osei-Antwi et al. results, their data will not be considered for the further calculations of the shear moduli.

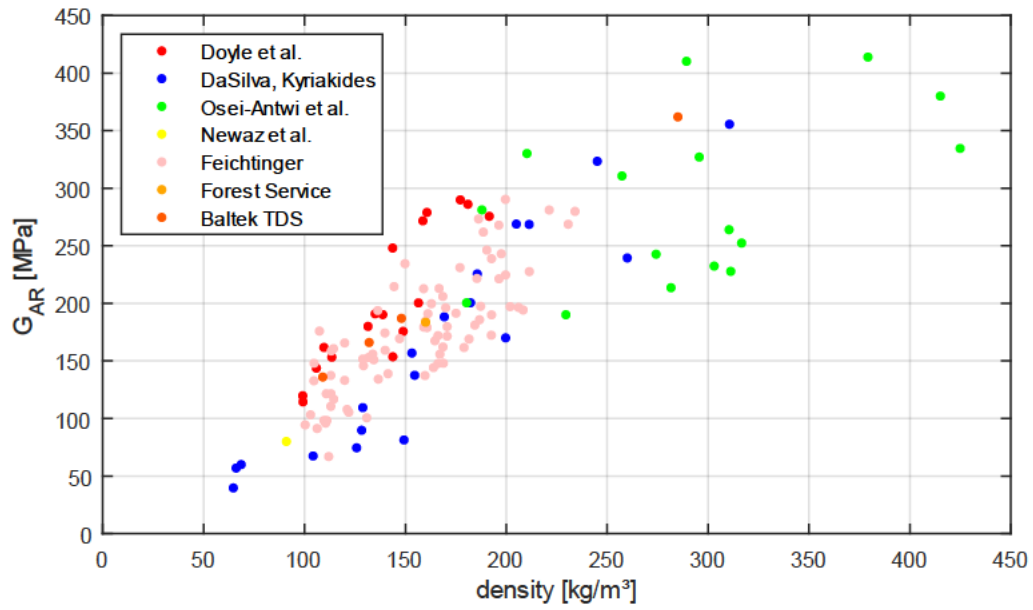


Figure 15: literature values shear modulus in axial-radial plane

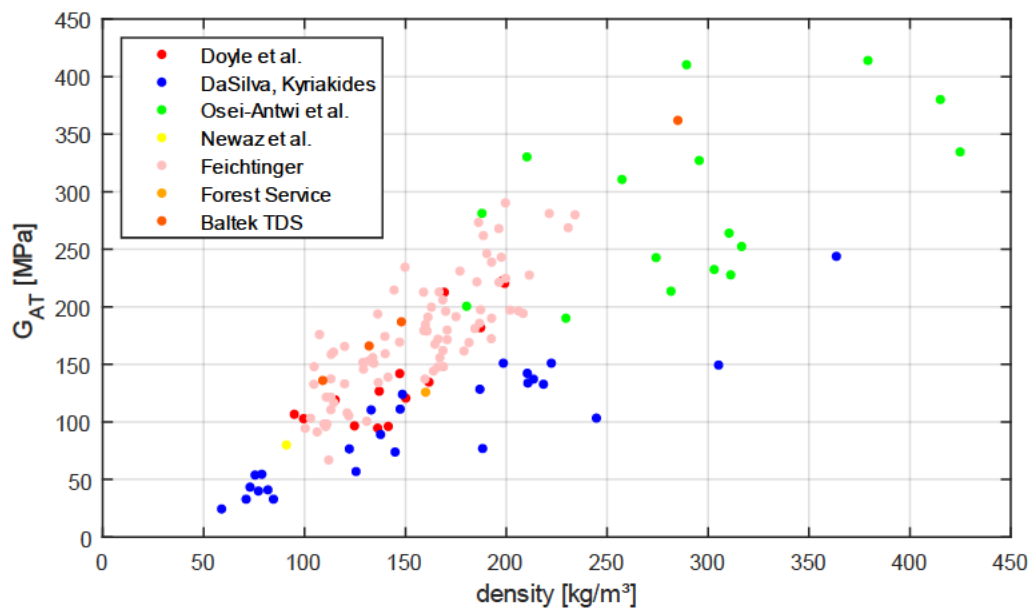


Figure 16: literature values shear modulus in axial-tangential plane



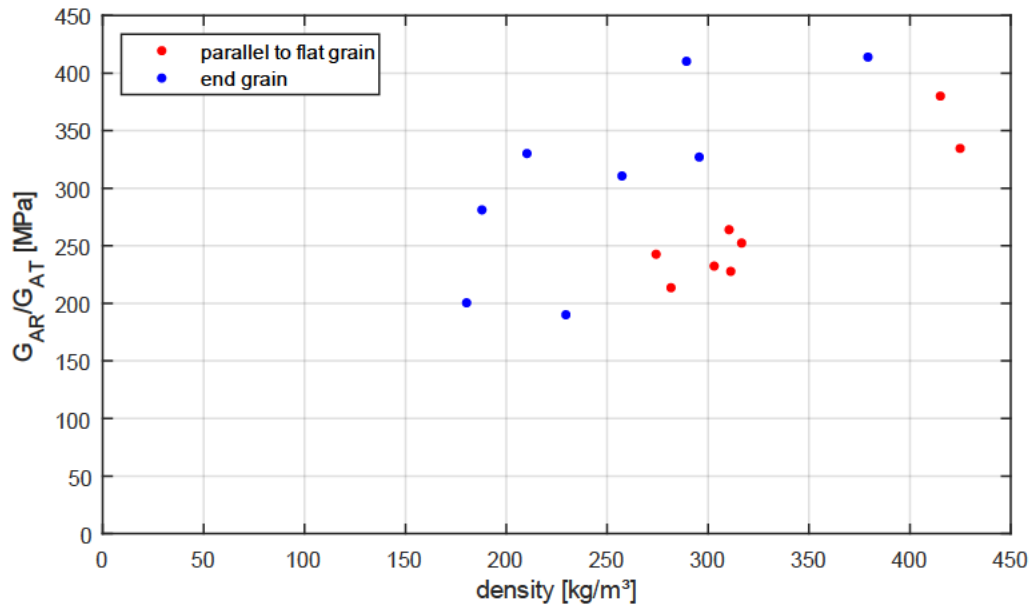


Figure 17: data sets Osei-Antwi et al. for shear moduli in axial-radial/axial-tangential plane

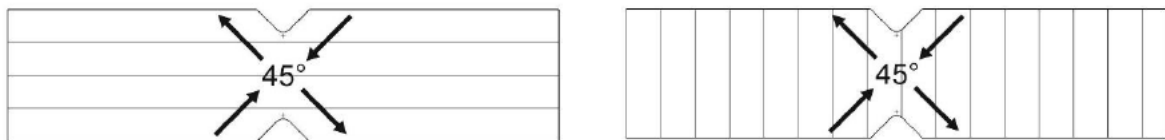


Figure 18: shear load in Iosipescu specimen with different grain orientation

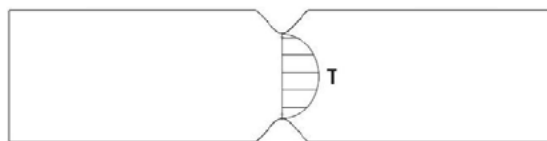


Figure 19: shear distribution in the notch of an Iosipescu specimen

Furthermore, it shall be mentioned again, that the data of Feichtinger for the shear moduli in axial-radial and axial-tangential plane is the same, because of the indistinguishable diagram data. The author delivers a function for the mixture occurring in balsa panels, too. For a better overview, the data is still displayed in both diagrams. Nonetheless, it will first be considered, when it comes to the final radial-tangential mixture for the model input value. The same applies to the Baltek TDS data. The data point of Newaz et al. is handled the same way, because a clear allocation of the data to the orientations is not possible.

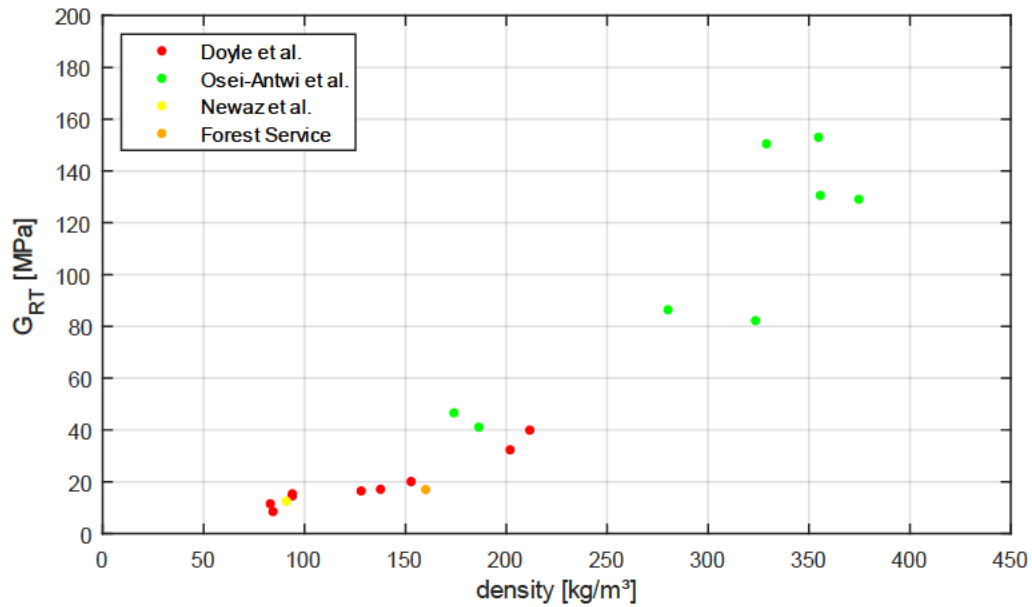


Figure 20: literature values shear modulus in radial-tangential plane

Figures 21 to 26 display the Poisson's ratios. Here, the first indication gives the load orientation and the second the reacting orientation that was measured. In general, the data set is less extensive than these for Young's moduli and shear moduli. For the axial load direction only three sources are available.

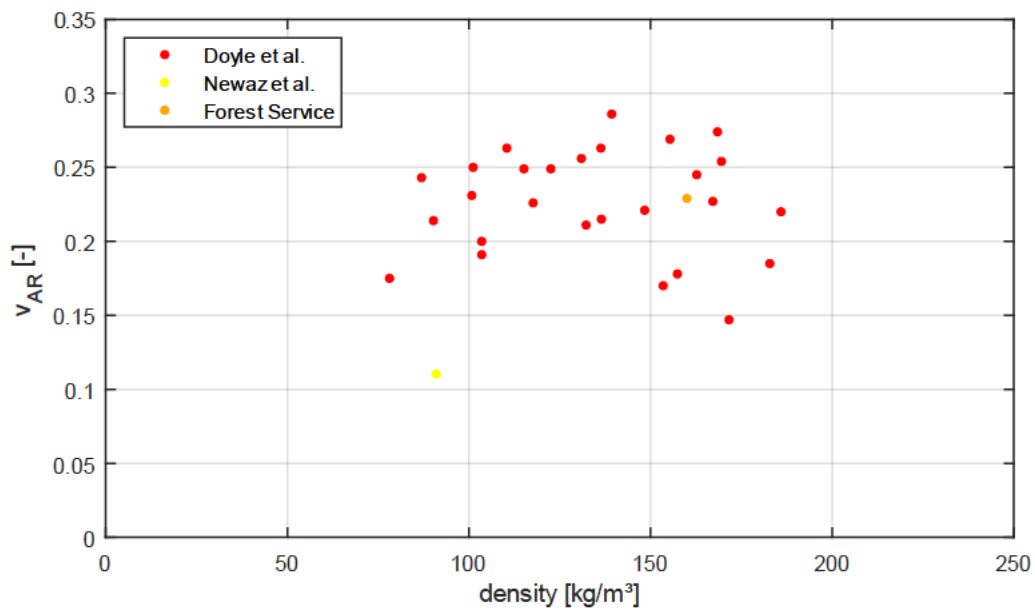


Figure 21: literature values axial-radial Poisson's ratio

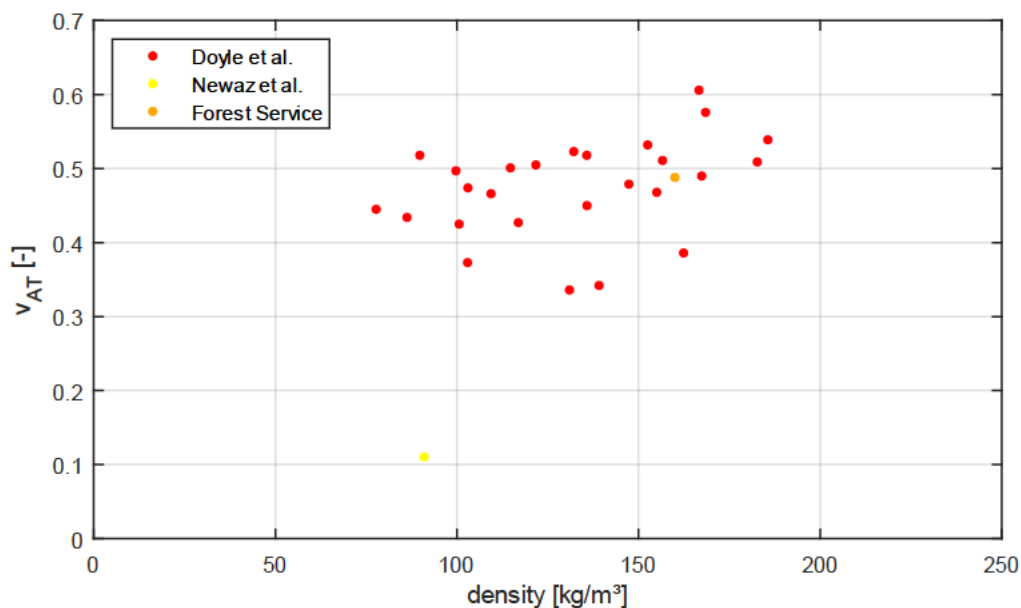


Figure 22: literature values axial-tangential Poisson's ratio

It can be noticed that the results from Newaz et al. are significantly lower than the rest. More important, they are the same for both orientations. Over all of their derived Poisson's ratios, there are three equal pairs of results. In their paper it is explained that the authors gain their Poisson's ratios from calculations based on an energy-preservation approach depending on the Young's moduli. The other sources derive their values from direct measurements of the strains. The first critical point in Newaz et al. theoretical approach is the fact, that it includes Young's moduli derived from compression and from tension tests. As outlined, the tension tests shall not be considered due to incomparability. The second critical point is that they do not distinguish between the radial and tangential orientation of their specimens. Thus, e.g. their axial-radial and axial-tangential results are the same. Meanwhile, the results from Doyle et al. and the Forest Service for the axial-tangential Poisson's ratio are approximately twice as high as for the axial-radial. The third critical point is the undiscussed use of the Maxwell-Betti Reciprocal Theorem [46, pp. 50–54]. It is a widely accepted, principally correct theory for the relations between Young's moduli and Poisson's ratios of an elastic material. However, its application for wood does not always meet with experimental results [9, p. 5-2]. This point shall only be mentioned, as the discussion about the applicability and potential constraints for it would exceed the scope of this thesis. For all of these reasons Newaz et al. results for the Poisson's ratios will not be taken into consideration for the further calculations within this thesis.

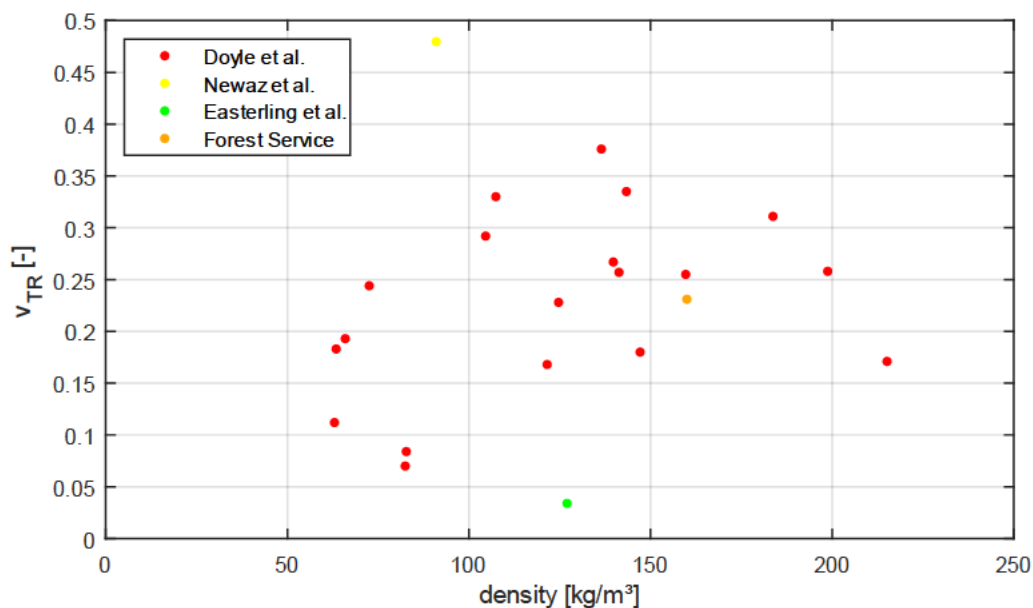


Figure 23: literature values tangential-radial Poisson's ratio

In the diagram for the tangential-radial Poisson's ratio in Figure 23, Easterling et al. result stands out, as it is much lower than the others. Looking at their results for the other directions in Figures 24 to 26, there is no such deviation noticeable. Even though the exact test setup for the measurement is not described in their paper, it is stated, that the Poisson's ratios are measured and not calculated. Furthermore, it is stated, that they result from compression tests. No potential systematic error can be found. The values are taken from Table 3 [13, p. 34] and are discussed at the end of chapter 5 [13, pp. 34–36]. There it is written that " $v_{TR}$  and  $v_{RT}$  [are] both roughly 0.5" [13, p. 36]. They are explicitly described to be higher than the other two values by a factor of more than 30. This leads to the conclusion, that there is a typing error in Table 3 and  $v_{TR}$  is meant to be 0.34 and not 0.034. This value would match with the results from the other sources. For this reason, the result is considered as 0.34. The other results from Easterling et al. remain.

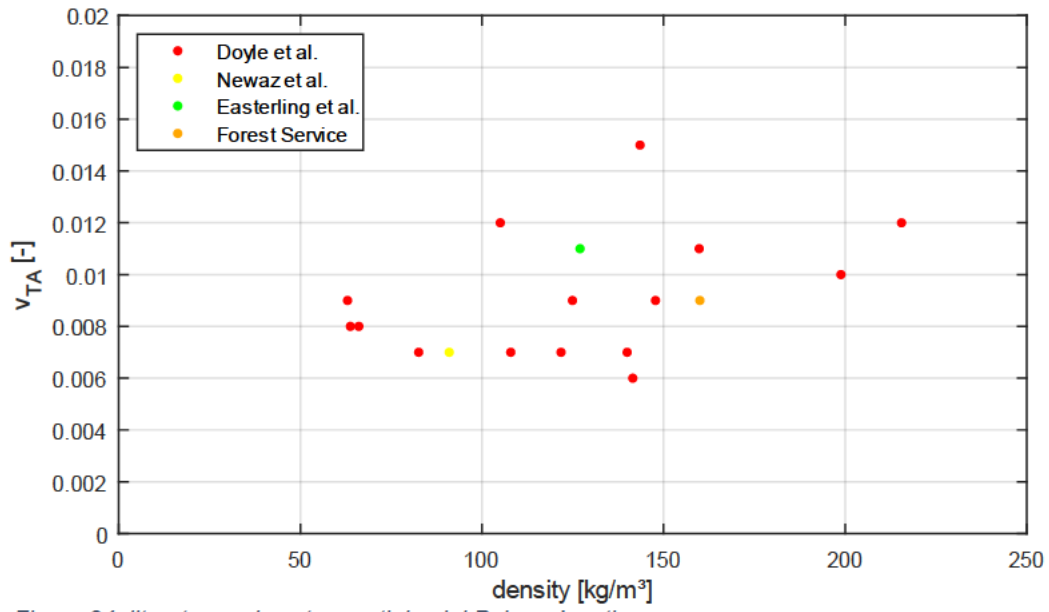


Figure 24: literature values tangential-axial Poisson's ratio

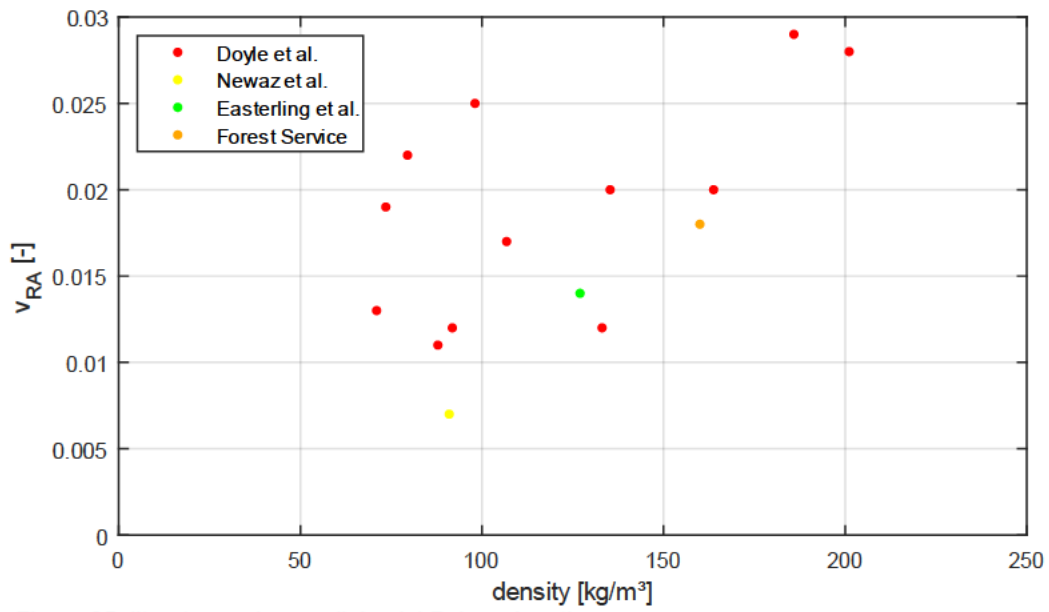


Figure 25: literature values radial-axial Poisson's ratio

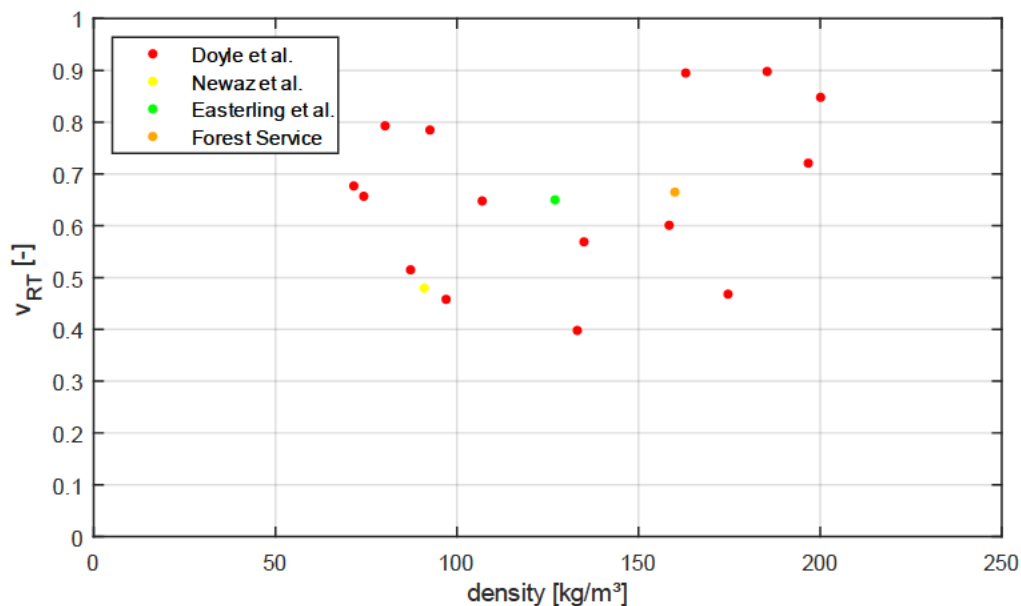


Figure 26: literature values radial-tangential Poisson's ratio

### 2.1.2.2 Influence of moisture content

Comparing the sources data regarding the moisture content of the balsa specimens, it must be noticed that it is handled with various accuracy. In some sources, for example in Doyle et al., the moisture content is listed for each density class [10, pp. 19 ff.] and measured on every specimen. In other sources, like Feichtinger [12], the moisture content is not noted at all. In some sources a common range is given, like in Da Silva et al., where a moisture content from 9 - 12%, [8, p. 8691] is noted. Overall, the available data is derived from balsa specimens with a moisture content of 8.97 - 13%, where it is noted. The moisture content influences the mechanical properties as well as the density of the balsa wood. Thus, the attempt to normalize the available data over the moisture content is made. It is performed on the example of axial Young's modulus because it has the most data available. To do so, the change of the mechanical property per percent moisture change shall be derived from the data. It shall then be compared with other literature data.

Sources with more than one data point and denoted moisture content are Doyle et al. [10], Da Silva and Kyriakides [8] and Soden and McLeish [17]. The measurement of the moisture content by Doyle et al. and Soden et al. is explained in detail. Doyle et al. condition the specimens in a standard climate. They weigh them before and after testing, average both values and measure the volume. Soden et al. oven-dry the specimens and measure weight reduction. In both cases the relative moisture content is noted. Da Silva et al. only note the moisture content as 9 - 12%, no further information is given. This leads to the mean moisture contents listed in Table 1.

source	moisture [%]
Doyle et al.	9.22
Da Silva et al.	10.5
Soden et al.	8.1

Table 1: mean moisture contents of balsa wood specimens of selected sources

Next, the functions for axial Young's modulus over density are derived by applying linear fittings to the data of each source. Why a linear fitting is appropriate, is discussed at the end of this chapter. The resulting functions with  $E_A$  in MPa and  $\rho$  in  $\text{kg/m}^3$  are

$$E_{A,Doyle} = 37.14 * \frac{10^6 m^2}{s^2} * \rho - 1240 MPa \quad (5.1)$$

$$E_{A,DaSilva} = 36.79 * \frac{10^6 m^2}{s^2} * \rho - 1794 MPa \quad (5.2)$$

$$E_{A,Soden} = 32.86 * \frac{10^6 m^2}{s^2} * \rho - 1655 MPa \quad (5.3)$$

The density of  $140 \text{ kg/m}^3$  is inserted in the equations to receive supporting points for a diagram, which displays Young's modulus over moisture content. It is displayed in Figure 27. There is also the range of the moisture content in each source displayed as a horizontal error bar.

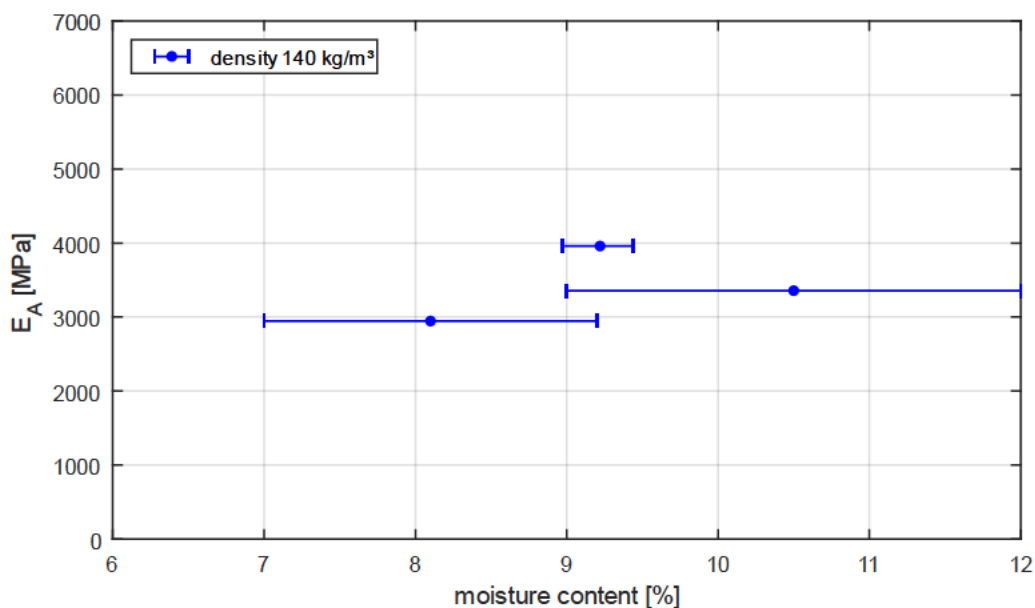


Figure 27: axial Young's modulus over moisture content for a specific density including moisture range

Most sources state a negative correlation between mechanical properties and increasing moisture content. For example, Soden et al. claim a “up to 6 per cent change in mechanical properties” [17, p. 230] per 1% moisture change for wood in general. Other sources assume a linear reduction of Young's modulus of wood in general in the relevant moisture content range of 9 - 13%, see Figures 28 and 29. In this linear correlated section, Báder et al. [47] state a mean reduction of about 4% per 1% moisture change [47, p. 1016]. From Neroth's [18] linear section, a mean reduction of about 2.5% [18, p. 840] is calculated. In Bhangu [48] the effect of moisture is investigated for balsa wood. From the data in Figure 5 [48, p. 5] a mean reduction of 1.25% is calculated for a moisture content change from dry to 20%. The author does not provide an own mathematical correlation. However, this reduction is in good agreement with Neroth's values. Here, the mean reduction from 0 - 20% is about 1.25% as well. Therefrom, a mean modulus change of 2.5% per 1%

moisture content increase is derived for balsa wood. It is at least valid in the defined relevant moisture content range. That this linear, negative influence of the moisture content on the mechanical property is not only applicable for axial Young's modulus, but for all Young's and shear moduli is suggested by the results of Keunecke et al. [49]. They carry out corresponding tests on yew and spruce [49, pp. 320–325]. Another factor to consider, when dealing with the moisture content of wood in general, can be an irrevocably alteration of its characteristics when oven-drying it [14, p. 2]. This alteration is also confirmed for balsa wood, if it is oven-dried after reaching relative moisture contents of up to 80% [48, p. 9]. During the manufacturing process of a FRP sandwich the balsa wood core is exposed to temperatures of 80°C. This is typically less than oven-drying temperatures e.g. listed in Figure 5-18 of the Wood Handbook [9, p. 5-38]. Whether there is still an alteration of the mechanical properties, exceeding the known alteration, caused by moisture content change during the process, is not quantified.

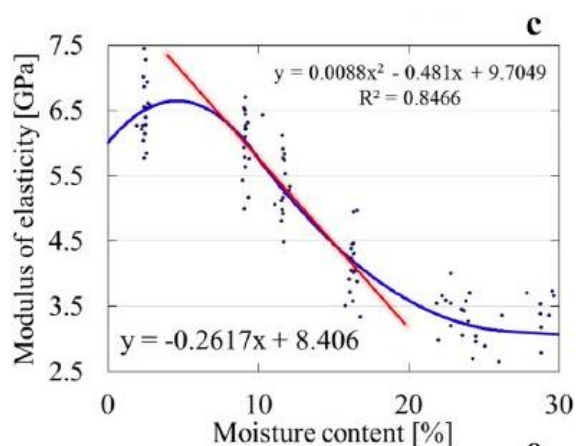


Figure 28: moisture diagram Bäder et al. [47, p. 1016]

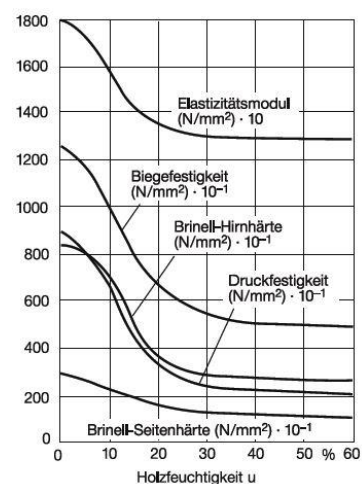


Figure 29: moisture diagram Neroth [18, p. 840]

However, none of these correlations corresponds with the calculated range of values, displayed in Figure 27. Thus, it does not seem expedient to normalize the available data from mixed sources by applying correctional functions derived from literature. Furthermore, there is no consensus in the literature about correctional values in general and no reliable sources for balsa wood in particular. Another uncertainty is the fact, that some sources only estimate the moisture content or do not denote it at all. According to the assumption derived from Bhangu and Neroth, the remaining moisture content range from 9 - 13% could result in a potential maximum 10% difference of the mechanical properties. Considering that the 13% only result from estimations in sources with a single provided data point, which have less influence on the evaluations, the impact of the moisture content deviations is potentially lower than 10%. Looking at the relatively high natural scattering of the data and the unquantified effects of temperature and drying of the balsa, the present moisture content range is considered to be neglectable for the scope of this thesis. This is also in the interest of keeping a larger database by considering the sources without any given moisture content to overall obtain more exact results. The available data is combined regardless of the moisture content. Though, the final results will be only applicable for balsa wood not significantly deviating from the given moisture content range from 9 - 13%.



### 2.1.2.3 Applicable fitting method

In the literature, there are different approaches for the fitting of the dependency of balsa wood's elastic properties on its density. The simplest fitting curve would be a linear one, for example suggested by Easterling et al. [13, pp. 38 ff], Doyle et al. in Figures 7 to 9 and 16 to 18 [10] and Da Silva and Kyriakides [8]. Kretschmann deals decisively with a more accurate approach by defining polynomic equations for the general description of Softwoods and Hardwoods in Table 5-11a [9, p. 5–29]. He specifies that these equations “are based on average values for the [different] species” [9, p. 5-26] and that they “do not accurately predict individual average species values” [9, p. 5–26]. He concludes that single species are better described by a linear analysis.

On the contrary, other authors suggest different kinds of non-linear fitting approaches. Already displayed are Feichtingers correlations that he derives from regression analysis. For the Young's modulus he finds a power function and for the shear modulus (axial-radial and axial-tangential mixed) an exponential function. The author does not describe his regression that leads to a “greater than [...] 99% confidence interval” [12, p. 342] in detail. But by the different and complex results from this regression, it is assumed that he performs a purely mathematical approach. Soden and McLeish base their potential correlation on a methodic approach. It states, that “the mechanical properties of wood [...] can usually be related to density by equations of the form  $P_\rho = K * \rho^n$  where  $n$  lies in the range 1.25 – 2.25” [17, p. 228]. The best fit for  $n$  is then calculated by the method of least squares.

Although more sources and more modern sources suggest a linear fitting, the linear fitting for the available data sets will be compared with non-linear fittings. Therefore, the coefficient of determination  $B$  is calculated. It is the square of the correlation coefficient  $r$  that is defined by

$$r = \frac{\sum_{i=1}^n x_i y_i - n \bar{x} \bar{y}}{\sqrt{(\sum_{i=1}^n x_i^2 - n \bar{x}^2)(\sum_{i=1}^n y_i^2 - n \bar{y}^2)}} \quad (6)$$

Here  $n$  is the number of data points and  $\bar{x}$  and  $\bar{y}$  are the respective arithmetic mean values [50, p. 90]. The correlation coefficient can have a value between -1 and +1 dependent on the quality of correlation. If  $r$  equals zero there is no correlation between the  $x$  and  $y$  values in the meaning of the chosen type of function (linear, power or else). Zero to  $\pm 0.5$  indicates a weak correlation.  $\pm 0.5$  to  $\pm 0.8$  indicates a medium correlation.  $\pm 0.8$  to  $\pm 1$  indicates a strong correlation. If  $r$  equals  $\pm 1$  there is a perfect functional correlation. This means that all points lie on the function curve without deviation. It is

$$B = r^2 \quad (7)$$

That means that  $B$  has values between 0 and 1. Again, the greater the value, the better is the correlation. This enables a quantification of the accuracy of the function types and a comparison between the different type.

To calculate the coefficient of determination for a linear, polynomial (grade 2), exponential and a power fitting for each mechanical property and each source, the software Matlab (The MathWorks Inc., Natick, Massachusetts, USA) is used. It offers various fitting calculations based on the function “fit”. All calculations operate with the method of least squares. This method identifies the minimum of the sum of the deviation-squares  $S$ , so the squares of the vertical difference between a given value and the regression function [51, p. 307].  $S$  is

$$S(a; b; c; \dots) = \sum_{i=1}^n [y_i - f(x_i)]^2 \quad (8)$$

dependent on  $a, b, c, \dots$  the parameters of the regression function. The Matlab function “fit” performs 400 iterations for the optimization of  $S$  and thus the curve fitting. It also delivers several statistical figures including  $B$ . The resulting coefficients of determination for the remaining sources with more than one value are displayed in Table 2. In the right column the mean value of the respective fitting for the different sources is given to make them comparable. The highest coefficient for each mechanical property is highlighted in green.

mechanical property	regression type	Doyle et al.	DaSilva, Kyriakides	Easterling et al.	Feichtinger	Soden, McLeish	Baltek TDS	mean (excl. Baltek)
$E_A$	lin.	0.9255	0.9110	0.9361	0.7511	0.9549	0.9982	0.8957
	pol.	0.9270	0.9177	0.9539	0.7548	0.9724	1.0000	0.9052
	exp.	0.8960	0.8201	0.8953	0.7529	0.9744	0.9891	0.8677
	pow.	0.9216	0.8931	0.9495	0.7539	0.9645	0.9962	0.8965
$E_R$	lin.	0.8885	0.8436	0.5741	-	-	-	0.7687
	pol.	0.9397	0.8968	0.5878	-	-	-	0.8081
	exp.	0.9372	0.8666	0.5667	-	-	-	0.7902
	pow.	0.9081	0.8927	0.5879	-	-	-	0.7962
$E_T$	lin.	0.8985	0.8002	0.6334	-	-	-	0.7774
	pol.	0.9104	0.8876	0.6345	-	-	-	0.8108
	exp.	0.8857	0.8661	0.5873	-	-	-	0.7797
	pow.	0.9107	0.8631	0.6245	-	-	-	0.7994
$G_{AR}$	lin.	0.8018	0.8753	-	0.6623	-	1.0000	0.7798
	pol.	0.8019	0.8758	-	0.6630	-	1.0000	0.7802
	exp.	0.7888	0.8094	-	0.6589	-	0.9944	0.7524
	pow.	0.8016	0.8745	-	0.6625	-	1.0000	0.7795
$G_{AT}$	lin.	0.7220	0.8402	-	0.6623	-	1.0000	0.7415
	pol.	0.8296	0.8419	-	0.6630	-	1.0000	0.7782
	exp.	0.7865	0.7778	-	0.6589	-	0.9944	0.7411
	pow.	0.7430	0.8402	-	0.6625	-	1.0000	0.7486
$G_{RT}$	lin.	0.9079	-	-	-	-	-	0.9079
	pol.	0.9587	-	-	-	-	-	0.9587
	exp.	0.9569	-	-	-	-	-	0.9569
	pow.	0.9255	-	-	-	-	-	0.9255

Table 2: coefficients of determination for fittings of literature mechanical properties

There are several observations to be made. The first is that all fittings lead to a high medium to strong correlation, which is also true for the mean values. As indicated,

the arithmetic mean values are calculated without the Baltek TDS values. This is because the data from Baltek leads to a coefficient of determination of 1 in many cases. This results from the low number of data points. It also gives rise to the assumption, that Baltek's data is already fitted. Including them in the mean values would lower values significance. Third point is that the values for  $G_{AR}$  and  $G_{AT}$  from Feichtinger and Baltek each are the same, because the data set is the same. That the values from Feichtinger are relatively low is caused by the large number of data points and thus more scattering. Also, the values from Easterling et al. for  $E_R$  and  $E_T$  are relatively low, which influences the mean values for these properties. This is caused by the low number of data points and one strongly deviating data point as it can be seen in Figures 10 and 11. Fourth point is that the polynomial fitting leads to the best coefficients of determination for all properties. The second-best option is varying with the property. Overall, it can be noticed that the differences between the respective coefficients are small. However, the coefficient of determination is a statistical value. A closer look on the indicated best fitting, the polynomial regression, is necessary to ensure that the results make sense regarding the mechanics of the balsa. In Figure 30 the data from Doyle et al. for the axial-tangential shear modulus is displayed in combination with the polynomial and the linear fitting curve. Here it becomes obvious that the linear fitting is much more sensible in the mechanical interpretation. The polynomial fitting would result in a modulus minimum at a density of about  $110 \text{ kg/m}^3$ , which is within the possible density range of balsa wood. Thus, with lower densities the shear modulus would become greater again. This is not physically reasonable and would contradict the trend observed in the literature. In addition, it can be stated that using other than the linear fittings leads to too large moduli for higher balsa wood densities. Furthermore, the differences between the coefficients of determination are small and most literature sources state a linear correlation. Therefore, it is assumed to be appropriate. All fittings are linear.

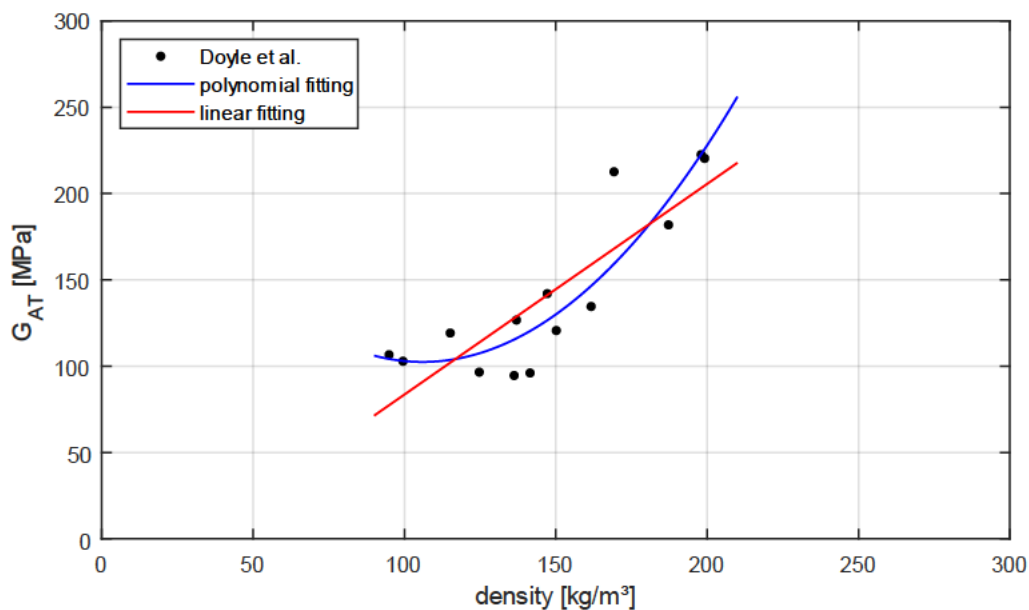


Figure 30: axial-tangential shear modulus from Doyle et al. with linear and polynomial fitting

The Poisson's ratios are assumed to be independent of the density. Thus, there is no fitting, but only a calculation of the arithmetic mean value for the determination.

### 2.1.3 Determination of universal literature values

In this chapter, universal literature values are derived from the discussed literature values. Currently the model offers the option to choose between the values from two literature sources. By determining universal literature values depending on more sources, a generally valid database is generated and can be implemented. The dependence on the correctness of the data of single sources, with their naturally caused scattering, is lowered. Besides, this thesis offers a basic data set of the mechanical properties of balsa for further research.

In general, for each Young's and shear modulus a linear fitting including all available data points from all sources is performed, resulting in a corresponding function. In the balsa panel the single orientations occur in combination with each other. To determine a function for each combination, e.g. for a combination of Young's modulus in radial and tangential direction, a similar number of data points within the relevant density range of 80 to 300 kg/m<sup>3</sup> is derived from the linear fitted functions. Then a new linear fitting is performed with this set of data points. Where it is necessary, the data from sources that already test mixed orientations or where no clear allocation is possible is added in this step. As mentioned, the Poisson's ratios are calculated from the available data with the arithmetic mean value.

Figure 31 shows all data points from all sources for Young's modulus in axial direction as black dots. The red line is the resulting linear regression. The resulting final function for Young's modulus in axial direction and thus in z-direction in the physically based model is

$$E_A(\rho) = E_{B,z}(\rho) = 36.6544 * \frac{10^6 m^2}{s^2} * \rho - 1579.2 MPa \quad (9)$$

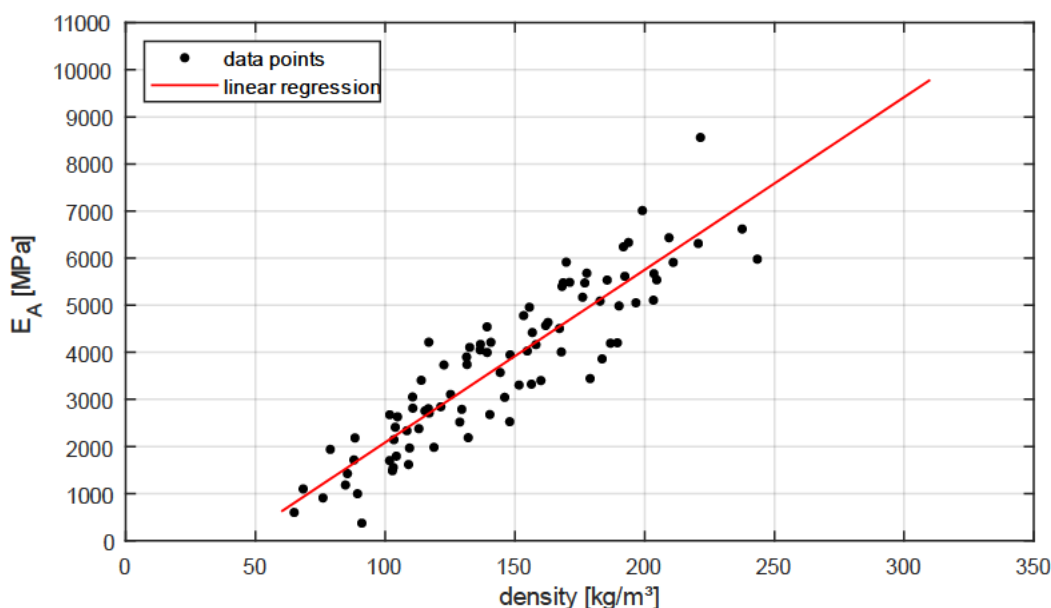


Figure 31: Young's modulus axial direction, linear regression

In the same way Young's moduli in radial (eq. 10) and tangential (eq. 11) direction are calculated, not yet including the data of Newaz et al.

$$E_R(\rho) = 2.2040 * \frac{10^6 m^2}{s^2} * \rho - 135.9354 MPa \quad (10)$$

$$E_T(\rho) = 0.5102 * \frac{10^6 m^2}{s^2} * \rho - 20.9717 MPa \quad (11)$$

The physically based model requires Young's modulus for a balsa panel in x- and y-direction as an input. It is assumed that the radial and tangential directions are randomly orientated in the panel, leading to an even 50-50 distribution of the properties. To determine this Young's modulus, the ones for radial and tangential direction are combined. This is done by performing a linear regression with six data points from the single fittings in the range from 80 to 300 kg/m<sup>3</sup>. Also, the data point from Newaz et al. is now included. This leads to

$$E_{B,x}(\rho) = E_{B,y}(\rho) = 1.3827 * \frac{10^6 m^2}{s^2} * \rho - 84.7810 MPa \quad (12)$$

The same procedure is applied for the calculation of the shear moduli. In the model one shear modulus each is required for the radial-axial and tangential-axial plane. The shear moduli in axial-radial (eq. 13) and axial-tangential (eq. 14) orientation derived from linear fittings of the literature data are

$$G_{AR}(\rho) = 1.2789 * \frac{10^6 m^2}{s^2} * \rho - 13.9288 MPa \quad (13)$$

$$G_{AT}(\rho) = 0.6374 * \frac{10^6 m^2}{s^2} * \rho + 14.0007 MPa \quad (14)$$

Again, these are combined with each other by performing a linear regression with six data points each leading to equation 15.1. Then they are compared and combined in the same way with the linear regression data of Feichtinger, Newaz et al. and Baltek TDS in equation 15.2. This equation already includes mixed orientations. Finally, this leads to equation 16.

$$G_{AR/AT,lin fit}(\rho) = 0.9581 * \frac{10^6 m^2}{s^2} * \rho + 0.0359 MPa \quad (15.1)$$

$$G_{AR/AT,direct}(\rho) = 1.2132 * \frac{10^6 m^2}{s^2} * \rho - 13.9306 MPa \quad (15.2)$$

$$G_{B,xz}(\rho) = G_{B,yz}(\rho) = 1.0856 * \frac{10^6 m^2}{s^2} * \rho - 6.9474 MPa \quad (16)$$

The shear modulus in radial-tangential plane is calculated as

$$G_{RT}(\rho) = G_{B,xy}(\rho) = G_{B,yx}(\rho) = 0.1846 * \frac{10^6 m^2}{s^2} * \rho - 5.4713 MPa \quad (17)$$

Poisson's ratios and standard deviations calculated with the arithmetic mean are displayed in Table 3.

	arithmetic mean	standard deviation absolute	standard deviation in %
$\nu_{AR}$	0.226	0.0343	15.1
$\nu_{AT}$	0.484	0.0792	16.4
$\nu_{TR}$	0.233	0.0825	35.5
$\nu_{TA}$	0.009	0.0023	24.6
$\nu_{RA}$	0.018	0.0056	30.4
$\nu_{RT}$	0.661	0.1463	22.1

Table 3: Poisson's ratios resulting from literature review

The assumption derived from the diagrams, that the standard deviation for some ratios is higher than for others is proofed. All deviations are higher than 10% up to a deviation of 35.5% for  $\nu_{TR}$ . The ideal relation between moduli of elasticity and Poisson's ratios for a homogeneous orthotropic material is [9, p. 5-2]

$$\frac{\nu_{ij}}{E_i} = \frac{\nu_{ji}}{E_j} \quad \text{with } i \neq j, \quad i, j = A, R, T \quad (18)$$

These relations are not exactly verified by the given arithmetic means, calculated with the derived Young's moduli for exemplary densities. As already mentioned in the Wood Handbook, these relations "are not always closely met" [9, p. 5-2] due to imprecise measurement because of very small displacements. Doyle et al. also suggest, to calculate the minor Poisson's ratios with the established equations [10, p. 4] but nonetheless measure them directly. Influences of specific gravity and moisture content are stated. Nonetheless, there is no noticeable correlation between the available Poisson's ratios data and the specific gravity in this thesis. What is confirmed, are the expectable relations of major and minor Poisson's ratios. Considering the high deviations, the derived values can be used within this thesis. The relevant Poisson's ratio for the calculation of the elastic properties of a sandwich is the in-plane ratio  $\nu_{B,xy} = \nu_{B,yx}$ . Considering the assumption of randomly orientated balsa blocks in the panels, it can be calculated with equation 19. This value is independent from the density. It replaces the value of 0.5, that is assumed in the existing model calculations. However, it can be noticed that the change of the value has only a small impact on the final results. It causes a change of about 0.001%.

$$\nu_{B,xy} = \nu_{B,yx} = \frac{\nu_{TR} + \nu_{RT}}{2} = \frac{0.233 + 0.661}{2} = 0.447 \quad (19)$$

During the work on this thesis, it was discussed to derive quantile functions with 90-10% or even 95-5% distribution of the values for the property equations. The purpose would be to ensure that the predictions performed on the basis of the derived functions are not too high. This is common practice in engineering models, especially for strength predictions. However, the existing physically based model's aim is to precisely predict the FRP sandwich mechanical properties as well as it was done with the mass prediction [5, p. 87]. It follows an academical approach in the first step. Starting the model based on already corrected and therefore lowered data would lead to a steady underestimation of the real properties and no precise prediction. Thus, a verification of predicted values with any kind of testing would not

be expedient but redundant. A safety correction of the data should happen in the last possible step before the physically based model predictions are used in a technical application. Otherwise, the influence of corrections could exponentiate and lead to an unusable model. Moreover the applicable standard for the design of wind turbine rotor blades DIN EN 61400-5 (VDE 0127-5) [52] stipulates that “structural models shall use mean values for material stiffness (modulus)” [52, ch. 6.6.1]. Safety factors are added afterwards. Following this argumentation and the applicable standard, the determined literature mean values for the mechanical properties are used without quantile corrections.

## 2.2 Theoretical background of experiments

The bending stiffness is considered to be one of the most critical stiffnesses with regard to the possible buckling failure modes of sandwich panels [5, p. 50]. In Otten’s Master’s Thesis it is decided to perform four-point bending tests because the constant bending load between the loading bars without an acting shear force “allows a simple calculative application of the bending line theory” [5, p. 50]. That a flexural test in form of a four-point bending test can be used for the determination of the bending stiffness as well as for the shear stiffness of a flat sandwich construction is also explained by Zenkert [53, pp. 337–340]. He refers to the ASTM C393 [6] as relevant standard, which is also chosen by Otten. Its advantages compared to other engineering standards for four-point bending, such as the DIN 53293 [54], are extensively discussed [5, pp. 50–52]. Furthermore, a test rig compliant with the ASTM C393 is already available at the IWES testing facility.

Following the bending line theory for a beam is explained. It is necessary for the evaluation of the tests. It is then compared with another measuring and evaluation method suggested by Zenkert. Furthermore, a third option to measure the bending stiffness based on strain is explained. A typical four-point bending setup according to ASTM C393 including the load distribution is displayed in Figure 32.

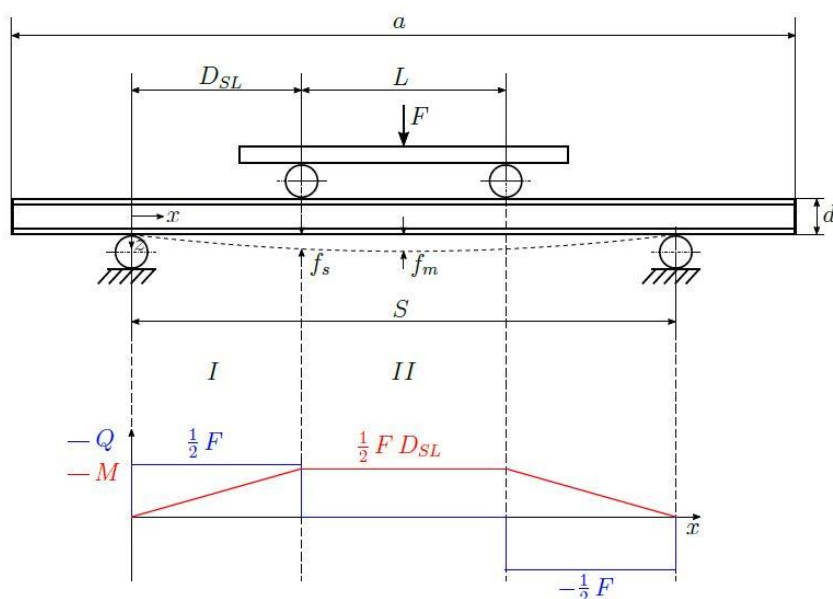


Figure 32: four-point bending test setup ASTM C393 incl. load distribution [5, p. 53]

## 2.2.1 Differential equation of the bending line

In previous four-point bending tests the evaluation of the bending line is based on the differential equation of the bending line for a Bernoulli beam. Conditions for the use of this beam theory are the Bernoulli assumptions. They state that the shear stiffness of the beam is very large. This means that a beam elements angle is not changed by shear force. The beam is shear rigid. All cross sections of the beam remain orthogonal to the bending line. Furthermore, it is assumed that the cross sections remain flat. With these assumptions the bending line theory is sufficiently precise and for sections without transverse force exact [55, p. 116]. This is the case between the loading bars.

However, the condition of a shear rigid beam is not applicable for a sandwich beam. The shear stiffness is relatively low and the shear deformation cannot be neglected [53, p. 57]. Thus, the Timoshenko beam theory is applicable for the description of the bending line of a sandwich beam [53, p. 51]. It models the overall deflection of the beam at a given point "as the sum of two independent deformations [...]. The bending deformation of the plate in absence of shear strain in the core [and] the additional deformation associated with shear strain in the core" [56, p. 128]. The fundamental differential equation of the bending line is [56, p. 130]

$$\frac{\partial^2 w}{\partial x^2} = \frac{\partial^2 w_b}{\partial x^2} + \frac{\partial^2 w_s}{\partial x^2} = -\frac{M_x}{D_x} + \nu_y \frac{M_y}{D_y} + \frac{1}{D_{Qx}} \frac{\partial Q_x}{\partial x} \quad (20)$$

Herein,  $x$  is the coordinate along the beam axis. In the case of four-point bending there is only the bending moment  $M_x$ . Thus,  $M_y$  equals zero and the corresponding summand can be neglected.  $w$  is the overall deflection.  $w_b$  and  $w_s$  are the partial deflections caused by bending and shear respectively.  $D_x$  is the bending stiffness,  $Q_x$  the transverse shear force normalized over the beam width and  $D_{Qx}$  the shear stiffness normalized over core thickness.

There are two sections with different acting moments and forces under four-point bending as displayed in Figure 32. The bending moments for sections I and II can be calculated as

$$M_I(x) = \frac{F}{2}x \quad \text{with} \quad 0 \leq x \leq D_{SL} \quad (21)$$

$$M_{II}(x) = \frac{F}{2}D_{SL} \quad \text{with} \quad D_{SL} \leq x \leq \frac{S}{2} \quad (22)$$

The transverse shear forces normalized over the beam width  $b$  for sections I and II can be calculated as

$$Q_I(x) = \frac{F}{2b} \quad \text{with} \quad 0 \leq x \leq D_{SL} \quad (23)$$

$$Q_{II}(x) = 0 \quad \text{with} \quad D_{SL} \leq x \leq \frac{S}{2} \quad (24)$$



Due to the symmetry of the bending line, the moments and the forces it is sufficient to only consider one half of the beam.

By inserting equations 21 and 22 in equation 20, the curvature based on bending can be sectionally calculated as

$$\frac{\partial^2 w_{b,I}}{\partial x^2} = -\frac{F}{2D_x} x \quad (25)$$

$$\frac{\partial^2 w_{b,II}}{\partial x^2} = -\frac{FD_{SL}}{2D_x} \quad (26)$$

Integrating equations 25 and 26 leads to the slopes based on bending

$$\frac{\partial w_{b,I}}{\partial x} = -\frac{F}{4D_x} x^2 + C_1 \quad (27)$$

$$\frac{\partial w_{b,II}}{\partial x} = -\frac{FD_{SL}}{2D_x} x + C_4 \quad (28)$$

Integrating equations 27 and 28 leads to the deflections based on bending

$$w_{b,I}(x) = -\frac{F}{12D_x} x^3 + C_1 x + C_2 \quad (29)$$

$$w_{b,II}(x) = -\frac{FD_{SL}}{4D_x} x^2 + C_4 x + C_5 \quad (30)$$

By inserting equations 23 and 24 in 20 the slopes based on shear can be calculated as

$$\frac{\partial w_{s,I}}{\partial x} = \frac{F}{2bD_{Qx}} \quad (31)$$

$$\frac{\partial w_{s,II}}{\partial x} = 0 \quad (32)$$

Integrating equations 31 and 32 leads to the deflections based on bending

$$w_{s,I}(x) = \frac{F}{2bD_{Qx}} x + C_3 \quad (33)$$

$$w_{s,II}(x) = C_6 \quad (34)$$

The remaining integration constants  $C_1$  to  $C_6$  are derived from six geometrical boundary conditions. At the first bearing there can be no deflection. This means

$$w_{b,I}(x = 0) = 0 \quad (35)$$

$$w_{s,I}(x = 0) = 0 \quad (36)$$

Due to the symmetry of the test setup and the bending line, the slope in the middle of the beam must be zero. The bending line has an extremum. This means

$$\frac{\partial w_{b,II}}{\partial x} \left( x = \frac{S}{2} \right) = 0 \quad (37)$$

At the first loading bar, the deflection and slope, each calculated with the equations for sections I and II, must be the same. Obviously, there is a continuous transition between the sections. This means

$$w_I(x = D_{SL}) = w_{II}(x = D_{SL}) \quad (38)$$

$$w'_I(x = D_{SL}) = w'_{II}(x = D_{SL}) \quad (39)$$

By inserting the geometrical boundary conditions in equations 29, 30, 33 and 34, the integration constants in equations 40.1 to 40.6 can be calculated.

$$C_1 = \frac{FD_{SL}S - FD_{SL}^2}{4D_x} \quad (40.1)$$

$$C_2 = 0 \quad (40.2)$$

$$C_3 = 0 \quad (40.3)$$

$$C_4 = \frac{FD_{SL}S}{4D_x} \quad (40.4)$$

$$C_5 = -\frac{FD_{SL}^3}{12D_x} \quad (40.5)$$

$$C_6 = \frac{FD_{SL}}{2bD_{Qx}} \quad (40.6)$$

This finally leads to the deflection equations for the two beam sections

$$w_I(x) = w_{b,I}(x) + w_{s,I}(x) = -\frac{F}{12D_x}x^3 + \frac{FD_{SL}S - FD_{SL}^2}{4D_x}x + \frac{F}{2bD_{Qx}}x \quad (41)$$

$$w_{II}(x) = w_{b,II}(x) + w_{s,II}(x) = -\frac{FD_{SL}}{4D_x}x^2 + \frac{FD_{SL}S}{4D_x}x - \frac{FD_{SL}^3}{12D_x} + \frac{FD_{SL}}{2bD_{Qx}} \quad (42)$$

They form an equation system with the two unknowns  $D_x$  and  $D_{Qx}$ . If the deflection of two points on the bending line is known,  $D_x$  and  $D_{Qx}$  can be calculated from equations 41 and 42. From  $D_{Qx}$  the shear modulus  $G_{xz}$  of the beam can be calculated as in equation 43. Here,  $c$  the core thickness and  $t_1$  and  $t_2$  are the face thicknesses [56, p. 135].

$$G_{xz} = \frac{D_{Qx} * c}{\left( c + \frac{t_1 + t_2}{2} \right)^2} \quad (43)$$

## 2.2.2 Four-point bending evaluation approaches

Beside the application of the described bending line theory for the evaluation of a four-point bending test, the evaluation approach of Zenkert [53, p. 340] shall be evaluated. He measures the deflection with a dial gauge mounted in a rig as displayed in Figure 30.

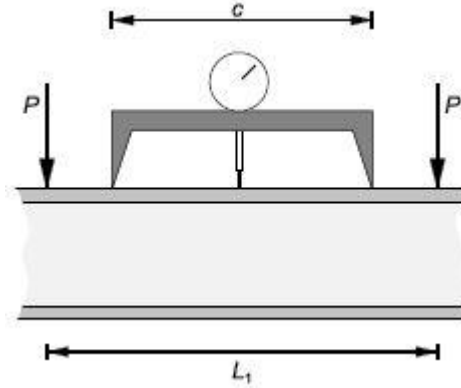


Figure 33: bending stiffness measurement with dial gauge by Zenkert [53, p. 340]

The corresponding determination equation is

$$w_Z = \frac{P * (L_2 - L_1) * c_Z^2}{16D} \quad (44)$$

The index  $Z$  distinguishes Zenkert's  $w$  and  $c$  from the one of this thesis. The single designations need to be transferred to this thesis' labelling system. This leads to

$$D = D_x \quad (45.1)$$

$$P = \frac{F}{2} \quad (45.2)$$

$$L_2 - L_1 = 2D_{SL} \quad (45.3)$$

The distance  $c$  is set to be the distance between the loading bars (eq. 46). Therefore, the deflection  $w$  can be calculated as the difference between the deflection in the middle of the beam and the deflection at the loading bar position (eq. 47). It can then be transformed.

$$c_Z = L = S - 2D_{SL} \quad (46)$$

$$\begin{aligned} w_Z &= w_{b,II} \left( x = \frac{S}{2} \right) - w_{b,II} (x = D_{SL}) \\ &= \left( -\frac{FD_{SL}S^2}{16D_x} + \frac{FD_{SL}S^2}{8D_x} - \frac{FD_{SL}^3}{12D_x} \right) - \left( -\frac{FD_{SL}^3}{4D_x} + \frac{FD_{SL}^2S}{4D_x} - \frac{FD_{SL}^3}{12D_x} \right) \\ &= \frac{FD_{SL}(S^2 - 4D_{SL}S + 4D_{SL}^2)}{16D_x} \end{aligned} \quad (47)$$

Inserting equations 45.1 to 45.3 and the result of equation 47 into equation 44 leads to

$$\frac{\frac{F}{2} 2D_{SL}(S - 2D_{SL})^2}{16D_x} = \frac{FD_{SL}(S^2 - 4D_{SL}S + 4D_{SL}^2)}{16D_x} \quad (48)$$

$$\Rightarrow FD_{SL}(S^2 - 4D_{SL}S + 4D_{SL}^2) = FD_{SL}(S^2 - 4D_{SL}S + 4D_{SL}^2) \quad q. e. d.$$

This shows, that Zenkert's approach can be traced to the Bernoulli bending line theory. It equals the deflection resulting from pure bending in the Timoshenko beam theory. The use of this evaluation approach is correct for section II of the beam, as "the curvature derives only from the bending of the beam" [53, p. 340]. The deflection caused by shear is the same in the whole section. This can be seen in equation 42. Notwithstanding, the evaluation approach offers no possibility to calculate the shear stiffness or the shear modulus of the specimen.

### 2.2.3 Correlation between strain and bending moment in a beam

Another option to derive the bending stiffness from a four-point bending test is to measure the strain on the beam's surfaces. Under four-point bending the upper face of a beam is compressed, while the lower face is elongated. This leads to negative strain on the upper and positive strain on the lower side. This strain depends on the distance of the surface to the neutral fiber  $z$  as in equation 49 [57, p. 176]. It is again based on the Bernoulli assumptions and thus is only applicable for the section between the loading bars in four-point bending.

$$\varepsilon(x, z) = -\frac{\partial^2 w}{\partial x^2} * z \quad (49)$$

With the beam thickness  $t$  this leads to equation 50 for the beam surface.

$$\frac{\partial^2 w}{\partial x^2} = -\frac{2\varepsilon(x)}{t} = \frac{\partial \psi}{\partial x} \quad (50)$$

With equation 22 and equation 51 [57, p. 178] the bending stiffness of the beam can be calculated as in equation 52.

$$M_y = E * I_y * \frac{\partial \psi}{\partial x} = D_x * \frac{\partial \psi}{\partial x} \quad (51)$$

$$D_x = \frac{FD_{SL}t}{4\varepsilon(x)} \quad (52)$$

## 2.3 Simplified rule of mixture approach by Thomsen and Larsen

During the literature research on the elastic properties of balsa wood and its use as core material in sandwich panels, a paper written by Thomsen and Larsen can be found [58]. In their paper, the authors develop a simplified rule of mixture approach for the estimation of the elastic properties of a grid-scored polymer foam sandwich

core. This approach and its applicability for balsa sandwich cores shall be evaluated. It could offer a further improvement of the existing physically based model.

The approach “is based on a “homogenization” technique for the core material, such that equivalent orthotropic elastic plate properties are assumed corresponding to a first-order shear deformation plate theory” [58, p. 262]. It can be used to determine the cores Young’s and shear moduli in-plane and out-of-plane. It does not deliver sufficient results for the Poisson’s ratios. The main idea of the approach is to describe a specified representative volume element (RVE) of the grid-scored core by “assuming sections of the [element] to be springs in parallel and series” [58, p. 263]. It is visualized in Figure 34. This description depends on several assumptions. First a perfect bonding between the core material and the resin grid is assumed [58, p. 263]. Second, all Poisson’s ratios’ effects are neglected. Third “it is assumed that the uniformly applied stresses cause uniform strains in both resin and foam” [58, p. 267].

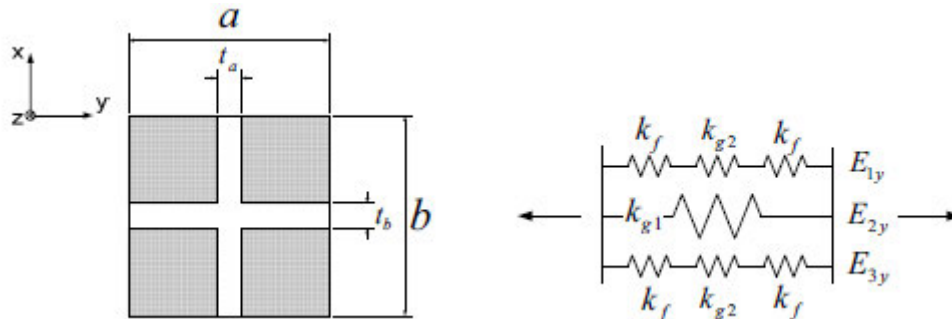


Figure 34: representative volume element described by combination of springs [58, p. 263]

The authors state, that the Young’s modulus in y-direction can be calculated with equation 53 [58, p. 264]. The index  $g$  indicates grid- and  $f$  foam-material. The index  $TL$  distinguishes Thomsen’s and Larsen’s symbols from the ones used in this Bachelor’s thesis.

$$E_{y,TL} = \frac{t_b}{b_{TL}} E_g + \left(1 - \frac{t_b}{b_{TL}}\right) \frac{E_g E_f}{\left(1 - \frac{t_a}{a_{TL}}\right) E_g + \frac{t_a}{a_{TL}} E_f} \quad (53)$$

The equation is derived from a volume-based mixture approached, which seems to be based on the spring analogy. This assumption and the mathematical correctness are evaluated in the following.

The spring constant for a linear spring can always be calculated with equation 54. Constants of springs in series are added by the summation of their reciprocals (eq. 55.1) and constants of parallel springs by direct summation (eq. 55.2).

$$k = \frac{E * A}{l_0} \quad (54)$$

$$\frac{1}{k_{all}} = \sum_{i=1}^n \frac{1}{k_i} \quad (55.1)$$

$$k_{all} = \sum_{i=1}^n k_i \quad (55.2)$$

Therefore, it is

$$k_f = \frac{E_f * A}{\frac{a_{TL} - t_a}{2}} = \frac{2 * E_f * A}{a_{TL} - t_a} \quad (56)$$

$$k_{g2} = \frac{E_g * A}{t_a} \quad (57)$$

With  $h$  for the thickness, the spring cross section  $A$  is

$$A = \frac{b_{TL} - t_b}{2} * h \quad (58)$$

According to equation 55.1 it is

$$\frac{1}{k_{1y}} = \frac{2}{k_f} + \frac{1}{k_{g2}} \quad (59)$$

With equation 56 and equation 57 this leads to

$$\frac{1}{k_{1y}} = \frac{2}{\frac{E_f * A}{\frac{a_{TL} - t_a}{2}}} + \frac{1}{\frac{E_g * A}{t_a}} = \frac{a_{TL} - t_a}{E_f * A} + \frac{t_a}{E_g * A} \quad (60)$$

Transformed to

$$k_{1y} = \frac{E_f * E_g * A}{E_g * (a - t_a) + E_f * t_a} = k_{3y} \quad (61)$$

As the middle part of the grid with the width  $t_b$  only consists of resin, it is

$$k_{2y} = \frac{E_g * A_g}{a_{TL}} \quad (62)$$

With

$$A_g = t_b * h \quad (63)$$

According to equation 55.2 it is

$$k_y = 2 * k_{1y} + k_{2y} \quad (64)$$

Furthermore, according to equation 54 it is

$$k_y = \frac{E_y * b_{TL} * h}{a_{TL}} \quad (65)$$

Inserting equations 61, 62 and 65 in 64 leads to

$$\begin{aligned} \frac{E_{y,TL} * b_{TL} * h}{a_{TL}} &= \frac{2 * E_f * E_g * A}{E_g * (a_{TL} - t_a) + E_f * t_a} + \frac{E_g * A_g}{a_{TL}} \\ \Rightarrow \frac{E_{y,TL} * b_{TL} * h}{a_{TL}} &= \frac{E_f * E_g * (b_{TL} - t_b) * h}{a_{TL} * \left[ E_g * \left( 1 - \frac{t_a}{a_{TL}} \right) + E_f * \frac{t_a}{a_{TL}} \right]} + \frac{E_g * t_b * h}{a_{TL}} \quad (66) \\ \Rightarrow E_{y,TL} &= \frac{E_f * E_g * \left( 1 - \frac{t_b}{b_{TL}} \right)}{E_g * \left( 1 - \frac{t_a}{a_{TL}} \right) + E_f * \frac{t_a}{a_{TL}}} + E_g * \frac{t_b}{b_{TL}} \quad q. e. d. \end{aligned}$$

Thus, equation 53 is mathematically based on the spring analogy. If the authors' predictions are precise, is not directly verified in their paper. The authors themselves do not perform corresponding tests, but evaluate their stiffness predictions with their own finite elements (FE) model [58, pp. 268–273].

To apply the approach for a balsa sandwich, core the spring analogy has to be adapted to another RVE. In a second step, it must be implemented in the physically based model. Its predictions can then be compared with the existing physically based model predictions and the experimental results. It is essential, to consider the differences between the structure of balsa and foam, mainly the vessel cells contained in the balsa. The following calculations are based on the RVE of Otten [5, p. 33], displayed in Figure 35. It contains one balsa panel block including the resin filled slits. In this RVE  $L_{RVE}$  is the length and  $W_{RVE}$  the width.  $s_x$  and  $s_y$  are the widths of the resin filled slits. The resin slits are placed on the outer side and not like a cross in the middle. However, the placement of the resin slits within the RVE is not relevant for the calculations.  $n$  is the number of vessel cells filled with resin in x- and  $m$  in y-direction.  $a$  is the width of the vessel cells. These are modelled as columns with a square base.  $b_x$  and  $b_y$  are the corresponding distances between the vessel cells. Not shown is  $t_{RVE}$ , it is the height of the RVE.

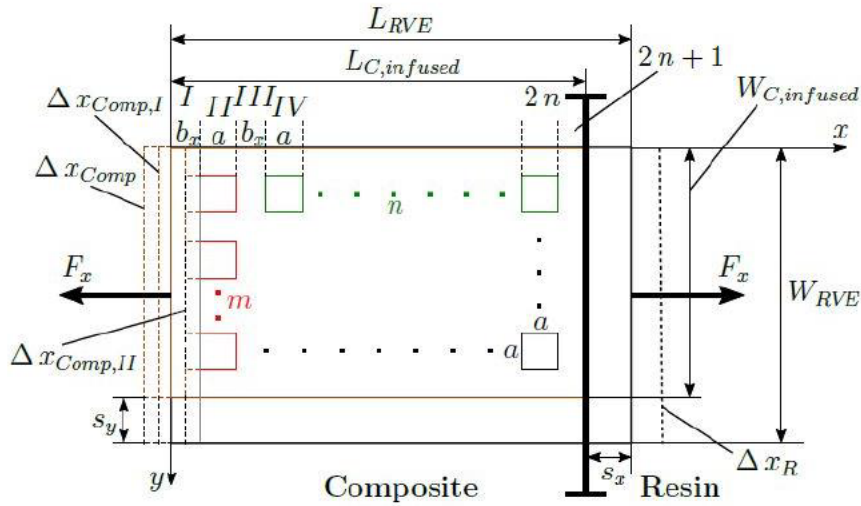


Figure 35: RVE Otten [5, p. 33]

The RVE can be described with spring constants, displayed in Figure 36.

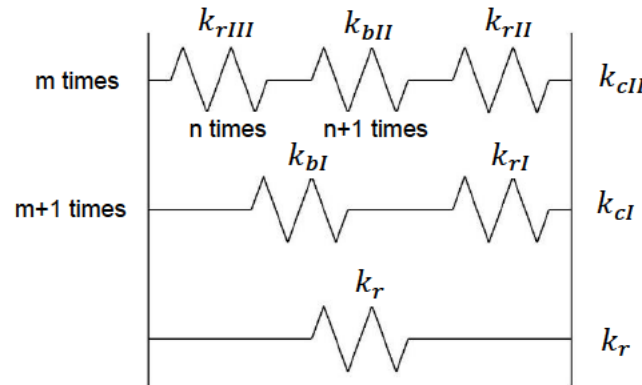


Figure 36: spring system RVE Otten

The single spring constants can be calculated with equation 54 as

$$k_r = \frac{E_r * s_y * t_{RVE}}{L_{RVE}} \tag{67}$$

$$k_{rI} = \frac{E_r * b_y * t_{RVE}}{s_x} \tag{68.1}$$

$$k_{rII} = \frac{E_r * a * t_{RVE}}{a} \tag{68.2}$$

$$k_{rIII} = \frac{E_r * a * t_{RVE}}{s_x} \tag{68.3}$$

$$k_{bI} = \frac{E_{B,x} * b_y * t_{RVE}}{L_{RVE} - s_x} \tag{68.4}$$

$$k_{bII} = \frac{E_{B,x} * a * t_{RVE}}{b_x} \tag{68.5}$$



$E_r$  is the resins Young's modulus.  $E_{B,x}$  is the balsa woods Young's modulus in x-direction. The single spring constants can then be added according to equations 55.1 and 55.2. This leads to

$$k_{cI} = \frac{k_{bI} * k_{rI}}{k_{bI} + k_{rI}} \quad (69)$$

$$k_{cII} = \frac{k_{rIII} * k_{bII} * k_{rII}}{k_{bII} * k_{rII} + (n + 1) * k_{rIII} * k_{rII} + n * k_{rIII} * k_{bII}} \quad (70)$$

Finally, the overall spring constant can be calculated as

$$k_x = k_r + (m + 1) * k_{cI} + m * k_{cII} \quad (71)$$

Therefrom the Young's modulus in x-direction is calculated as

$$E_{x,RVE} = \frac{k_x * L_{RVE}}{W_{RVE} * t_{RVE}} \quad (72)$$

Inserting equations 67 to 71 in 72 finally leads to

$$E_{x,RVE} = \frac{L_{RVE}}{W_{RVE}} * E_r * \left[ \frac{s_y}{L_{RVE}} + \frac{(m + 1)E_{B,x}b_y}{E_{B,x}s_x + E_r * (L_{RVE} - s_x)} + \frac{mE_{B,x}a}{E_{B,x}(s_x + na) + (n + 1)E_r b_x} \right] \quad (73)$$

The calculations of the Young's moduli in y- and in z-direction are performed analogously. In y-direction the perspective on the RVE is changed, which leads to corresponding changes in equation 73, resulting in equation 74. In z-direction all springs are parallel and can simply be totaled (eq. 75). This leads to a summation via the volume fraction as performed by Otten [5, p. 37]. The resulting calculation for Young's modulus in z-direction can be found in equation 76.

$$E_{y,RVE} = \frac{W_{RVE}}{L_{RVE}} * E_r * \left[ \frac{s_x}{W_{RVE}} + \frac{(n + 1)E_{B,y}b_x}{E_{B,y}s_y + E_r * (W_{RVE} - s_y)} + \frac{nE_{B,y}a}{E_{B,y}(s_y + ma) + (m + 1)E_r b_y} \right] \quad (74)$$

$$k_z = \frac{E_r W_{RVE} s_x}{t_{RVE}} + \frac{E_r s_y (L_{RVE} - s_x)}{t_{RVE}} + \frac{E_r a^2 mn}{t_{RVE}} + \frac{E_{B,z} [(W_{RVE} - s_y)(L_{RVE} - s_x) - a^2 mn]}{t_{RVE}} \quad (75)$$

$$E_{z,RVE} = \frac{k_z * t_{RVE}}{W_{RVE} * L_{RVE}} \quad (76)$$

$$= \frac{E_r [W_{RVE} s_x + s_y (L_{RVE} - s_x) + a^2 mn] + E_{B,z} [(W_{RVE} - s_y)(L_{RVE} - s_x) - a^2 mn]}{W_{RVE} * L_{RVE}}$$

Thomsen and Larsen continue with the calculations of the out-of-plane shear moduli. Although there is no physical correlation between the spring constant and the shear modulus as it is between the spring constant and the Young's modulus in equation 54, the same approach is used. That is possible because the original approach via the spring constants leads to volume fraction dependent mixture rules. These are also applicable for the shear moduli. This is proven in equations 54 to 66. Thus, the same equations can be used, simply replacing the Young's moduli with

the corresponding shear moduli of the balsa wood and the resin. The balsa woods shear moduli depend on its orientation. For the calculation of  $G_{xz,RVE}$  equation 73 is modified by replacing  $E_r$  with  $G_r$  and  $E_{B,x}$  with  $G_{B,xz}$ . Analogously, for the calculation of  $G_{yz,RVE}$ ,  $E_r$  is again replaced with  $G_r$  and  $E_{B,y}$  with  $G_{B,yz}$  in equation 74.

For the calculation of the in-plane shear stiffness  $G_{xy,RVE}$  the single spring constants are considered to not be parallel as for  $E_z$  but to be in series. Including the replacement of  $E_r$  with  $G_r$  and  $E_{B,z}$  with  $G_{B,xy}$  this leads to equation 77.

$$G_{xy,RVE} = \frac{G_r * G_{B,xy} * L_{RVE} * W_{RVE}}{[W_{RVE}s_x + s_y(L_{RVE} - s_x) + a^2mn]G_{B,xy} + [(L_{RVE} - s_x)(W_{RVE} - s_y) - a^2mn]G_r} \quad (77)$$

### 3 Experimental methods and procedures of four-point bending test

Following, the test setup, specimen preparation and test procedure for the four-point bending tests are described. The governing standard for the four-point bending test is the ASTM C393 [6]. Its use and the applied evaluation methods are prescribed by the research team at IWES, based on the given advantages outlined in chapter 2.2. The conditions derived from ASTM C393 are briefly summarized.

#### 3.1 Test Setup according to ASTM C393

The ASTM C393 [6] offers the option of a three-point or a four-point loading configuration, from which the four-point configuration is chosen. It is the non-standard configuration. The specimen shall be set on two support bars and is loaded with two loading bars on top of it. All bars shall cover the specimen's width. The support bars shall be fixed in place and the loading bars shall apply the force by vertical movement. The bars shall be 25 mm wide flat aluminum blocks with rubber pressure pads of the same width and a nominal thickness of 3 mm. The bars shall be designed to allow free rotation of the specimen at the loading and support points. The bars and the whole test rig shall have sufficient stiffness to avoid significant deflection under load.

Tests shall be performed on at least five specimens per condition. The chosen non-standard configuration of the specimen geometry shall fulfill the following conditions:

- the width shall be not less than twice the total sandwich thickness
- the width shall not be more than six times the total thickness
- the width shall not be less than three times the dimension of a core cell
- the width shall not be greater than one half of the span length
- the length shall be equal to the greater of the support span length plus 50mm or plus one half of the thickness
- the facing thickness shall be small relative to the core thickness, which is defined as the face thickness being approximately 10% or less of the core's thickness

#### 3.2 Testing machine and tools

The tests are performed on a hydraulic coupon test bench of the type inova FU250-1500 HM01 (INOVA Praha s.r.o., Prague, Czech Republic). It is capable of force and path controlled movement and of indicating the total force as required by ASTM C393 [6]. The test rig was built at the IWES and is constructed with aluminum profiles by item (item Industrietechnik GmbH, Solingen, Germany). The distance between the supporting and the loading bars can be adjusted by hand. The overall construction follows the standards of ASTM C393. The free rotation of all bars is enabled by bearing them in ball bearings, which are located on the rigs item profiles. The test rig installed in the machine can be seen in Figure 37.



Figure 37: four-point bending test rig according to ASTM C393

### 3.3 Preparation of specimens

The test specimens are cut from sandwich panels manufactured directly at IWES. They consist of a balsa wood core and biaxial glass fiber fabric face sheets. The used manufacturing technique is vacuum assisted resin transfer molding (VARTM). After the manufacturing, the panels are cut into single specimens. They are then prepared for the measuring of the bending line with the method of digital image correlation (DIC). The nominal width and length of the specimens shall be 80 mm times 551 mm. All specimens are considered to be beams.

#### 3.3.1 Infusion and manufacturing process of balsa core sandwich specimens

In the process of resin transfer molding “the reinforcement is first placed in the mold whereupon the liquid resin is infused into the reinforcement fabric through the difference in pressure” [53, p. 422]. In the vacuum assisted variant a one-sided mold is usually covered by a vacuum bag. This bag is sealed against the mold and then a vacuum is drawn under the bag. The liquid resin is then injected in the mold. In VARTM the “sole force driving the impregnation is vacuum drawn from under the vacuum bag” [53, p. 422]. The resin used is typically preformulated and the impregnation time can range from a few minutes to a few hours, as the resin is reacting slowly. The principle schematic of the VARTM is displayed in Figure 38.

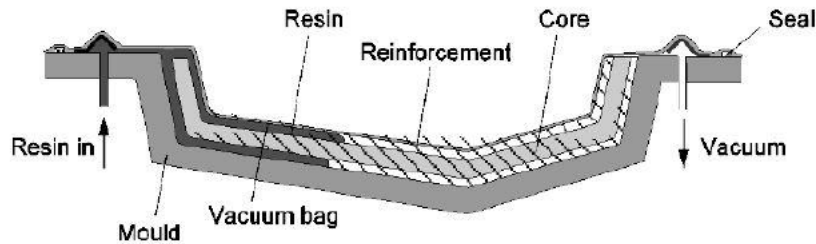


Figure 38: schematic vacuum assisted resin transfer moulding [53, p. 423]

For the four-point bending tests, plane specimens are manufactured. Thus, a plane sandwich plate is required. As the mold a special laminating table is used. It provides a plane surface and the option of heating it. A peel ply is placed on the table to enable the easy separation of the sandwich. Then the face sheet laminate is placed. The chosen layout is symmetric and starts with biaxial glass fiber fabrics. The balsa core is placed on it, with the support mesh directed to the table. The upper face sheet glass fiber fabric is placed mirrored. Another peel ply is applied, covered by a perforated foil and a green mesh working as flow aid. It assures the fast and uniform distribution of the resin over the panel. Also, it supports the airflow when evacuating the vacuum bag and thus air inclusions in the panel are prevented. To further support an even resin distribution, the resin is introduced via a spiral tube. It enables a linear resin front. A similar spiral tube, covered by a resin-tight hull, is also used to assist the evacuation of the vacuum bag. The vacuum bag is built with a vacuum foil sealed directly on the table. To ensure the continuity of the vacuum over the whole process, a second vacuum bag is built over the first one covering the sandwich. It is again sealed on the table and evacuated with the support of a spiral tube. The principle layout of the VARTM vacuum bag can be seen in Figure 39. Figure 40 is a photo taken during the evacuation of the two vacuum bags.

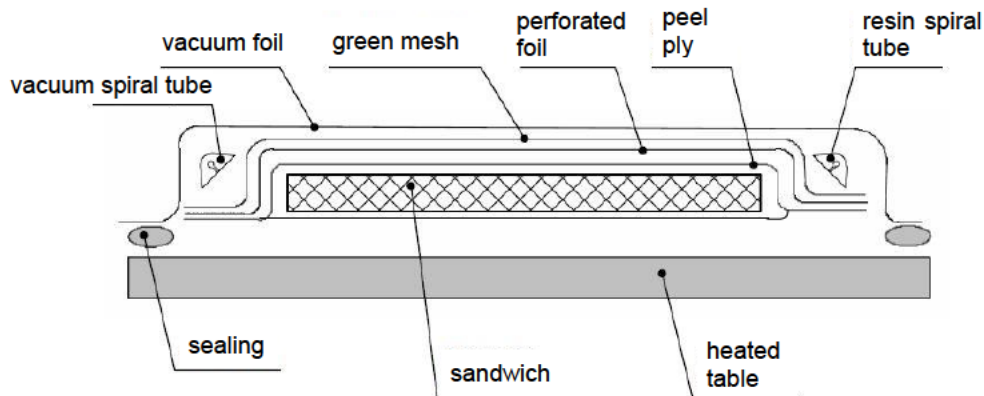


Figure 39: principle layout of sandwich manufacturing with VARTM [59, slide 57]



Figure 40: VARTM panel manufacturing with two vacuum bags

Two plates of different thickness are manufactured. Both have the same symmetrical layout. The difference between them is the thickness of the balsa core. One is manufactured with a core thickness of 12.7 mm (0.5 inch). The other one is manufactured with a core thickness of 25.4 mm (1 inch). Both balsa cores are of the type Baltek SB 100 with a nominal density of 148 kg/m<sup>3</sup>. Its TDS can be found in appendix B. Both cores are slit in the described way, resulting in a pattern with a block size of 50.8 mm times 25.4 mm. The laminates are made of biaxial E-glass fiber fabric of the type SAERTEX X-E-812g/m<sup>2</sup>-1270mm with a grammage of 812 g/m<sup>2</sup>. Its TDS can be found in appendix C. The laminate layer stacking sequence is

$$[(0^\circ|90^\circ)_2| \pm 45^\circ| \mp 45^\circ]$$

with the +45° orientation next to the core. This leads to eight unidirectional layers, two each contained in one biaxial fabric. It should be mentioned that the used fabric is more than three and a half years old at the time of use. It is not stored in enclosed wrapping. The chosen laminate stacking sequence and overall sandwich layout results from experience with former flexural beam tests and four-point bending fatigue tests.

The used resin is EPIKOTE Resin MGS RIMR 035c by Hexion (Hexion Inc., Columbus, Ohio) with the corresponding EPIKURE Curing Agent MGS RIMH 037 by the same manufacturer. The TDS can be found in Appendix D. The resin and curer are mixed with a mass proportion of 100:28 right before the infusion process. The mixture is then evacuated in a vacuum chamber to extract remaining air

enclosures. During the infusion process the table is heated to 40°C. After the infusion, the sandwich is left for curing on the heated table for 12h. Afterwards it is tempered at 80°C for at least 7h.

Finally, the specimens are cut from the two sandwich panels manually with a circular saw. Eight specimens per thickness are manufactured, which leads to a total sum 16 specimens.

### 3.3.2 Measuring Systems

To measure the exact deflection of the bending line of the beam specimens, the method of digital image correlation (DIC) is used. It offers the advantage that displacements and strains can be directly measured on the specimen. Thus, potential measuring inaccuracies occurring in indirect methods are prevented. For example, the ASTM C393 [6] explicitly mentions, that the use of crosshead or actuator displacement leads to inaccurate results.

“In classical image correlation the deformation of an object is determined by observation with a [charge-coupled device] CCD camera. Then a digital image correlation process determines the shift and/or rotation and distortion of little facet elements determined in the reference image. [...] For 3-dimensional measurement, two cameras are used. If the object is observed by two cameras from different directions, the position of each object point is focused on a specific pixel in the camera plane. If the positions of the two cameras relatively to each other, the magnifications of the lenses and all imaging parameters are known, the absolute 3-dimensional coordinates of any surface point in space can be calculated [...]. If this calculation is done for every point of the object surface, the 3D surface contour of the object can be determined in all areas, which are observed by both cameras. However, it is important, that the object surface shows enough structure to allow the algorithms to correlate identical points from both cameras” [60, p. 1].

Therefore, one side of each specimen is covered with white paint as primer. Then a black speckle pattern is applied with airbrush with a speckle size of about 0.8 mm. The size is governed by the distance of the cameras to the specimen. This distance is about 50 cm. The used DIC system is the Q400 from Dantec Dynamics (Dantec Dynamics GmbH, Ulm, Germany) operated with the ISTR4 4D software (version 4.4.6.160, Dantec Dynamics GmbH, Ulm, Germany). The used cameras are two Prosilica GT3300 (Allied Vision Technologies GmbH, Stadtroda, Germany) with a resolution of 8.1 megapixel. Due to the limited space around the test machine the cameras are positioned above each other, as it can be seen in Figure 41. Here, also the speckle pattern on a specimen can be seen. Before testing, the DIC system is calibrated with a calibration plate as described in the corresponding technical note [60, pp. 2 f]. Additional to the speckle pattern, thin crossmarks on the pattern support the identification of the middle point and the points beneath the loading bars. They are necessary for the subsequent evaluation with the DIC software.



Figure 41: four-point bending test setup with installed DIC system

In addition to the DIC measurement of the deflection of the bending line, the bending stiffness is determined by measuring the strains on the beams' surfaces during the test. This is done because it is the first use of the DIC system in a four-point bending test at IWES. The strain measurement method offers a second set of results from a well-established measuring method. It is performed on all thin specimens and six out of eight thick specimens.

Two Tokyo Measuring Instruments Lab. strain gauges of the type FLAB-10-350-11-3LQM-F are applied to the specimens upper and lower face sheet. They are placed exactly in the middle on the x- and y-symmetry axes to measure the strain in x-direction. The measuring grid size is 10mm, the resistance is  $350 \pm 1 \Omega$  and the gauge factor is 2.09. The bending stiffness can then be calculated with equation 52. The strain to be inserted in the equation is calculated by the upper and lower strain with equation 78. Due to the subtraction of the upper and lower strain, any strain influences by unintended normal forces are eliminated and pure bending strain remains [61, p. 43].

$$\varepsilon(x) = \frac{\varepsilon_l - \varepsilon_u}{2} \quad (78)$$

### 3.4 Test procedure

Before testing, each specimen's dimensions are measured with a caliper gauge. Only the length is measured with a metallic ruler. Each dimension is measured at three places in the test section. The specimens are openly stored in the testing facility, which is conditioned to  $23 \pm 2$  °C and  $50 \pm 5$  % relative humidity. Directly before testing, the specimens' relative moisture content is measured with the moisture measuring device Trotec T510 (Trotec GmbH, Heinsberg, Germany). The test rig is adjusted to a support distance of 440 mm with a loading bar distance of 82 mm. They were used in other tests before and are mandatory in the beginning.



The test specimen is placed on the support bars. The test rig is manually closed until the loading bars come nearly into contact with the specimen. Then the symmetrical alignment of the specimen in the test rig is checked by measuring the distances from the marked middle line on the specimen to the loading bars. If necessary, the specimen is realigned. The cables of the attached strain gauges are connected with the test computer. Then the test rig is manually closed until the loading bars rubber pads are in contact with the specimen. The machine control is changed from manual to automatically path controlled. According to ASTM C393 the speed for cross head displacement is set to the standard speed of 6 mm/min as the specimens will be tested in the elastic regime and no failure shall occur [6, p. 5]. The machine path and the strain gauge signals are set to zero. The strain measurement system is calibrated once, before performing all tests. Before every test the DIC image is reviewed to ensure that it is still sharp and the specimen and the cameras are still positioned correctly.

During the testing, the actuator path, the applied force, the surrounding temperature, and the strain data of both strain gauges over time are recorded with a rate of 10 Hz. The DIC system records the whole specimen surface in the relevant area with 4 Hz. A higher frequency is not possible because this would lead to limitations of the recordable area due to limited data storage. Displacements and strains of specific points and areas are evaluated in the post processing. Due to technical problems with the DIC software, it is not possible to directly connect the force signal from the test machine with the single DIC images. Thus, the recording on both systems is started at the same moment to enable a correlation over time. As the overall evaluations are based on time respectively strain differences in the linear regime, this method is sufficiently accurate. Contrary to past tests, the specimens are not loaded until failure. The thin specimens are loaded until a machine path of 10.5 mm and the thick specimens until a machine path of 7.1 mm. These values are found to be safely in the linear regime and also provide a sufficient data span.

### 3.5 Determination of bending stiffness and shear modulus

For each specimen, the bending stiffness and the shear modulus are determined with different approaches. In a first step, the linear regime in the data curves, caused by the linear-elastic behavior of the material, must be determined. Based on experiences of previous tensile tests according to DIN EN ISO 527-4 [62] the relevant linear regime for the evaluation is defined to be between 500 to 2500  $\mu\text{m}/\text{mm}$  strain. In this way the initial nonlinearity of the whole setup is excluded and the upper strain limit is within the linear regime of the sandwich. This fits well with the present data as can be seen in chapter 4.2. At a higher strain, the utilized glass fibers tend to show a nonlinear behavior and plastic deformation. For all calculations, the difference between the data points, which are defined by the strain boundaries, is used.

For the determination of the bending stiffness based on the DIC data, the deflection equations for the bending line 41 and 42 are used. The measured deflection of the middle point of the beam is inserted in equation 42, so  $\Delta w_{II}(x = \frac{S}{2})$ . The two measured deflections at the points on the bending line, which are centered beneath the loading bars, are first averaged. This is necessary, because the deflections tend

to be not exactly the same, which would be assumed by theory. The average is then inserted in equation 41, so  $\Delta w_I(x = D_{SL})$ . The resulting equation system with the two unknowns  $D_x$  and  $D_{Qx}$  is solved. Finally, the shear modulus is determined with equation 43. The different recording speeds of the test machine with 10 Hz and the DIC with 4 Hz make it necessary to perform linear interpolations of the DIC data, if the time point of the reached strain boundaries lies between to DIC frames.

The determination of the bending stiffness based on the strain gauge data is performed with equation 52, after averaging the strain of the upper and lower gauge with equation 78. The shear modulus can then be calculated with equation 79 [56, p. 135].

$$G_{xz} = \frac{Q_x}{\frac{\partial w_{s,II}(x = D_{SL})}{\partial x}} * \frac{c}{d^2} = \frac{\frac{\Delta F}{2b}}{\frac{\Delta w_{s,II}(x = D_{SL})}{D_{SL}}} * \frac{c}{\left(c + \frac{t_1 + t_2}{2}\right)^2} \quad (79)$$

The deflection beneath the loading bars caused by shear is calculated with equation 80 derived from equation 42.

$$\Delta w_{s,II}(x = D_{SL}) = \Delta w_{II}(x = D_{SL}) - \Delta w_{b,II}(x = D_{SL}) \quad (80)$$

The total deflection of the bending line beneath the loading bars  $\Delta w_{II}(x = D_{SL})$  in equation 80, is the same measured with the DIC, which is already used before. As outlined the use of the machine cross head displacement is not suitable.

### 3.6 Modified tests and other test configurations

During the test performance with the described setup, possible factors of uncertainty are discovered. In an attempt to counter them, the following modifications to the setup are done and another set of tests is performed. Main modification is to remove the 25 mm wide aluminum blocks with rubber pads prescribed by the standard. Instead, the load is then directly applied via the cylindrical bars. This is done to exclude the relatively soft rubber pads from the setup. The deflection in the middle of each specimen is additionally measured with a LVDT, placed central under the specimen in the test rig. Its head is adhered to the specimen's surface. Furthermore, the machine crosshead displacement is considered to equal the deflection at the loading bar positions in this case, because of the removed rubber pads. It shall be noticed that even without the rubber pads, thus a more punctual loading, no visible damage on the specimen occurred. Beside the LVDT measurement the bending stiffness is again measured via strain gauges.

The ASTM C393 [6], which the previous test configurations are based on, refers to the ASTM D7250 [63] as the standard practice for the determination of sandwich beam's flexural and shear stiffness. In the ASTM D7250 the performance of a four-point quarter-span and a four-point third-span loading configuration test is suggested to determine the flexural stiffness, shear rigidity and core shear modulus [63, p. 5]. Both configurations shall be performed as described in ASTM C393 on each specimen. Therefore, depending on the actual specimen sizes, the supporting distance is set to 450 mm. The resulting loading bar distances are 225 mm (quarter

span) and 150 mm (third span). For each configuration, the deflection in the middle of the beam is measured with a LVDT, placed central under the specimen. From the two measured force-deflection curves for each specimen the mentioned properties can be derived.

## 4 Experimental results

### 4.1 Specimen geometry

The measured dimensions of the specimens can be found in Table 4. Hereby is  $l$  the length,  $b$  the width,  $t$  the sandwich thickness and  $t_c$  the core thickness. All are measured as described in chapter 3.4. The mean face sheet thickness is 2.58 mm for the thin and 2.53 mm for the thick specimens. The mean core thickness is 12.00 mm respectively 24.78 mm. This leads to facing to core thickness ratios of 0.215 and 0.102. They are relevant for the calculations in ASTM C393 [6].

	No	$l$ [mm]	$b$ [mm]	$t$ [mm]	$t_c$ [mm]
thin	1	551.00	80.15	17.32	12.07
	2	550.80	79.93	17.23	12.02
	3	550.67	80.27	17.20	11.90
	4	550.70	80.33	17.16	11.91
	5	550.73	80.34	17.21	11.98
	6	550.80	80.17	17.11	11.89
	7	550.73	80.16	17.25	12.03
	8	550.77	80.26	17.12	12.20
	mean	550.78	80.20	17.20	12.00
	abs. stand. dev.	0.10	0.12	0.06	0.10
rel. stand. dev. [%]	0.02	0.15	0.38	0.81	
thick	9	551.17	80.56	30.01	25.03
	10	551.00	80.65	29.83	24.63
	11	551.00	80.31	29.87	24.92
	12	550.23	80.50	29.79	24.68
	13	551.00	80.82	29.88	24.92
	14	550.93	80.85	29.95	24.47
	15	551.00	81.05	29.90	24.73
	16	551.00	80.59	30.09	24.84
	mean	550.92	80.67	29.92	24.78
	abs. stand. dev.	0.27	0.22	0.09	0.17
rel. stand. dev. [%]	0.05	0.27	0.31	0.69	

Table 4: specimen geometries

### 4.2 Bending stiffness and shear modulus

In Figure 42, the strains measured with the upper and lower strain gauge are displayed over the applied force. This is done exemplarily for specimen nine. As mentioned in chapter 3.5, the strain over force curve is linear in the section from 500 to 2500  $\mu\text{m}/\text{mm}$ . This is the case for all specimens. Thus, the further results are based on this definition of linearity. The relative wood moisture content is approximately 6% in all specimens before each test.

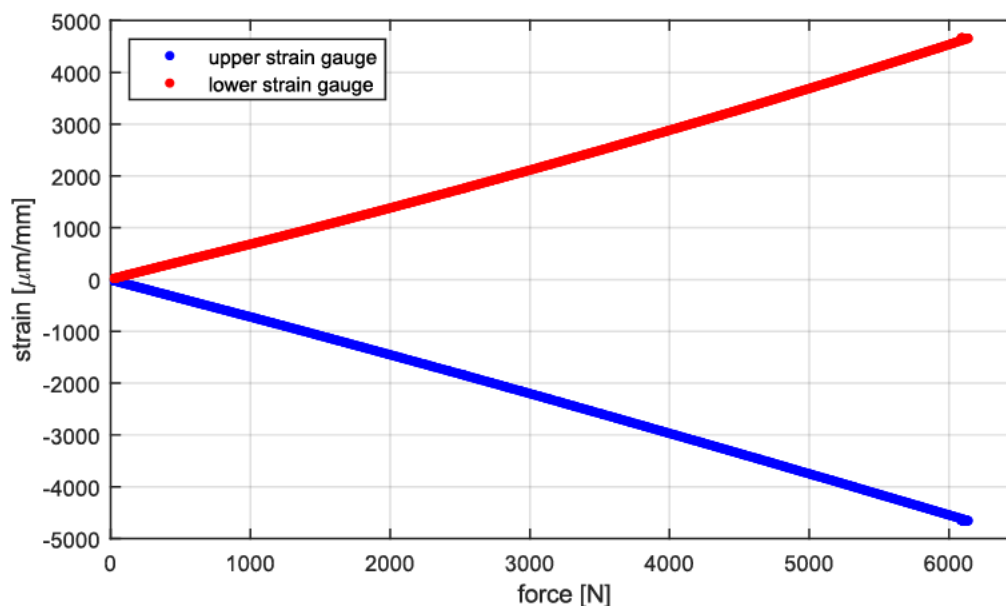


Figure 42: strain over force four-point bending, specimen 9

The results for the determined bending stiffness and shear modulus for each specimen can be found in Table 5. The results based on strain and on DIC measurement are compared for each specimen. No results are displayed for specimen number three, because it was not sufficiently aligned in the test rig at the time of testing. Therefore, it was damaged in a way that it is not possible to repeat the test. There is no strain data for specimens 13 and 14 as they are not prepared with strain gauges initially. The results based on strain data are all calculated with the averaged strains as in equation 78, except the results for specimen five. Its results are only based on the strain data of the upper strain gauge, as the lower one's data recording or transmission was disturbed during the test performance. Remarkable are the results for the shear modulus of the thin specimens. For specimen one, a negative shear modulus is determined which is physically impossible. The other extreme is the determined shear modulus of specimen five, which is much higher than the other moduli.

	No	bending stiffness [N/m <sup>2</sup> ]		shear modulus [Mpa]	
		strain	DIC	strain	DIC
thin	1	523.53	459.43	181.40	-741.61
	2	525.73	498.90	136.52	212.52
	3	-	-	-	-
	4	521.34	511.12	138.76	160.64
	5	529.71	484.27	182.18	1065.44
	6	515.71	467.68	157.53	787.77
	7	538.87	499.08	134.29	274.31
	8	533.93	503.18	179.22	383.34
thick	9	1843.68	1666.29	207.23	438.57
	10	1730.29	1576.05	208.29	427.83
	11	1793.29	1563.64	199.80	703.90
	12	1703.76	1623.73	163.34	205.77
	13	-	1602.49	-	443.06
	14	-	1601.58	-	409.86
	15	1745.10	1588.47	203.86	412.61
	16	1775.57	1602.34	182.40	355.35

Table 5: four-point bending results, based on strain and on DIC data

The mean values for the thin and thick specimens for each property can be found in Table 6. It also contains the absolute and relative standard deviation. Looking at the bending stiffness, it can be noticed that the standard deviation is less than 4% in all cases. The bending stiffness of the thick specimens is much higher than the one of the thin specimens, which is expected. There is a significant difference between the results based on strain and DIC, even though they are measured simultaneously. The bending stiffness calculated from strain is 7.65% higher for the thin specimens, respectively 10.12% higher for the thick.

The standard deviations of the shear moduli are higher than for the bending stiffnesses. Especially the relative standard deviation of 172.15% of the shear modulus of the thin specimens, derived from DIC data, is extraordinarily high. This results from the mentioned extreme values. Beside that, a high scattering of the shear moduli derived from DIC data can be observed in general. The relative standard deviation of 30.21% is the second highest in the data set.

		bending stiffness [N/m <sup>2</sup> ]		shear modulus [Mpa]	
		strain	DIC	strain	DIC
thin	mean	526.52	489.09	154.62	306.06
	standard deviation abs.	7.26	17.89	20.61	526.88
	standard deviation [%]	1.38	3.66	13.33	172.15
thick	mean	1765.28	1603.07	194.15	424.62
	standard deviation abs.	45.56	29.42	16.25	128.26
	standard deviation [%]	2.58	1.84	8.37	30.21

Table 6: mean values and standard deviations of four-point bending test results

The results of the modified test described in chapter 3.6 and other test configurations are not presented in detail because they do not deliver usable results. For example, the modified test setup with the same distances but without the aluminum blocks at the loading bars, leads to obviously wrong bending stiffnesses for the thick specimens. They are in the range of -45133 N/m<sup>2</sup> up to 17647 N/m<sup>2</sup> based on the LVDT measurement. The tests and evaluation according to ASTM D7250 [63] leads to results stating a dependence of the bending stiffness on applied load. With increasing load, the derived bending stiffness increases as well as. This effect is displayed in Figure 43 on the example of specimen nine. For the derived shear moduli, a dependence on the applied load can be observed, too. Here, the data curve shows the behavior of a fractional-rational function caused by the mathematics of the applied equations, displayed in Figure 44. A physical reason for this behavior is not possible. The used evaluation equations are prescribed by the standard. Thus, the measurement is assumed to be incorrect. The strain-based measurement of the bending stiffnesses is in the range of ±10% of the original strain-based values.

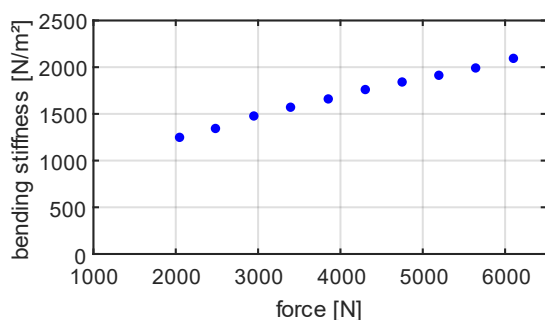


Figure 43: resulting bending stiffness ASTM D7250

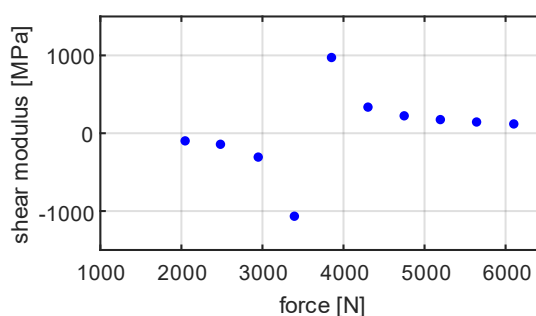


Figure 44: resulting shear modulus ASTM D7250

## 5 Model validation

In this chapter, the updated model predictions for the bending stiffness and shear modulus of the sandwich are displayed. Furthermore, the experimental results are discussed. Finally, the model predictions are compared and validated with the experimental results. When validating the accuracy of the model predictions and their sufficiency, the natural scattering of the experimental results due to the utilized natural material balsa wood as to be kept in mind. Another factor for scattering can be the manual manufacturing of the sandwich specimens.

### 5.1 Implementation of literature database and resulting predictions

The generated literature database results in the equations 9, 12, 16, 17 and 19. To implement them in the, in chapter 1.2 described, physically based model in a first step, a balsa properties “library” is added on a new Excel sheet. This offers the opportunity for the user to choose the values and equations from single, different literature sources or from the literature database. This enables a comparison between different approaches and theories. Furthermore, this library can be extended later, with values and equations from other sources or own tests. However, the developed literature database is set as the default configuration. This is also the case, if the user chooses a single source for the calculations, which does not provide values and equations for every necessary mechanical property. As it can be seen in chapter 2.1.1, most sources only determine data for some of the properties. The missing properties are then automatically calculated with the equations from the literature database. For the validation of the implemented literature database equations, all model calculations are based on them.

For the combination of Baltek SB 100 balsa panels with the EPIKOTE resin system, the in Table 7 listed sandwich core properties for each model version can be derived. These interim results are then used in the further calculation of the sandwich properties. Model 1 includes the balsa literature database and the application of the simplified mixture approach of Thomsen and Larsen for balsa wood, described in chapter 2.3. Model 2 is based on the balsa literature database but calculates without the simplified mixture approach. Model 3 is the old model, without any supplements. Model 2 and 3 provide two different values for  $G_{xy}$  respectively  $G_{yx}$ , based on Otten's equations [5, p. 42]. The difference to the simplified mixture approach is discussed in chapter 5.3. Furthermore, as a general trend, it can be noticed that due to the literature database implementation the bending stiffnesses in all directions become higher. Beyond that, no systematic change can be recognized. This is expected when implementing a completely new generic database.



	model 1	model 2		model 3	
$E_x$ [Mpa]	187.12	223.21		105.59	
$E_y$ [Mpa]	166.68	199.00		78.05	
$E_z$ [Mpa]	3783.79	3783.79		3426.87	
$G_{xz}$ [Mpa]	184.36	203.83		309.06	
$G_{yz}$ [Mpa]	178.41	197.47		304.24	
$G_{xy}$ [Mpa]	23.97	55.37	45.79	31.45	21.15

Table 7: balsa-resin core properties; model 1 including mixture approach of Thomsen and Larsen and literature database; model 2 including literature database; model 3 without supplements (old model)

For the model predictions, a fiber volume content (FVC) of  $\varphi = 0.49$  is assumed. The FVC is calculated from the used fabric and the measured face thicknesses with an IWES intern tool and is not experimentally validated. The face thicknesses that can be entered in the physically based model are not processed in the stiffness predictions. Furthermore, it must be noticed that in the “Model Input” interface, in the section “Geometry of dry Plate”, the measured core thickness after manufacturing the plate must be entered. The physically based model does not correct this value by the manufacturing shrinkage for the stiffness calculations. The predicted sandwich bending stiffnesses and shear moduli for each specimen can be found in Table 8, including the mean values for the thin and thick specimens.

	No	bending stiffness [N/m <sup>2</sup> ]			shear modulus [Mpa]		
		model 1	model 2	model 3	model 1	model 2	model 3
thin	1	492.59	493.03	491.64	190.38	210.48	319.14
	2	488.03	488.46	487.09	190.42	210.53	319.21
	3	482.42	482.84	481.51	190.53	210.64	319.39
	4	483.42	483.85	482.51	190.52	210.63	319.37
	5	487.96	488.39	487.03	190.46	210.56	319.27
	6	481.18	481.61	480.28	190.54	210.65	319.40
	7	490.07	490.51	489.14	190.41	210.52	319.20
	8	501.68	502.14	500.70	190.27	210.36	318.96
thick	9	1698.30	1702.22	1689.84	186.02	205.66	311.84
	10	1652.03	1655.77	1643.95	186.07	205.71	311.92
	11	1679.77	1683.63	1671.44	186.03	205.67	311.86
	12	1654.93	1658.68	1646.82	186.06	205.71	311.91
	13	1690.44	1694.32	1682.06	186.03	205.67	311.86
	14	1637.01	1640.68	1629.07	186.09	205.74	311.95
	15	1672.26	1676.06	1664.04	186.06	205.70	311.90
	16	1675.98	1679.81	1667.71	186.04	205.69	311.88
mean	thin	488.42	488.85	487.49	190.44	210.55	319.24
	thick	1670.09	1673.90	1661.87	186.05	205.69	311.89

Table 8: model predictions for bending stiffness and shear modulus; model 1 including mixture approach of Thomsen and Larsen and literature database; model 2 including literature database; model 3 without supplements (old model)

Taking a look on the bending stiffness, it can first be noticed that the three model predictions are close to each other. The maximum difference between the mean

values of the thin specimens is 0.28% and 0.72% for the thick specimens. Both values are relative to the resulting means of the old model. The nearly similar predicted bending stiffness is explained by the relatively small influence of the core material on the bending stiffness in a sandwich construction in general. In a sandwich, the bending stiffness is governed by the face sheet material. But neither the supplemented literature database nor the simplified mixture approach have an influence on the face sheets. The slightly higher difference between the mean maximum and minimum of the models for the thin and thick specimens can also be explained by the relatively higher influence of the thicker core on the overall stiffness. Looking at the predicted shear moduli, there is a significant difference between the results. For both specimen types, the mean prediction without the simplified mixture approach is 34.05% lower than the old models' one. Including the simplified mixture approach, reduces the prediction based on literature data for another 9.55%. The predicted out-of-plane shear modulus is mostly determined by the core shear modulus. As it can be seen in Table 8, it is significantly changed by the model supplements, thus changing the sandwich's shear modulus in the same way. Again, the difference between the absolute values between the thin and thick specimens of 2.36% can be explained by the relatively higher influence of the core material on the overall modulus. This difference results from the remaining influence of the face sheet material on the shear modulus. It is confirmed by the, compared to the pure core material's, higher shear moduli.

## 5.2 Discussion of experimental results and validation of model predictions

In this section, the experimental results are discussed. Furthermore, the influence of potential factors of uncertainty in the test procedure are determined. Then the presented model predictions are validated with the experimental data.

Looking at the in chapter 3.1 listed conditions for the applicability of ASTM C393, it can be noticed, that two of them are not fulfilled by the present test configuration. The specimen length of averaged 551 mm is longer than the span length plus 50 mm, which equals 490 mm. But the additional 61 mm are found to be negligible. Not neglectable is the face to thickness ratio of 0.215 for the thin specimens, as it is higher than the in ASTM C393 specified ratio of 0.1 [6, p. 4]. This means that "the transverse shear force [could] be carried to a considerable extent by the facings" [6, p. 4], which has to be kept in mind for the evaluation of the experimental results.

Another unplanned possible influence on the results occurs during the test performance. It is observed, that although the loading bars are mounted rotatable, in some cases one or even both supporting bars do not turn to follow the specimen's curvature. This means that the regarding specimen has no full contact with the rubber pad at greater deflections. This effect is documented in Figure 45. Thus, the supporting span is shortened for a few millimeters. The loading is not exactly centric within the four-point bending anymore. These effects cannot be met by corrections of the evaluation calculations, as the deviations are in the range of a few millimeters and occur irregularly. None of the measures to prevent the loss of contact, like lubricating the bearings, is effective. This influence should also be kept in mind when discussing the accuracy of the results.

Furthermore, the possibility that a relatively soft sandwich core can be locally compressed under the loading bars shall be mentioned. This could result in a changed height of the sandwich and thus, a non-linear bending behavior. This could have an influence on the deflection measured via DIC beneath the loading bars. However, the faces of the sandwiches do not show any damages after testing, which experientially occur, if the core is compressed. Also, no noticeable deformations of the core surface can be seen in the DIC tracking during the testing. Thus, it is assumed that the core is not compressed in the present case and the measurement is not influenced by this effect.

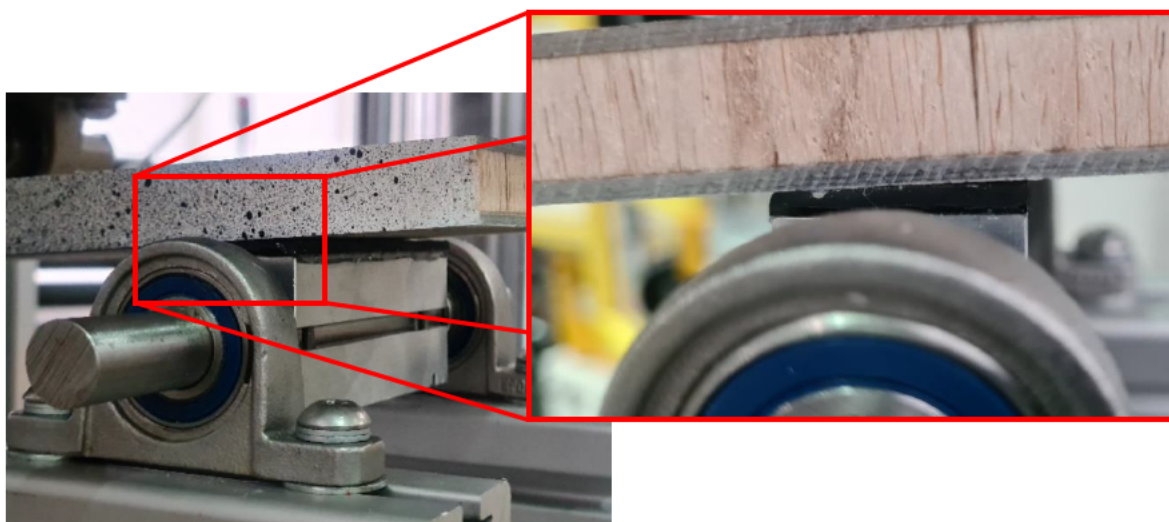


Figure 45: detailed view of gap between specimen and rubber pads occurring irregularly during testing (photos taken during two different tests)

The described differences between the results measured via strain gauges and measured via DIC could partly result from an inexact bearing. The strain gauges directly measure on the specimen's surface at only one point and have a certain tolerance when being marginally positioned out of the center due to their own length. However, the DIC evaluation is based on the measured deflection of three points on the specimen. This means that the probability of measurement deviations is much higher. An analysis of the Timoshenko bending line equations, the DIC evaluation is based on, shows that they are extremely sensitive to changes respective inaccuracies in the deflection measurement. For example, a difference of 0.01 mm in the deflection of the middle position can cause changes of the calculated shear modulus in the range of hundreds of megapascal. In this context, another critical point in the DIC measurement could be, that the camera system is installed on an item profile directly connected with the test machine as it can be seen in Figure 41. Thus, minimal vibrations of the machine, occurring even in a static test, could have an influence on the accuracy as well. Furthermore, the evaluation of the DIC video data in the present system requires the manual definition of evaluation axis orientations and of the exact points to be evaluated via "point and click". Thus, the reliability of the DIC based results can be doubted. This is also reflected in the standard deviations listed in Table 6.

Although the strain-based shear modulus is calculated with the DIC-measured deflection of the specimen beneath the loading bars, too, it is found to be more accurate. The influence of measurement deviations on the resulting shear modulus in this case is about 30 MPa for 0.1 mm difference. As already mentioned in the

ASTM C393 [6, p. 4], the attempt to do the calculations with the machine cross head displacement leads to unreasonable results. Even the use of correction values for the test rig compliance, measured in a compression test without a specimen, does not improve them. Thus, the validation of the model predictions is done with the experimental results based on strain. An interesting additional observation in the results based on strain is that, if the linearity limits of 500 to 2500  $\mu\text{m}/\text{mm}$  are set to higher strains up to 4000  $\mu\text{m}/\text{mm}$ , the derived bending stiffness gets lower. This results from an increasing, but in Figure 42 barely visible, nonlinearity of the strain with increasing load. A reason for this could be the overextension of the face sheet glass fibers and a corresponding nonlinear strain behavior due to occurring damages or plastic deformations on a micromechanical level.

For a better overview, the mean experimental results and the model predictions are directly compared in Table 9.

	bending stiffness [ $\text{N}/\text{m}^2$ ]				shear modulus [ $\text{Mpa}$ ]			
	strain	model 1	model 2	model 3	strain	model 1	model 2	model 3
thin	526.52	488.42	488.85	487.49	154.62	190.44	210.55	319.24
thick	1765.28	1670.09	1673.90	1661.87	194.15	186.05	205.69	311.89

Table 9: overview experimental results and model predictions

Comparing the experimental and model bending stiffnesses in general, it can be noticed that the measured bending stiffnesses are significantly higher than the predicted. For the thin specimens, the predictions are approximately 7.3% lower and for the thick specimens 5.2 to 5.9%. The bending stiffness is crucially influenced by the face sheets and the core thickness, but less by the core material itself. This is the reason for the low differences between the model predictions, which are far below the threshold of the natural scattering of the values. Given the additional measurement uncertainties, it is not possible to prove which model delivers the more accurate prediction of bending stiffnesses. Furthermore, it is unclear if the balsa wood literature database supplements the bending stiffness prediction. Taking the range of the strain-based bending stiffness results of the modified tests into account, it can be stated that the bending stiffness prediction in general meets the reality.

Because of the relatively low impact of the core Young's modulus on the overall bending stiffness, it is not possible to investigate the influence of the moisture content of the balsa wood. The measured relative moisture content of 6% is below the range of 9 to 13% the literature database is derived from. Hence, according to Figures 28 and 29, a higher Young's modulus could be expected. But as outlined in chapter 2.1.2.2, there are several other effects correlated with the moisture content that cannot be quantified. In combination with the low influence of the core's Young's modulus and the measurement uncertainties, it is not satisfactory to correlate the relatively higher measured bending stiffness with the lower than modelled moisture content. To investigate this correlation further tests with different moisture contents of pure balsa are necessary.

Comparing the predicted shear moduli with the experimental results, it can be noticed, that the mean result for the thin specimens is lower than all model predictions. In detail it is 18.8% below the prediction from model one, including the simplified mixture approach, and 26.6% below the one of model two. The old

model's prediction without any supplements is more than twice as high as the experimental result. The apparent overestimation of the specimens' shear moduli could at least partly result from the measurement inaccuracies. In ASTM C393 a higher apparent shear modulus due to high face to core thickness ratios, which lead to a stronger contribution of the face sheets' high shear modulus, is suggested [6, p. 4]. Nevertheless, the measured shear modulus is below the predictions. This is a sign for the physical model also working for higher face to thickness ratios than 0.1. It does not result in an overestimation of the face sheets' influence on the overall shear modulus. For the thick specimens, the experimental result lies between the model predictions with and without the simplified mixture approach. Thus, it is again significantly below the old models' prediction. From both cases it can be stated that the implementation of the balsa wood literature database supplements the modulus and thus the stiffness prediction of the physically based model. It improves its accuracy significantly.

As outlined, the additional modified test configurations do not lead to usable results, which is why they are not discussed in detail. The reason for the obviously incorrect measurements is assumed to be the LVDT or its installation. Due to the limited time for experiments within the scope of this thesis, the LVDT is only adhered to the specimen's surface. This connection could allow unwanted movement and thus a deviation of the measured deflection. Future tests should be performed with a more rigid connection, like a clamp or bracket.

### 5.3 Discussion of the simplified rule of mixture approach by Thomsen and Larsen

The sandwich core properties calculated with the simplified rule of mixture approach are generally lower than without, as it can be seen in Table 7. Only exception is the Young's modulus in z-direction. Here, the mixture approach leads to the same equation than before. The other Young's moduli are about 16% lower. The out-of-plane shear moduli are about 9.5% lower. The in-plane shear modulus is up to 56.7% lower. These differences are considered significant. Furthermore, the influence on the eventual overall sandwich bending stiffness is much lower. On the contrary, the difference in the out-of-plane core shear moduli is completely reflected in the sandwich's modulus.

An important systematic difference between the simplified rule of mixture approach by Thomsen and Larsen and the old model calculations developed by Otten can be found in the calculation of the in-plane shear modulus  $G_{xy}$ . Otten derives two different shear moduli for the same plane  $G_{xy}$  and  $G_{yx}$  [5, p. 42]. They depend on the considered perspective of the RVE. This does not meet the reality, where only three independent shear moduli exist orthogonal to each other [9, p. 5-2]. The in-plane shear modulus is necessary for the calculation of the  $\underline{\underline{Q}}$  matrix within the calculation of the mechanical properties of the sandwich based on the CLT [5, p. 45]. Although in cell K93 on the page "Model Input" of the physically based model the arithmetic mean of both shear moduli is calculated, this mean is not used for the calculation of the matrix. It is calculated with only one of both values, dependent on the chosen direction for the  $0^\circ$ -definition within the CLT. This seems insufficient, as the in-plane shear modulus of the core must be independent of any direction

definitions. Following this argumentation, the model's weakness of the doubled in-plane shear modulus is corrected with the simplified rule of mixture approach, as only one in-plane shear modulus is derived.

Comparing the model values predicted with the simplified rules of mixture approach with the experimental results, it is not possible to decide whether the approach leads to more accurate predictions. Additionally, the factors of uncertainty in the evaluation of the experiments as well as the strong natural scattering of the results per se must be considered. Furthermore, there is nearly no difference between the predicted bending stiffnesses. Regarding the shear moduli, the experimental results lie between the models' predictions, at least for the thick specimens. All in all, this does not allow a reliable validation of the implementation of Thomsen and Larsen's simplified rule of mixture approach for balsa wood.

## 6 Conclusions and future research

Most widely, the goal of this thesis to receive sufficiently accurate model predictions for bending stiffness and shear modulus of an FRP sandwich verified by experimental results is achieved. The database for the elastic properties of balsa wood derived from the relevant literature gives a comprehensive summary of the available corresponding research. It is successfully implemented in the model and improved the accuracy of the model's shear stiffness predictions significantly.

An underestimation of the bending stiffness of clearly less than 10% is observed. Reasons for this, beside the natural scattering of the material's properties, could be the described uncertainties in the measurement of the tests. For future research, it is suggested to further improve the four-point bending test configuration by eliminating the single potential sources of uncertainty. A combination of strain, DIC and LVDT measurement would enable a comparison of the measuring methods. Especially another four-point bending test with all measurements performed simultaneously is assumed to deliver pursuing results, if considering the listed suggestions for improvement of the single methods. In addition to this, alternative test methods for the measurement of elastic sandwich properties, which are potentially less sensible against measurement deviations, should be analysed and considered. Howsoever, the implemented balsa wood literature database has only little influence on the predicted bending stiffnesses. To improve the prediction on a theoretical level, a more accurate analysis and description of the real face sheet laminates should be performed.

The prediction of the shear moduli and thus of the shear stiffness is significantly improved by the implemented balsa wood literature database. The thick specimens' shear modulus is well met. The remaining overestimation of the shear modulus for the thin specimens is attributable to the inaccuracies in the measurement. Assurance for this could be reached by performing an own test programme on balsa wood of different densities. The whole literature database could directly be verified by this and extended under controlled test circumstances. The experiences from the tests displayed in the literature review of this thesis should be utilized for the test design. Besides, an own test programme should be performed to further investigate the influence of the relative moisture content on balsa wood mechanical properties. The present literature database is not sufficient to quantify its influence. But that there is a strong influence that is worth to be researched and described is not doubted. With tests under controlled climatic conditions and predetermined moisture contents this goal could be achieved.

The analysis and implementation of the simplified rule of mixture approach of Thomsen and Larsen for balsa wood sandwich cores is performed additionally to the scope of this thesis. Its experimental verification, respectively the verification of its supplemental effect on the model's stiffness predictions, is not possible with the conducted tests. However, it could not be debunked either. For future research, it seems promising to perform tests to characterize the elastic properties directly on the sandwich core material. This offers the opportunity to utilize the larger differences between the property predictions of the two core models for the

verification of one or another. This is not possible within this thesis due to their reduced effect on the overall sandwich properties.



## 7 References

- [1] Geschäftsstelle der Arbeitsgruppe Erneuerbare Energien-Statistik (AGEE-Stat) am Umweltbundesamt (2021): *Erneuerbare Energien in Deutschland: Daten zur Entwicklung im Jahr 2020*. URL [https://www.umweltbundesamt.de/sites/default/files/medien/5750/publikationen/2021\\_hgp\\_erneuerbareenergien\\_deutsch\\_bf.pdf](https://www.umweltbundesamt.de/sites/default/files/medien/5750/publikationen/2021_hgp_erneuerbareenergien_deutsch_bf.pdf). Last viewed: 28.03.2021.
- [2] Bundesverband Windenergie e.V.: *Numbers and Facts*. URL <https://www.wind-energie.de/english/statistics/international-statistics/>. Last viewed: 28.03.2021.
- [3] Hau, Erich (2016): *Windkraftanlagen: Grundlagen, Technik, Einsatz, Wirtschaftlichkeit*. Springer Vieweg, Berlin, Germany.
- [4] Fraunhofer-Institut für Energiewirtschaft und Energiesystemtechnik (2019): *Windenergie Report Deutschland 2018.*, Stuttgart, Germany. URL [http://windmonitor.iee.fraunhofer.de/opencms/export/sites/windmonitor/img/Windmonitor-2018/WERD\\_2018.pdf](http://windmonitor.iee.fraunhofer.de/opencms/export/sites/windmonitor/img/Windmonitor-2018/WERD_2018.pdf). Last viewed: 28.03.2021.
- [5] Otten, Tobias (2020): *A physically based FRP Sandwich Model implementing the Resin Uptake of Balsa Wood as Core Material*. Master's Thesis. University of Applied Sciences Aachen, Aachen, Germany. FB6 Aerospace Engineering.
- [6] ASTM International: *Standard Test Method for Core Shear Properties of Sandwich Constructions by Beam Flexure*. ASTM C393/C393M - 16, West Conshohocken, PA, U.S.
- [7] Rosemeier, M., Buriticá, P., and Antoniou, A. (2018): *Impact of resin uptake of core materials on buckling of wind turbines blades*. Journal of Physics: Conference Series Vol. 1037 Issue 4.
- [8] Da Silva, Andre and Kyriakides, Stelios (2007): *Compressive response and failure of balsa wood*. International Journal of Solids and Structures No. 44: pp. 8685–8717.
- [9] Forest Products Laboratory (2010): *Wood Handbook: Wood as an Engineering Material*, Madison, Wisconsin, U.S.
- [10] Doyle, D. V., Drow, J. T., and McBurney, R. S. (1962): *ELASTIC PROPERTIES OF WOOD: The Young's Moduli, Moduli of Rigidity, and Poisson's Ratios of Balsa and Quipo*. Report No. 1528. Forest Products Laboratory, Madison, Wisconsin, U.S. URL [https://ir.library.oregonstate.edu/xmlui/bitstream/handle/1957/1286/FPL\\_1528ocr.pdf;jsessionid=610FCE038A05C7B88BDFD3AD4C0AB5B1?sequence=1](https://ir.library.oregonstate.edu/xmlui/bitstream/handle/1957/1286/FPL_1528ocr.pdf;jsessionid=610FCE038A05C7B88BDFD3AD4C0AB5B1?sequence=1). Last viewed: 28.03.2021.

- [11] Osei-Antwi, Michael, Castro, Julia de, Vassilopoulos, Anastasios P., and Keller, Thomas (2013): *Shear mechanical characterization of balsa wood as core material of composite sandwich panels*. Construction and Building Materials No. 41: pp. 231–238.
- [12] Feichtinger, Kurt A. (1989): *Test Methods and Performance of Structural Core Materials -1. Static Properties*. Journal of Reinforced Plastics and Composites Vol. 8: pp. 334–357.
- [13] Easterling, K. E., Harryson, R., Gibson, L. J., and Ashby, M. F. (1982): *On the mechanics of balsa and other woods*. Proceedings of the Royal Society London A 383: pp. 31–41.
- [14] Eckelman, Carol A. (1997): *Wood Moisture Calculations*. FNR-156. Department of Forestry & Natural Resources, West Lafayette, Indiana, U.S. URL <https://www.extension.purdue.edu/extmedia/FNR/FNR-156.pdf>. Last viewed: 28.03.2021.
- [15] Harrington, Jonathan J. (2002): *Hierarchical modelling of softwood hygro-elastic properties*. Dissertation. University of Canterbury, Christchurch, New Zealand.
- [16] Malek, S. and Gibson, Lorna J. (2017): *Multi-scale modelling of elastic properties of balsa*. International Journal of Solids and Structures 113-114: pp. 118–131.
- [17] Soden, P. D. and McLeish, R. D. (1976): *Variables Affecting the Strength of Balsa Wood*. Journal of Strain Analysis Vol 11 No 4: pp. 225–234.
- [18] Neroth, Günter and Vollenschaar, Dieter (2011): *Wendehorst Baustoffkunde: Grundlagen - Baustoffe - Oberflächenschutz*. Vieweg+Teubner, Wiesbaden, Germany.
- [19] March, H. W., Kuenzi, E. W., and Kommers, W. J. (1942): *METHOD OF MEASURING THE SHEARING MODULI IN WOOD*. Report No. 1301. Forest Products Laboratory, Madison, Wisconsin, U.S. URL <https://www.google.com/url?sa=t&rct=j&q=&esrc=s&source=web&cd=&ved=2ahUKEwik5tSTroXwAhUn8LsIHao7C1MQFjAAegQIBBAD&url=https%3A%2F%2Ffir.library.oregonstate.edu%2Fdownloads%2F37720h337&usg=AOvVaw3A0-dyipQ1sFLlrLshpGGu>. Last viewed: 17.04.2021.
- [20] ASTM International: *Standard Test Method for Shear Properties of Composite Materials by the V-Notched Beam Method*. ASTM D5379/D5379M-05, West Conshohocken, PA, U.S.
- [21] ASTM International: *Standard Test Methods for Direct Moisture Content Measurement of Wood and Wood-Base Materials*. ASTM D4442-07, West Conshohocken, PA, U.S.
- [22] ASTM International: *Standard Test Method for Shear Properties of Sandwich Core Materials*. ASTM C273-94, West Conshohocken, PA, U.S.

- [23] Newaz, G., Mayeed, M., and Rasul, A. (2016): *Characterization of balsa wood mechanical properties required for continuum damage mechanics analysis*. Journal of Materials: Design and Applications 230 (1): pp. 206–218.
- [24] Yao, Wen-juan and Ye, Zhi-ming (2004): *Analytical Solution of Bending-Compression Column Using Different Tension-Compression Modulus*. Applied Mathematics and Mechanics Vol. 25 No. 9: pp. 983–993.
- [25] ASTM International: *Standard Test Methods for Small Clear Specimens of Timber*. ASTM D143-09, West Conshohocken, PA, U.S.
- [26] Kotlarewski, Nathan J., Belleville, Benoit, Gusamo, Benson K., and Ozarska, Barbara (2016): *Mechanical properties of Papua New Guinea balsa wood*. European Journal of Wood and Wood Products Vol. 74: pp. 83–89.
- [27] Australian/New Zealand Standard: *Timber-Methods of test, Method 1: Moisture content*. AS/NZS 1080.1:2012, Sydney, Australia.
- [28] Australian/New Zealand Standard: *Timber-Methods of test, Method 3: Density*. AS/NZS 1080.3:2000, Sydney, Australia.
- [29] ASTM International: *Standard Test Method for Flatwise Compressive Properties of Sandwich Cores*. ASTM C365-57, West Conshohocken, PA, U.S.
- [30] ASTM International: *Standard Test Method for Shear Properties of Sandwich Core Materials*. ASTM C273-61, West Conshohocken, PA, U.S.
- [31] U.S. Department of Defense: *Military Standard. Sandwich Constructions and Core Materials; General Test Methods*. MIL-STD-401B, Washington D.C., U.S.
- [32] ASTM International: *Testing small clear specimens of timber*. ASTM D143-52, West Conshohocken, PA, U.S.
- [33] British Standards Institution: *British Standard - Methods of testing small clear specimens of timber*. BS 373:1957.
- [34] DIN Deutsches Institut für Normung e.V.(2019): *Rigid cellular plastics - Determination of compression properties*. DIN EN ISO 844:2019, Berlin, Germany.
- [35] ASTM International: *Standard Test Method for Flatwise Tensile Strength of Sandwich Constructions*. ASTM C297/C297M-16, West Conshohocken, PA, U.S.
- [36] ASTM International: *Standard Test Method for Shear Properties of Sandwich Core Materials*. ASTM C273/C273M-20, West Conshohocken, PA, U.S.
- [37] Borrega, Marc, Ahvenainen, Patrik, Serimaa, Ritva, and Gibson, Lorna (2015): *Composition and structure of balsa (Ochroma pyramidale) wood*. Wood Science and Technology Vol. 49: pp. 403–420.

- [38] Brøndsted, Povl and Toftegaard, Helmuth: *Methods for Qualification of the Mechanical Properties of Sandwich Core Materials for Wind Turbine Blades*. Proceedings of ICCM 2009: 17th International Conference on Composite Materials: A7:10. Edinburgh, Scotland, 27.-31.07.2009.
- [39] Monti, Arthur, El Mahi, Abderrahim, Jendli, Zouhaier, and Guillaumat, Laurent (2018): *Quasi-static and fatigue properties of a balsa cored sandwich structure with thermoplastic skins reinforced by flax fibres*. Journal of Sandwich Structures and Materials Vol. 21: pp. 2358–2381.
- [40] Branner, K. and Berring, P.: *Compressive Strength of Thick Composite Panels*. Composite materials for structural performance: towards higher limits: Proceedings of the 32nd International Symposium on Materials Science: pp. 221–228. Roskilde, Denmark, 05.-09.09.2011.
- [41] Widagdo, Djarot, Kuswoyo, Andi, Nurpratama, Taufiq O., and Hadi, Bambang K. (2020): *Experimental flatwise tensile strength dataset of carbon fiber reinforced plastic sandwich panels with different core material preparations*. Data in brief Vol. 28: pp. 1–9.
- [42] Caprino, G. and Langella, A. (2000): *Study of a Three-Point Bending Specimen for Shear Characterisation of Sandwich Cores*. Journal of Materials Vol. 34: pp. 791–814.
- [43] Grenestedt, Joachim L. and Bekisli, Burak (2003): *Analysis and preliminary tests of a balsa sandwich core with improved shear properties*. International Journal of Mechanical Sciences Vol. 45: pp. 1327–1346.
- [44] Shishkina, Oksana, Lomov, Stepan V., Verpoest, Ignaas, and Gorbatikh, Larissa (2014): *Structure-property relations for balsa wood as a function of density: modelling approach*. Archive of Applied Mechanics Vol. 84: pp. 789–805.
- [45] Yoshihara, Hiroshi, Ohsaki, Hisashi, Kubojima, Yoshitaka, and Ohta, Masamitsu (1999): *Applicability of the Iosipescu shear test on the measurement of the shear properties of wood*. Journal of Wood Science Vol. 45: pp. 24–29.
- [46] Hyer, M. W. (1998): *Stress analysis of fiber-reinforced composite materials: with contributions on fibers, matrices, interfaces, and manufacturing by S. R. White*. WCB McGraw-Hill, Boston, Massachusetts, U.S.
- [47] Báder, Mátyás and Németh, Róbert (2019): *Moisture-dependent mechanical properties of longitudinally compressed wood*. European Journal of Wood and Wood Products Vol. 77: pp. 1009–1019.
- [48] Bhangu, Shubhdeep Singh (2012): *Effect of Moisture Absorption on the Mechanical Properties of Balsa Wood*. ADFA Journal of Undergraduate Engineering Research Vol. 5 No. 1.

- [49] Keunecke, Daniel, Sonderegger, Walter, Pereteanu, Karol, Lüthi, Thomas, and Niemz, Peter (2007): *Determination of Young's and shear moduli of common yew and Norway spruce by means of ultrasonic waves*. Wood Science and Technology Vol. 41: pp. 309–327.
- [50] Schiefer, Hartmut and Schiefer, Felix (2018): *Statistik für Ingenieure: Eine Einführung mit Beispielen aus der Praxis*. Springer Vieweg, Wiesbaden, Germany.
- [51] Papula, Lothar (2009): *Mathematische Formelsammlung: für Ingenieure und Naturwissenschaftler*. Vieweg+Teubner, Wiesbaden, Germany.
- [52] DIN Deutsches Institut für Normung e.V.(2019): *Wind energy generation systems - Part 5: Wind turbine rotor blades (IEC 88/675/CDV:2018)*. draft DIN EN 61400-5, Berlin, Germany.
- [53] Zenkert, Dan (1997): *The Handbook of Sandwich Construction*, Cradley Heath, West Midlands, U.K.
- [54] DIN Deutsches Institut für Normung e.V.(1982): *Testing of sandwiches; flexure test of flat sandwiches*. DIN 53293, Berlin, Germany.
- [55] Gross, Dietmar, Hauger, Werner, Schröder, Jörg, and Wall, Wolfgang A. (2012): *Technische Mechanik 2: Elastostatik*. Springer-Verlag, Berlin, Heidelberg, Germany.
- [56] Allen, Howard G. (1969): *Analysis and Design of Structural Sandwich Panels*. Pergamon Press, Oxford, U.K.
- [57] Spura, Christian (2019): *Technische Mechanik 2. Elastostatik: Nach fest kommt ab*. Springer Vieweg, Wiesbaden, Germany.
- [58] Thomsen, Ole Thybo and Larsen, Jesper (2008): *Simplified Rule of Mixtures Approach for the Accurate Estimation of the Elastic Properties of Grid-Scored Polymer Foam Core Sandwich Plates. Proceedings of the 8th International Conference on Sandwich Structures (ICSS8) 2008*: pp. 261–274.
- [59] Seibel, Michael (2019): *Faserverbundtechnologie, Vorlesungsskript*. Hochschule für Angewandte Wissenschaften, Hamburg. Department Fahrzeugtechnik und Flugzeugbau.
- [60] Herbst, Christian and Splitthof, Karsten: *Basics of 3D Digital Image Correlation: Q400 Application Note - T-Q-400-Basics-3DCORR-002a-EN*. Dantec Dynamics GmbH, Ulm, Germany. URL <https://www.dantecdynamics.com/notes/basics-of-3d-digital-image-correlation-dic/?sourceid=764>. Last viewed: 28.03.2021.
- [61] Nickel, Andreas (2011): *Optimierung der Designparameter von GFK-Kern-Verbunden unter Berücksichtigung der Harzaufnahme des Kerns*. Diplomarbeit. Technische Universität Berlin, Berlin, Germany. Institut für Luft- und Raumfahrt.

- [62] DIN Deutsches Institut für Normung e.V.(1997): *Plastics - Determination of tensile properties - Part 4: Test conditions for isotropic and orthotropic fibre-reinforced plastic composites (ISO 527-4:1997)*. DIN EN ISO 527-4, Berlin, Germany.
- [63] ASTM International: *Standard Practice for Determining Sandwich Beam Flexural and Shear Stiffness*. ASTM D7250/D7250M - 20, West Conshohocken, PA, U.S.







78,12				0,175							
86,92				0,243							
90,21				0,214							
100,77				0,231							
101,15				0,250							
103,49				0,200							
103,52				0,191							
110,42				0,263							
115,12				0,249							
117,66				0,226							
122,53				0,249							
130,95				0,256							
132,26				0,211							
136,31				0,263							
136,46				0,215							
139,29				0,286							
148,37				0,221							
153,48				0,170							
155,34				0,269							
157,39				0,178							
162,69				0,245							
167,12				0,227							
168,42				0,274							
169,50				0,254							
171,60				0,147							
182,82				0,185							
185,90				0,220							
77,75					0,445						
86,24					0,434						
89,76					0,518						
99,72					0,497						
100,59					0,425						
102,91					0,373						
103,00					0,474						
109,36					0,466						
114,71					0,501						
116,89					0,427						
121,72					0,505						
130,97					0,336						
132,14					0,523						
135,73					0,518						
135,78					0,450						
139,12					0,342						
147,33					0,479						
152,51					0,532						
155,00					0,468						
156,60					0,511						
162,39					0,386						
166,63					0,606						
167,37					0,490						
168,45					0,576						
170,29					0,737						
182,68					0,509						
185,59					0,539						
70,98								0,013			
73,51								0,019			
79,50								0,022			
87,86								0,011			
91,84								0,012			
98,07								0,025			
106,78								0,017			
133,07								0,012			
135,29								0,020			
163,77								0,020			
185,87								0,029			
201,09								0,028			

71,57							0,677			
74,33							0,657			
80,20							0,793			
87,22							0,515			
92,55							0,785			
97,00							0,458			
106,94							0,648			
133,13							0,398			
134,96							0,569			
158,42							0,601			
162,97							0,895			
174,63							0,468			
185,39							0,898			
196,73							0,721			
200,12							0,848			
62,99						0,009				
63,76						0,008				
66,09						0,008				
82,57						0,007				
105,04						0,012				
107,92						0,007				
121,77						0,007				
124,91						0,009				
139,97						0,007				
141,52						0,006				
143,52						0,015				
147,78						0,009				
159,80						0,011				
198,83						0,010				
215,51						0,012				
62,96						0,112				
63,43						0,183				
65,94						0,193				
72,54						0,244				
82,43						0,070				
82,74						0,084				
104,57						0,292				
107,39						0,330				
121,52						0,168				
124,66						0,228				
136,44						0,376				
139,74						0,267				
141,31						0,257				
143,35						0,335				
147,12						0,180				
159,68						0,255				
183,70						0,311				
198,77						0,258				
215,10						0,171				

Table A-1: literature data Doyle et al.

Density		Moisture content	E <sub>A</sub>	E <sub>R</sub>	E <sub>T</sub>	v <sub>AR</sub>	v <sub>AT</sub>	v <sub>TR</sub>	v <sub>TA</sub>	v <sub>RA</sub>	v <sub>RT</sub>	G <sub>AR</sub>	G <sub>AT</sub>	G <sub>RT</sub>
[-]	[kg/m <sup>3</sup> ]	[%]	[N/mm <sup>2</sup> ]	[N/mm <sup>2</sup> ]	[N/mm <sup>2</sup> ]	[-]	[-]	[-]	[-]	[-]	[-]	[N/mm <sup>2</sup> ]	[N/mm <sup>2</sup> ]	[N/mm <sup>2</sup> ]
relative														
0,043	64,5	9 - 12	610									39,5		
0,047	70,5	9 - 12			18,9									
0,049	73,5	9 - 12		34,6									43,9	
0,076	114	9 - 12			24,1									
0,079	118,5	9 - 12	1990											
0,085	127,5	9 - 12		88,1										
0,086	129	9 - 12										109,4		
0,092	138	9 - 12											89,6	
0,097	145,5	9 - 12	3040											
0,111	166,5	9 - 12			54,9									
0,121	181,5	9 - 12										200,6		
0,125	187,5	9 - 12		246,6										
0,140	210	9 - 12											133,7	
0,128	192	9 - 12	5620											
0,130	195	9 - 12			78,9									
0,141	211,5	9 - 12										268,8		
0,145	217,5	9 - 12		345,2										
0,203	304,5	9 - 12											149,4	
0,150	225	9 - 12			98,3									
0,156	234	9 - 12		428,3										
0,158	237	9 - 12	6620											
0,207	310,5	9 - 12										355,9		
0,242	363	9 - 12											243,8	

Table A-2: literature data Da Silva, Kyriakides

Density	Moisture content	E <sub>A</sub>	E <sub>R</sub>	E <sub>T</sub>	v <sub>AR</sub>	v <sub>AT</sub>	v <sub>TR</sub>	v <sub>TA</sub>	v <sub>RA</sub>	v <sub>RT</sub>	G <sub>AR</sub>	G <sub>AT</sub>	G <sub>RT</sub>
[kg/m <sup>3</sup> ]	[%]	[N/mm <sup>2</sup> ]	[N/mm <sup>2</sup> ]	[N/mm <sup>2</sup> ]	[-]	[-]	[-]	[-]	[-]	[-]	[N/mm <sup>2</sup> ]	[N/mm <sup>2</sup> ]	[N/mm <sup>2</sup> ]
78	n.d.	903	53	13									
127	n.d.	2870	67	32			0,034	0,011	0,014	0,65			
160	n.d.	3330	86	39									
218	n.d.	5900	172	59									

Table A-3: literature data Easterling et al.

Density	Moisture content	E <sub>A</sub>	E <sub>R</sub>	E <sub>T</sub>	v <sub>AR</sub>	v <sub>AT</sub>	v <sub>TR</sub>	v <sub>TA</sub>	v <sub>RA</sub>	v <sub>RT</sub>	G <sub>AR</sub>	G <sub>AT</sub>	G <sub>RT</sub>
[kg/m <sup>3</sup> ]	[%]	[N/mm <sup>2</sup> ]	[N/mm <sup>2</sup> ]	[N/mm <sup>2</sup> ]	[-]	[-]	[-]	[-]	[-]	[-]	[N/mm <sup>2</sup> ]	[N/mm <sup>2</sup> ]	[N/mm <sup>2</sup> ]
274,2	12										242,7	242,7	
281,6	12										213,6	213,6	
303,0	12										232,4	232,4	
310,4	12										264,0	264,0	
311,2	12										227,8	227,8	
316,6	12										252,4	252,4	
415,1	12										380,1	380,1	
424,9	12										334,6	334,6	
174,0	12												46,6
186,4	12												41,1
280,1	12												86,4
323,5	12												82,2
328,9	12												150,5
354,7	12												153
355,6	12												130,6
374,7	12												129,1
180,3	12										200,5	200,5	
187,9	12										281,2	281,2	
210,2	12										330,2	330,2	
229,5	12										190,1	190,1	
257,3	12										310,7	310,7	
289,3	12										410,3	410,3	
295,6	12										327,1	327,1	
379,2	12										414	414	

Table A-4: literature data Osei-Antwi et al.

Density	Moisture content	E <sub>A</sub>	E <sub>R</sub>	E <sub>T</sub>	v <sub>AR</sub>	v <sub>AT</sub>	v <sub>TR</sub>	v <sub>TA</sub>	v <sub>RA</sub>	v <sub>RT</sub>	G <sub>AR</sub>	G <sub>AT</sub>	G <sub>RT</sub>		
[kg/m <sup>3</sup> ]	[%]	[N/mm <sup>2</sup> ]	[N/mm <sup>2</sup> ]	[N/mm <sup>2</sup> ]	[-]	[-]	[-]	[-]	[-]	[-]	[N/mm <sup>2</sup> ]	[N/mm <sup>2</sup> ]	[N/mm <sup>2</sup> ]		
		compression	compression	tension	compression	tension									
90,98	12	371,57	23,49	48,27	23,49	48,27	0,1103	0,1103	0,4797	0,0070	0,0070	0,4797	80,0	80,0	12,5

Table A-5: literature data Newaz et al.

testing type	thickness	length	width
	[mm]	[mm]	[mm]
compression along fiber direction	9,57 ±0,03	24,50 ±0,07	- -
tension along fiber direction	5,50 ±0,20	25,40 ±0,00	12,60 ±0,25
compression across fiber direction	9,40 ±0,00	24,00 ±0,50	24,00 ±0,15
tension across fiber direction	4,40 ±0,10	36,00 ±0,50	18,20 ±0,25
shear across fiber direction	19,05 -	25,40 -	25,40 -
shear along fiber direction	19,05 -	25,40 -	25,40 -

Table A-6: specimens' dimensions Newaz et al.

Density	Moisture content	E <sub>A</sub>	E <sub>R</sub>	E <sub>T</sub>	v <sub>AR</sub>	v <sub>AT</sub>	v <sub>TR</sub>	v <sub>TA</sub>	v <sub>RA</sub>	v <sub>RT</sub>	G <sub>AR</sub>	G <sub>AT</sub>	G <sub>RT</sub>
[kg/m <sup>3</sup> ]	[%]	[N/mm <sup>2</sup> ]	[N/mm <sup>2</sup> ]	[N/mm <sup>2</sup> ]	[-]	[-]	[-]	[-]	[-]	[-]	[N/mm <sup>2</sup> ]	[N/mm <sup>2</sup> ]	[N/mm <sup>2</sup> ]
80 ≤ 120	13	1222,14									only max shear stress		
120 ≤ 180	13	2037,07											
180 ≤ 220	13	-											

Table A-7: literature data Kotlarewski et al.

Density	Moisture content	E <sub>A</sub>	E <sub>R</sub>	E <sub>T</sub>	v <sub>AR</sub>	v <sub>AT</sub>	v <sub>TR</sub>	v <sub>TA</sub>	v <sub>RA</sub>	v <sub>RT</sub>	G <sub>AR</sub>	G <sub>AT</sub>	G <sub>RT</sub>
[kg/m <sup>3</sup> ]	[%]	[N/mm <sup>2</sup> ]	[N/mm <sup>2</sup> ]	[N/mm <sup>2</sup> ]	[-]	[-]	[-]	[-]	[-]	[-]	[N/mm <sup>2</sup> ]	[N/mm <sup>2</sup> ]	[N/mm <sup>2</sup> ]
101,70	n.d.	1700,2											
103,10	n.d.	1555,7											
104,74	n.d.	2629,5											
108,36	n.d.	2334,3											
110,55	n.d.	3051,4											
112,97	n.d.	2377,6											
113,89	n.d.	3405,8											
116,80	n.d.	4214,5											
116,92	n.d.	2708,7											
125,18	n.d.	3106,2											
128,74	n.d.	2518,0											
129,51	n.d.	2787,6											
131,53	n.d.	3740,5											
139,25	n.d.	4540,7											
140,33	n.d.	2678,0											
140,72	n.d.	4212,2											
151,59	n.d.	3303,7											
155,59	n.d.	4956,6											
158,09	n.d.	4162,0											
161,85	n.d.	4567,9											
167,88	n.d.	4007,0											
169,78	n.d.	5913,9											
176,08	n.d.	5168,9											
177,71	n.d.	5679,5											
183,60	n.d.	3860,0											
189,49	n.d.	4201,4											
193,79	n.d.	6331,2											
203,57	n.d.	5670,4											
220,67	n.d.	6310,0											
221,51	n.d.	8562,3											
100,30	n.d.										94,44		
102,96	n.d.										103,17		
104,61	n.d.										132,72		
104,71	n.d.										147,95		
106,23	n.d.										91,29		
107,38	n.d.										175,93		
109,61	n.d.										98,22		
110,43	n.d.										95,98		
110,75	n.d.										121,51		
111,05	n.d.										98,22		
111,96	n.d.										66,87		
113,00	n.d.										110,53		
113,00	n.d.										137,40		
113,10	n.d.										121,50		
113,21	n.d.										158,67		
114,34	n.d.										160,68		
114,43	n.d.										116,79		
119,86	n.d.										133,13		



Density	Moisture content	E <sub>A</sub>		E <sub>R</sub>	E <sub>T</sub>	v <sub>AR</sub>	v <sub>AT</sub>	v <sub>TR</sub>	v <sub>TA</sub>	v <sub>RA</sub>	v <sub>RT</sub>	G <sub>AR</sub>	G <sub>AT</sub>	G <sub>RT</sub>
[kg/m <sup>3</sup> ]	[%]	[N/mm <sup>2</sup> ]	[N/mm <sup>2</sup> ]	[N/mm <sup>2</sup> ]	[N/mm <sup>2</sup> ]	[-]	[-]	[-]	[-]	[-]	[-]	[N/mm <sup>2</sup> ]	[N/mm <sup>2</sup> ]	[N/mm <sup>2</sup> ]
		compression	tension											
84,67	8,1 ± 1,1	1181,7												
85,42	8,1 ± 1,1	1423,2												
102,77	8,1 ± 1,1	1483,6												
104,29	8,1 ± 1,1	1794,1												
109,38	8,1 ± 1,1	1966,6												
178,98	8,1 ± 1,1	3441,6												
186,85	8,1 ± 1,1	4192,1												
190,13	8,1 ± 1,1	4985,6												
203,39	8,1 ± 1,1	5106,4												
204,65	8,1 ± 1,1	5537,7												
90,24	8,1 ± 1,1		1914,9											
103,75	8,1 ± 1,1		2363,4											
120,56	8,1 ± 1,1		2975,8											
128,47	8,1 ± 1,1		3062,1											
158,00	8,1 ± 1,1		4390,5											
169,93	8,1 ± 1,1		5623,9											
171,52	8,1 ± 1,1		4588,8											
175,33	8,1 ± 1,1		4985,6											
180,34	8,1 ± 1,1		6728											
183,51	8,1 ± 1,1		4709,6											
192,81	8,1 ± 1,1		7443,9											
233,62	8,1 ± 1,1		7840,7											
247,01	8,1 ± 1,1		10609,5											

Table A-9: literature data Soden et al.

Density	Moisture content	E <sub>A</sub>	E <sub>R</sub>	E <sub>T</sub>	v <sub>AR</sub>	v <sub>AT</sub>	v <sub>TR</sub>	v <sub>TA</sub>	v <sub>RA</sub>	v <sub>RT</sub>	G <sub>AR</sub>	G <sub>AT</sub>	G <sub>RT</sub>
[kg/m <sup>3</sup> ]	[%]	[N/mm <sup>2</sup> ]	[N/mm <sup>2</sup> ]	[N/mm <sup>2</sup> ]	[-]	[-]	[-]	[-]	[-]	[-]	[N/mm <sup>2</sup> ]	[N/mm <sup>2</sup> ]	[N/mm <sup>2</sup> ]
160	12	3400	156,4	51	0,229	0,488	0,231	0,009	0,018	0,665	183,6	125,8	17

Table A-10: literature data Wood Handbook

Density	Moisture content	E <sub>A</sub>		E <sub>R</sub>	E <sub>T</sub>	v <sub>AR</sub>	v <sub>AT</sub>	v <sub>TR</sub>	v <sub>TA</sub>	v <sub>RA</sub>	v <sub>RT</sub>	G <sub>AR</sub>	G <sub>AT</sub>	G <sub>RT</sub>
[kg/m <sup>3</sup> ]	[%]	[N/mm <sup>2</sup> ]	[N/mm <sup>2</sup> ]	[N/mm <sup>2</sup> ]	[N/mm <sup>2</sup> ]	[-]	[-]	[-]	[-]	[-]	[-]	[N/mm <sup>2</sup> ]	[N/mm <sup>2</sup> ]	[N/mm <sup>2</sup> ]
		compression	tension											
109	n.d.	1616	1682									136	136	
132	n.d.	2187	2337									166	166	
148	n.d.	2526	2791									187	187	
285	n.d.	4428	6604									362	362	

Table A-11: literature data Baltek TDS

# Appendix B: Baltek SB technical data sheet

## BALTEK

**3A** CORE  
COMPOSITE MATERIALS

### BALTEK® SB

GM-TDS-103

*Select Grade Structural Balsa*

DATA SHEET 02.2016 - Replaces 10.2014

#### DESCRIPTION



**BALTEK® SB** is a core material produced from select kiln-dried balsa wood in the 'end-grain' configuration. It has extremely high strength and stiffness to weight ratios, and achieves an excellent bond with all types of resins and adhesives. It is compatible with a variety of manufacturing processes and is resistant to temperature changes, or exposure to fire, or chemicals such as styrene.

**BALTEK® SB** is an ideal core material for an extensive range of applications subjected to static or dynamic loads in service. All while being a renewable resource.

#### CHARACTERISTICS

- Outstanding strength and stiffness to weight ratios
- First-class, select grade lumber
- Ecological product
- Broadest range of available balsa densities worldwide
- Certified for a range of applications by DNV, Germanischer Lloyd, Lloyd's Register, American Bureau of Shipping and Korean Register
- Excellent fatigue and impact resistance
- Fulfills most FST (flame, smoke, toxicity) requirements
- Good sound and thermal insulation
- Extremely wide operating temperature range (-212 °C to +163 °C (-414 °F to +325 °F))

#### APPLICATIONS

- **Marine:** Hulls, decks, bulkheads, superstructures, interiors, tooling/molds
- **Road and Rail:** Floors, roofs, side skirts, front-ends, doors, interiors, covers
- **Wind energy:** Rotor blades (shear webs and shells), nacelles, spinners
- **Industrial:** Tanks, containers, architectural panels, impact limiters, sporting goods
- **Aerospace:** Floors, cargo pallets, cargo containers, bulkheads, general aviation
- **Defense:** Naval vessels, containers, cargo pallets, shelters, ballistic panels

#### PROCESSING

- Adhesive bonding
- Compression molding
- Contact molding (hand/spray)
- Pre-preg processing (up to 180 °C, 355 °F)
- Resin injection (RTM)
- Vacuum infusion

[www.3ACorematerials.com](http://www.3ACorematerials.com)

Europe | Middle East | India | Africa  
Alex AG  
5943 Sina, Switzerland  
T +41 41 789 86 00 | F +41 41 789 66 60  
[corematerials@3AComposites.com](mailto:corematerials@3AComposites.com)

North America | South America  
Baltek Inc.  
High Point, NC 27261, USA  
T +1 336 398 1900 | F +1 336 398 1901  
[corematerials.americas@3AComposites.com](mailto:corematerials.americas@3AComposites.com)

Asia | Australia | New Zealand  
3A Composites (China) Ltd.  
201201 Shanghai, China  
T +86 21 585 86 006 | F +86 21 338 27 208  
[corematerials.asia@3AComposites.com](mailto:corematerials.asia@3AComposites.com)






MECHANICAL PROPERTIES						
Typical properties for BALTEK® SB		Unit (metric)	SB.50	SB.80	SB.100	SB.150
Apparent nominal density	ASTM C-271	kg/m <sup>3</sup>	109	132	148	285
Minimum sheet density	ASTM C-271	kg/m <sup>3</sup>	84	113	136	248
Compressive strength perpendicular to the plane	ISO 844	N/mm <sup>2</sup>	5.5	7.7	9.2	22
Compressive modulus perpendicular to the plane	ISO 844	N/mm <sup>2</sup>	1616	2187	2526	4428
Tensile strength perpendicular to the plane (polyester)	ASTM C-297	N/mm <sup>2</sup>	3.9	5.0	5.7	12.2
Tensile strength perpendicular to the plane (epoxy)	ASTM C-297	N/mm <sup>2</sup>	9	10.9	12	18.3
Tensile modulus perpendicular to the plane	ASTM C-297	N/mm <sup>2</sup>	1682	2337	2791	6604
Shear strength <sup>1</sup>	ASTM C-273	N/mm <sup>2</sup>	1.8	2.3	2.6	5.2
Shear modulus	ASTM C-273	N/mm <sup>2</sup>	136	166	187	362
Thermal conductivity at room temperature	ASTM C-177	W/m <sup>2</sup> K	0.048	0.059	0.066	0.084
Standard sheet	Width	mm ± 5	610	610	610	610
	Length	mm ± 10	1220	1220	1220	1220
	Thickness	mm +0.25 -0.75	4.7 to 76	4.7 to 76	4.7 to 76	6 to 76
ContourKore (CK)	Thickness	mm +0.25 -0.75	4.7 to 50	4.7 to 50	4.7 to 50	6 to 50

Please specify Lamprep surface treatment or AL600 coating (decreases porosity and increases bond strength) when ordering.

Perforations (breather holes), grooves and other finishing options are also available. Other sheet sizes are available on request.

<sup>1</sup> All samples tested @ ¼" thick. Please apply appropriate shear strength reduction factors for greater thickness.

Fire Performance*	Standard		SB.50	SB.100	SB.150
Aircraft	FAR 25.853	Flammability	Passed	Passed	Not tested
		Smoke density	Passed	Passed	
		Toxicity	Passed	Passed	
		Heat release	Failed	Failed	
Rail	ASTM E 162	Flame spread factor	2.22	2.22	Not tested
		Heat Evolution factor	6.24	6.24	
		Flame spread index	14	14	
Rail	ASTM E 662 (non-flaming mode)	Ds @ 90 sec	3	3	Not tested
		Ds @ 4min	39	39	
Rail	ASTM E 662 (flaming mode)	Ds @ 90 sec	8	8	Not tested
		Ds @ 4min	25	25	

\* All samples tested with phenolic resin FRP skins.

The data provided gives approximate values for the nominal density. Due to density variations these values can be lower than indicated above. Minimum values to calculate sandwich constructions can be provided upon request. The information contained herein is believed to be correct and to correspond to the latest state of scientific and technical knowledge. However, no warranty is made, either expressed or implied, regarding its accuracy or the results to be obtained from the use of such information. No statement is intended or should be construed as a recommendation to infringe any existing patent.

GM-TDS-103



MECHANICAL PROPERTIES						
Typical properties for BALTEK® SB		Unit (Imperial)	SB.50	SB.80	SB.100	SB.150
Nominal sheet density	ASTM C-271	lb/ft³	6.8	8.2	9.3	17.8
Minimum sheet density	ASTM C-271	lb/ft³	5.2	7.1	8.5	15.5
Compressive strength perpendicular to the plane	ISO 844	psi	798	1117	1336	3184
Compressive modulus perpendicular to the plane	ISO 844	psi	234400	317198	366200	642000
Tensile strength perpendicular to the plane (polyester)	ASTM C-297	psi	558	725	831	1770
Tensile strength perpendicular to the plane (epoxy)	ASTM C-297	psi	1299	1581	1737	2654
Tensile modulus perpendicular to the plane	ASTM C-297	psi	243900	338954	404700	957600
Shear strength <sup>1</sup>	ASTM C-273	psi	267	334	378	761
Shear modulus	ASTM C-273	psi	19700	24076	27100	52600
Thermal conductivity at room temperature	ASTM C-177	BTU.in/ft².hr.°F	0.331	0.407	0.456	0.581
Standard sheet	Width	in ± 3/16	24	24	24	24
	Length	in ± 3/8	48	48	48	48
	Thickness	in +0.01 -0.03	3/16 to 3	3/16 to 3	3/16 to 3	1/4 to 3
ContourKore (CK)	Thickness	in +0.01 -0.03	3/16 to 2	3/16 to 2	3/16 to 2	1/4 to 2

Please specify Lamprep surface treatment or AL600 coating (decreases porosity and increases bond strength) when ordering.

Perforations (breather holes), grooves and other finishing options are also available. Other sheet sizes are available on request.

<sup>1</sup> All samples tested @ 1/4" thick. Please apply appropriate shear strength reduction factors for greater thickness.

Fire Performance*	Standard		SB.50	SB.100	SB.150
Aircraft	FAR 25.853	Flammability Smoke density Toxicity Heat release	Passed Passed Passed Failed	Passed Passed Passed Failed	Not tested
Rail	ASTM E 162	Flame spread factor Heat Evolution factor Flame spread index	2.22 6.24 14	2.22 6.24 14	Not tested
Rail	ASTM E 662 (non-flaming mode)	Ds @ 90 sec Ds @ 4min	3 39	3 39	Not tested
Rail	ASTM E 662 (flaming mode)	Ds @ 90 sec Ds @ 4min	8 25	8 25	Not tested

\* All samples tested with phenolic resin FRP skins.

The data provided gives approximate values for the nominal density. Due to density variations these values can be lower than indicated above. Minimum values to calculate sandwich constructions can be provided upon request. The information contained herein is believed to be correct and to correspond to the latest state of scientific and technical knowledge. However, no warranty is made, either expressed or implied, regarding its accuracy or the results to be obtained from the use of such information. No statement is intended or should be construed as a recommendation to infringe any existing patent.

GM-TDS-103

# Appendix C: Saertex X-E-812g/m<sup>2</sup>-1270mm technical data sheet



## TECHNICAL DATASHEET

SAP No. 30000687 Article Description X-E-812g/m<sup>2</sup>-1270mm

Textile Structure 7000715 SAERTEX®

### ARTICLE CONSTRUCTION (in accordance with EN 13473-1)

Layer	Construction	Areal weight	Tolerance	Material
4	45 °	401 g/m <sup>2</sup>	+/- 5 %	E-glass 600 TEX
3	90 °	3 g/m <sup>2</sup>	+/- 5 %	E-glass 68 TEX
2	0 °	1 g/m <sup>2</sup>	+/- 5 %	E-glass 34 TEX
1	-45 °	401 g/m <sup>2</sup>	+/- 5 %	E-glass 600 TEX
Stitching		6 g/m <sup>2</sup>	+/- 1 g/m <sup>2</sup>	PES [Polyester] 76 dtex

Fiber input can be determined individually

### FURTHER CHARACTERISTICS

Gauge	5,0	Stitching pattern	warp	Width (nominal)	1.270 mm
Stitch length	2,60 mm	Total tolerance	5,1 %	Total areal weight	812 g/m <sup>2</sup>

**Labelling (Standard)** Every roll is equipped with a label in the core. A further label is located outside on the foil or on the box.

**Packaging (Standard)** Every roll is wound on a cardboard core and wrapped in foil. Further packaging options can be determined individually.

**Storage recommendation** With original packaging: Temperature 15-35°C and 20-80% humidity. No moisture and direct sunlight. To avoid problems with humidity and electrostatic charge, fabrics to be conditioned 24 hours prior to processing, independent of storage conditions.

# Appendix D: EPIKOTE Resin MGS RIMR 035c, EPIKURE Curing Agent MGS RIMH 037 technical data sheet



## Starting Formulation

### EPIKOTE™ Resin MGS™ RIMR035c EPIKURE™ Curing Agent MGS™ RIMH036, 0366, 037, 038, 038F APPLICATION

EPIKOTETM Resin MGS™ RIMR035c is a low-viscous infusion resin system approved by German Lloyd and can be used for processing of glass, carbon and aramid fibres. Due to its excellent mechanical properties, this system is suitable for the production of components featuring high static and dynamic loadability.

The range of pot lives is between approx. 2 hours and approx. 5.5 hours. Curing at higher temperatures (up to approx. 80-100°C) is possible, depending on laminate thickness and geometry of the parts to be manufactured. The infusion resin system does not contain any unreactive components. The raw materials used feature a very low vapour pressure. This permits processing of the material under vacuum even at elevated temperatures. For processing at elevated temperatures lower reactive curing agents like RIMH037 and especially RIMH038 are available in order to keep exotherm temperatures during curing at a low level. The optimum processing temperature is in the range of 20°C to 35°C. Higher temperatures are possible, but will shorten pot life. A temperature increase of 10°C will approx. halve the pot life. Different temperatures during processing are not known to have significant impact on the mechanical properties of the cured product.

All curing agents except of RIMH038F (F = free of pigment) are coloured for easier identification of a correct mixing process. Although unlikely, deviations in colour are possible (e.g. due to UV radiation after longer exposure to sun light), but are not known to have an effect on the processing and final properties of the material.

Compatibility problems are not to be expected in combination with UP gelcoats, coatings (e.g. PUR-based), etc. However, comprehensive tests are indispensable.

Although RIMR035c is very unlikely to crystallize at low temperatures, storage conditions of 15°C - 30°C and low humidity are recommended. If crystallisation of either component should be observed, it can be removed by warming up while stirring. Slow warming up to approx. 50 - 60°C in an oven or heating cabinet and stirring or shaking will clarify the contents of the container without any loss of quality. Use only completely transparent products. Before warming up, open containers slightly to permit equalization of pressure. Caution during warm-up! Do not warm up over an open flame! While stirring up use safety equipment (gloves, eyeglasses, respirator equipment, long sleeves and trousers, safety shoes).

After dispensing material, the containers must again be closed carefully, to avoid contamination or absorption of water. All amine hardeners show a chemical reaction when exposed to air, known as „blushing“. This reaction is visible as white carbamide crystals, which could make the materials unusable.

The materials have a shelf life of minimum 2 years, when stored in their originally sealed containers.

The relevant industrial safety regulations for the handling of epoxy resins and curing agents and our instructions for safe processing are to be observed.

### EPIKOTE™ Resin MGS™ RIMR035c EPIKURE™ Curing Agent MGS™ RIMH036, 0366, 037, 038, 038F SPECIFICATIONS

		Infusion resin RIMR035c
Density <sup>1)</sup>	[g/cm <sup>3</sup> ]	1,11 – 1,14
Viscosity <sup>1)</sup>	[mPa·s]	1000 – 1500
Refractory index <sup>1)</sup>	[-]	1,5530 – 1,5580

Generated: April 21, 2021  
Issue Date:  
Revision:

© and ™ Licensed trademarks of Hexion Inc.

#### DISCLAIMER

The information provided herein was believed by Hexion Inc. ("Hexion") to be accurate at the time of preparation or prepared from sources believed to be reliable, but it is the responsibility of the user to investigate and understand other pertinent sources of information, to comply with all laws and procedures applicable to the safe handling and use of the product and to determine the suitability of the product for its intended use. All products supplied by Hexion are subject to Hexion's terms and conditions of sale. HEXION MAKES NO WARRANTY, EXPRESS OR IMPLIED, CONCERNING THE PRODUCT OR THE MERCHANTABILITY OR FITNESS THEREOF FOR ANY PURPOSE OR CONCERNING THE ACCURACY OF ANY INFORMATION PROVIDED BY HEXION, except that the product shall conform to Hexion's specifications. Nothing contained herein constitutes an offer for the sale of any product.

		Curing agent		
RIMH036	RIMH0366	RIMH037		
Density <sup>1)</sup>	[g/cm <sup>3</sup> ]	0,93 – 0,96	0,92 – 0,96	0,92 – 0,96
Viscosity <sup>1)</sup>	[mPa·s]	5 – 25	5 – 25	5 – 25
Refractory index <sup>1)</sup>	[-]	1,460 – 1,465	1,458 – 1,467	1,458 – 1,464
Pot life <sup>2)</sup>	[min]	110 – 170	150 – 250	190 – 290
T <sub>G, mid, pot</sub>	[°C]	Approx. 80 – 85 (unconditioned)		

		Curing agent	
RIMH038 / RIMH038F			
Density <sup>1)</sup>	[g/cm <sup>3</sup> ]	0,91 – 0,95	
Viscosity <sup>1)</sup>	[mPa·s]	5 – 25	
Refractory index <sup>1)</sup>	[-]	1,460 – 1,463	
Pot life <sup>2)</sup>	[min]	240 – 330	
T <sub>G, mid, pot</sub>	[°C]	Approx. 80 (unconditioned)	

Measuring conditions:

1) measured at 25°C

2) measured in 30°C water bath, 100g sample

## EPIKOTE™ Resin MGS™ RIMR035c EPIKURE™ Curing Agent MGS™ RIMH036, 0366, 037, 038, 038F CHARACTERISTI

Generated: April 21, 2021  
Issue Date:  
Revision:

© and ™ Licensed trademarks of Hexion Inc.

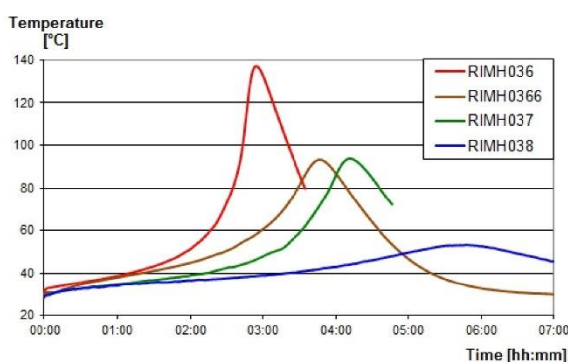
### DISCLAIMER

The information provided herein was believed by Hexion Inc. ("Hexion") to be accurate at the time of preparation or prepared from sources believed to be reliable, but it is the responsibility of the user to investigate and understand other pertinent sources of information, to comply with all laws and procedures applicable to the safe handling and use of the product and to determine the suitability of the product for its intended use. All products supplied by Hexion are subject to Hexion's terms and conditions of sale. HEXION MAKES NO WARRANTY, EXPRESS OR IMPLIED, CONCERNING THE PRODUCT OR THE MERCHANTABILITY OR FITNESS THEREOF FOR ANY PURPOSE OR CONCERNING THE ACCURACY OF ANY INFORMATION PROVIDED BY HEXION, except that the product shall conform to Hexion's specifications. Nothing contained herein constitutes an offer for the sale of any product.

Page 2 of 6

Approval	DNV-GL SE (Germanischer Lloyd)
Application	Rotor blades for wind energy turbines, boat and shipbuilding, sports and recreation equipment, model construction, tooling
Operational temperature	-60°C to +70°C after heat treatment
Processing	Generally infusion at temperatures between 15°C and 50°C, depending on production parameters
Features	Low viscosity, extremely long pot life, excellent cost performance ratio
Storage	Shelf life of 24 months in originally sealed containers

**EPIKOTE™ Resin MGS™ RIMR035c EPIKURE™ Curing Agent MGS™ RIMH036, 0366, 037, 038, 038 TEMPERATURE**



Measuring conditions: 100g mixture at 30°C in a water basin

Water (e.g. high humidity or contained in the fabrics) can cause an acceleration of the resin/curing agent reaction and influence mechanical properties.

Do not mix large quantities – particularly of higher reactive systems – at elevated processing temperatures. As the heat dissipation in the mixing container is very slow, the contents will be heated up by the reaction heat (exothermic resin-curing agent reaction) rapidly. This can result in temperatures of more than 200°C in the mixing container, which may cause smoke-intensive burning of the resin mass.

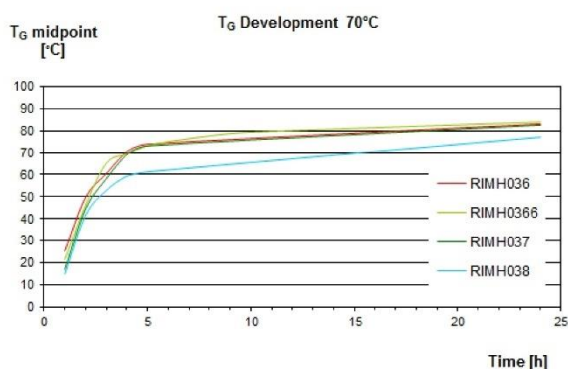
**EPIKOTE™ Resin MGS™ RIMR035c EPIKURE™ Curing Agent MGS™ RIMH036, 0366, 037, 038, 038 TG DEVELOPMENT**

Generated: April 21, 2021  
 Issue Date:  
 Revision:

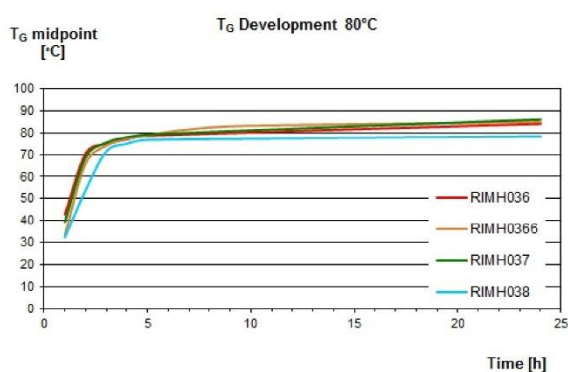
© and ™ Licensed trademarks of Hexion Inc.

**DISCLAIMER**

The information provided herein was believed by Hexion Inc. ("Hexion") to be accurate at the time of preparation or prepared from sources believed to be reliable, but it is the responsibility of the user to investigate and understand other pertinent sources of information, to comply with all laws and procedures applicable to the safe handling and use of the product and to determine the suitability of the product for its intended use. All products supplied by Hexion are subject to Hexion's terms and conditions of sale. HEXION MAKES NO WARRANTY, EXPRESS OR IMPLIED, CONCERNING THE PRODUCT OR THE MERCHANTABILITY OR FITNESS THEREOF FOR ANY PURPOSE OR CONCERNING THE ACCURACY OF ANY INFORMATION PROVIDED BY HEXION, except that the product shall conform to Hexion's specifications. Nothing contained herein constitutes an offer for the sale of any product.



Measuring conditions: DSC, T<sub>G, midpoint</sub> at 70°C cure according to MMS 4000



Measuring conditions: DSC, T<sub>G, midpoint</sub> at 80°C cure according to MMS 4000

**EPIKOTE™ Resin MGS™ RIMR035c EPIKURE™ Curing Agent MGS™ RIMH036, 0366, 037, 038, 038 MECHANICAL DAT**

Generated: April 21, 2021  
 Issue Date:  
 Revision:

© and ™ Licensed trademarks of Hexion Inc.

**DISCLAIMER**

The information provided herein was believed by Hexion Inc. ("Hexion") to be accurate at the time of preparation or prepared from sources believed to be reliable, but it is the responsibility of the user to investigate and understand other pertinent sources of information, to comply with all laws and procedures applicable to the safe handling and use of the product and to determine the suitability of the product for its intended use. All products supplied by Hexion are subject to Hexion's terms and conditions of sale. HEXION MAKES NO WARRANTY, EXPRESS OR IMPLIED, CONCERNING THE PRODUCT OR THE MERCHANTABILITY OR FITNESS THEREOF FOR ANY PURPOSE OR CONCERNING THE ACCURACY OF ANY INFORMATION PROVIDED BY HEXION, except that the product shall conform to Hexion's specifications. Nothing contained herein constitutes an offer for the sale of any product.

Mechanical data		
Density DIN EN ISO 1183-1	[g/cm <sup>3</sup> ]	Approx. 1,15
Flexural strength DIN EN ISO 178	[MPa]	Approx. 115
Modulus of elasticity DIN EN ISO 178	[GPa]	Approx. 3,1
Tensile strength DIN EN ISO 527-2	[MPa]	Approx. 70
Elongation at break DIN EN ISO 527-2	[%]	7 - 10
Water absorption at 23°C DIN EN ISO 175	24h [%] 7d [%]	Approx. 0,20 Approx. 0,40
Curing: 8h 70°C		

Advice:

Mechanical data are typical for the combination of infusion resin RIMR035C with curing agent RIMH037. Data can differ in other applications.

**EPIKOTE™ Resin MGS™ RIMR035c EPIKURE™ Curing Agent MGS™ RIMH036, 0366, 037, 038, 038 MIXING RATIOS**

	RIMR035c with all curing agents
Parts by weight	100 : 28 ± 2
Parts by volume	100 : 34 ± 2

The mixing ratio stated must be observed carefully. Adding more or less curing agent will not result in a faster or slower cure, only incomplete curing with limited performance, that can not be corrected in any way.

Resin and curing agent must be mixed carefully. Mix until no clouding is visible in the mixing container. Special attention must be paid to the walls and bottom of the mixing container.

**EPIKOTE™ Resin MGS™ RIMR035c EPIKURE™ Curing Agent MGS™ RIMH036, 0366, 037, 038, 038 VISCOSITY DEVE**

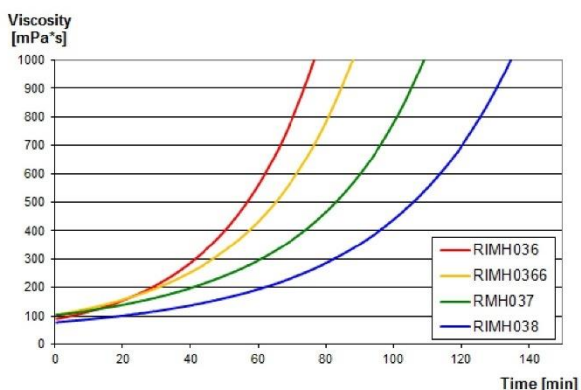
Generated: April 21, 2021  
 Issue Date:  
 Revision:

© and ™ Licensed trademarks of Hexion Inc.

DISCLAIMER

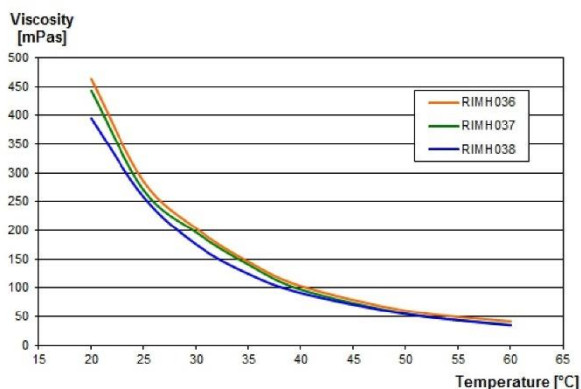
The information provided herein was believed by Hexion Inc. ("Hexion") to be accurate at the time of preparation or prepared from sources believed to be reliable, but it is the responsibility of the user to investigate and understand other pertinent sources of information, to comply with all laws and procedures applicable to the safe handling and use of the product and to determine the suitability of the product for its intended use. All products supplied by Hexion are subject to Hexion's terms and conditions of sale. HEXION MAKES NO WARRANTY, EXPRESS OR IMPLIED, CONCERNING THE PRODUCT OR THE MERCHANTABILITY OR FITNESS THEREOF FOR ANY PURPOSE OR CONCERNING THE ACCURACY OF ANY INFORMATION PROVIDED BY HEXION, except that the product shall conform to Hexion's specifications. Nothing contained herein constitutes an offer for the sale of any product.





Measuring conditions: 40°C, cone-plate configuration, gap d=0,1 mm

EPIKOTE™ Resin MGS™ RIMR035c EPIKURE™ Curing Agent MGS™ RIMH036, 0366, 037, 038, 038 VISCOSITY OF



Measuring conditions: 100g mixture at 30°C in a water basin

Disclaimer

© and ™ Licensed trademarks of Hexion Inc.

The information provided herein was believed by Hexion Inc. ("Hexion") to be accurate at the time of preparation or prepared from sources believed to be reliable, but it is the responsibility of the user to investigate and understand other pertinent sources of information, to comply with all laws and procedures applicable to the safe handling and use of the product and to determine the suitability of the product for its intended use. All products supplied by Hexion are subject to Hexion's terms and conditions of sale. HEXION MAKES NO WARRANTY, EXPRESS OR IMPLIED, CONCERNING THE PRODUCT OR THE MERCHANTABILITY OR FITNESS THEREOF FOR ANY PURPOSE OR CONCERNING THE ACCURACY OF ANY INFORMATION PROVIDED BY HEXION, except that the product shall conform to Hexion's specifications. Nothing contained herein constitutes an offer for the sale of any product.

Generated: April 21, 2021  
 Issue Date:  
 Revision:

© and ™ Licensed trademarks of Hexion Inc.

DISCLAIMER

The information provided herein was believed by Hexion Inc. ("Hexion") to be accurate at the time of preparation or prepared from sources believed to be reliable, but it is the responsibility of the user to investigate and understand other pertinent sources of information, to comply with all laws and procedures applicable to the safe handling and use of the product and to determine the suitability of the product for its intended use. All products supplied by Hexion are subject to Hexion's terms and conditions of sale. HEXION MAKES NO WARRANTY, EXPRESS OR IMPLIED, CONCERNING THE PRODUCT OR THE MERCHANTABILITY OR FITNESS THEREOF FOR ANY PURPOSE OR CONCERNING THE ACCURACY OF ANY INFORMATION PROVIDED BY HEXION, except that the product shall conform to Hexion's specifications. Nothing contained herein constitutes an offer for the sale of any product.

**Declaration of honor**

I hereby declare that I,

Name: Garcia Merida

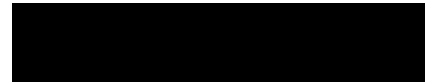
First name: David Joaquin

wrote this Bachelor's thesis with the title:

Theoretical and experimental determination of balsa wood elastic properties to supplement the stiffness prediction of a physically based FRP Sandwich Model

without the assistance of others and only used the indicated literature and aids. Direct quotes or the use of ideas of other authors are marked at the corresponding locations in the Bachelor's thesis.

Hamburg, 30.04.2021



*original signature*